IMPACT OF INTESTINAL INFLAMMATION ON OSTEOCLAST DIFFERENTIATION AND FUNCTION

By

Christopher Peek

Dissertation

Submitted to the Faculty of the

Graduate School of Vanderbilt University

in partial fulfillment of the requirements

for the degree of

DOCTOR OF PHILOSOPHY

in

Microbe-Host Interactions

May 31, 2022

Nashville, Tennessee

Approved:

James E. Cassat, M.D., Ph.D.
David Aronoff, M.D.
Christopher Williams, M.D., Ph.D.
Keith Wilson, M.D.
Rachelle W. Johnson, Ph.D.
Jeremy Goettel, Ph.D.

DEDICATION

To my friends, family, wife, and dog.

ACKNOWLEDGMENTS

This work would have been possible without the financial support through F30DK120114-04 (NIH, CTP), T32M007347 (NIH, Vanderbilt MSTP), Career Award for Medical Scientists from the Burroughs Wellcome Fund (JEC), pilot funding from the Vanderbilt University Medical Center Digestive Disease Research Center grant P30DK058404 (NIH, JEC), and Senior Research Award #709139 from the Crohn's and Colitis Foundation (JEC).

Completing this work would not have been possible without the incredible support of so many amazing scientists and friends. This is especially true during a global pandemic. The shared resources cores and facilities at Vanderbilt University and Vanderbilt University Medical Center have been integral to the completion of this project. Thank you to the Vanderbilt Flow Cytometry Shared Resources core for their training and assistance with more experiments than I can recall. To Dave Flaherty and Brittany Matlock – thank you for assisting with sorting samples, unclogging machines, and providing a fun environment to talk about science and life. Thank you to the Vanderbilt University Institute of Imaging Sciences Center for Small Animal Imaging for your training and assistance with micro-computed tomography and Scanco software. To Sasi Uppuganti – thank you for your prompt replies to emails and diligent, often thankless, work to maintain the machines and servers. Thank you to the Vanderbilt University Medical Center Translational Pathology Shared Resource for processing, embedding, and staining the many samples generated from this work. Thank you to the Vanderbilt Center for Bone Biology for access to microscopes and histomorphometry software. To Josh Johnson – thank for your technical expertise and assistance with processing, sectioning, and staining femurs. To Alysa Merkel – thank you for the many protocols and assistance you provided. Thank you to the Vanderbilt Digestive Diseases Research Center (thanks, Dad) for providing shared resources and

space to conduct research. To, Margarette Allaman – thank you for technical assistance with Luminex. To Blanca Piazuelo and Kay Washington – thank you both for offering your expertise in scoring samples for histologic injury.

I also want to thank the many labs that touched this project in one way or another. To the Marvin Whitely laboratory, specifically Caroline Ibberson, thank you all for taking the time to teach me both the computational and bench protocols required for transposon sequencing. To the Keith Wilson laboratory, specifically Yvonne Latour, thank you for your assistance with *Citrobacter rodentium* experiments. To the Jeremy Goettel laboratory, specifically Justin Jacobse, thank you so much with your generosity in sharing equipment, time, reagents, and being a sounding board for ideas. To Leigh Knodler, thank you for your generosity in sharing *Salmonella enterica* strains. To the Mariana Byndloss laboratory, specifically Woongjae Yoo, Catie Shelton, Nic Shealy, and Teresa Torres, thank you for your generosity in time, sharing *Salmonella enterica* strains, and assistance with experiments. To Mariana Byndloss – thank you for your unofficial mentorship and kindness. To Zach – it was an honor to get to know you in the time we worked together.

To my past and present lab mates – thank you for providing such an amazing environment to work. Aimee – thank you for taking me on as a rotation student. Niki – thank you for your time in helping co-developing flow cytometry protocols and your shared enthusiasm about osteoclasts. Tom – thank you for always genuinely checking in on me and making the lab a better place. Jacob, Laura, Teresa, Virginia, Ian, and Caroline – you all were amazing laboratory technicians. Helping me with the often-undesirable tasks of weighing mice, collecting stool specimens, managing mouse colonies, counting cells, and enumerating osteoclasts truly moved the needle on what would have been impossible days to more manageable days. The work you

all did every day ensured that the lab was able to function – thank you. Caleb – my lab big brother – thank you for your mentorship and willingness to help with my project even in the face of your own needs. I was lucky to be on the receiving end of your friendship and support. Jenna – thank you so much for holding the lab together with the little things you do that often go unnoticed, reflecting my enthusiasm for osteoclasts and immunology, and being a great sounding board for data discussion or experimental ideas. Casey – your infectious energy made lab such a great place to come to work. Thank you for your willingness to help with any lab task and being the ultimate team player. Brittney, Juan, and Kara – thank you for providing some post-doctoral seniority to keep us trainees in check. To Kara in particular – you are such an amazing lab member – your willingness to drop everything and help even when it's inconvenient for you inspires me to be better for others in the lab. Clara – it's been an honor to mentor you. I'm so excited to see the things you'll do and the places you'll go. Thank you so much for all your hard work over the past few months – it truly helped this work progress.

To my past mentors, I would not be here without you. Mark Denison – thank you for taking a chance on a high school kid and teaching me to ask bold scientific questions and persevere in the face of rejection. Megan Culler-Freeman – you were such an amazing mentor and friend. Thank you for introducing me to the Vanderbilt MSTP and for teaching me more skills than I can remember. Barney Graham – thank you so much for allowing me to grow in your laboratory and demonstrating what quiet, humble leadership looks like. Syed Moin – thank you for pushing me scientifically and showing me what a truly well controlled experiment looks like. Kayvon Modjarrod – thank you for your friendship, mentorship, and for reminding me to not take myself too seriously. Thank you to my mentors from Davidson College, Malcolm Campbell and Dave Wessner, for your mentorship, support, and encouragement. Thank you to

Terry Dermody for creating such a welcoming MSTP that drew me in and to Chris Williams along with the current MSTP leadership team for continuing to grow the program.

To my thesis committee – David Aronoff, Chris Williams, Keith Wilson, Rachelle Johnson, and Jeremy Goettel – thank you all sincerely for the time and energy you devoted to my training. Your input was invaluable to my growth as a scientist. Thank you for challenging me throughout this process and creating a space where my ideas felt respected and heard.

To my mentor, Jim Cassat, thank you for everything. You've built such an amazing research program and laboratory culture which makes saying goodbye so hard. I was lucky to be a small part of it. Thank you for trusting me to take on a project that represented a new frontier for the laboratory and for giving me the creative freedom to explore new ideas. It often felt like we were learning side by side, which was both exciting and scary. Thank you for highlighting the excitement and helping me confront the scary. I'm grateful for the opportunities you entrusted to me to contribute to grant writing and appreciate the massive amount of time and energy you took to provide valuable feedback – it truly impacted me as a writer and future mentor. Thank you for pushing me to conduct rigorous science and constantly showing me what good mentorship looks like. Above all, thank you for being an amazing friend throughout this process.

To my MSTP friends – Brad, Matt, Kelsey, Maggie, Abin, Connor, and Lizzie – thank you all for being there throughout this entire process and for allowing me to be a cheerleader to your successes. To my non-MSTP friends – Mikeie, Natalie, Josh, Liz, Ben, Cat, Scott, Erol, Nashville 'Shine, and others – thank you for reminding me that there's a life outside of science and medicine and for keeping me grounded. To Mikeie especially, thank you for being a brother to me.

Most of all, to my family – Mom, Dad, and Jennifer – I can't thank you all enough for constantly being there for me and reminding me what's most important in life. Jennifer – it's been truly amazing watching you grow and I'm so excited to see what you accomplish. Mom and Dad – thank you for being examples of the people I want to become, for your unconditional love, and for your unending support. To Zeus – you are the best dog and writing partner. To my wife, Jenny, you are my hero. I am in constant awe of all you do. Thank you for lifting me up when I'm down, providing the encouragement to keep going, and celebrating my successes. I could not have done this without you. I love you.

TABLE OF CONTENTS

Page

LIST OF TABLES

Table Page

LIST OF FIGURES

Figure Page

LIST OF ABBREVIATIONS

Antigen presenting cells (APCs)
Adenosine triphosphate (ATP)
B lymphocyte-induced maturation protein-1 (BLIMP-1)
Bone formation rate (BFR)
Bone marrow macrophages (BMMs)
Bone surface (BS)
Bone volume (BV)
Bone multicellular unit (BMU)
Bovine serum albumin (BSA
Bruton's tyrosine kinase (BTK)
Clustered regularly interspaced short palindromic repeats (CRISPR)
Colony stimulating factor 1 receptor (CSF1R)
C-terminal telopeptide (CTX)
C-type lectin domain family 5, member A (CLEC5A)
Dextran sulfate sodium (DSS)
DNA methyltransferase 3 alpha (DNMT3A)
DNAX activating protein of 12 kDa (DAP12)
Dimethylsulfoxide (DMSO)
Enhancer of Zeste Homolog 2 (EZH2)
Eroded surface (ES)
Extracellular acidification rate (ECAR)
FcεR1 gamma chain (FcRγ)
Follicle associated epithelia (FAE)
Germ-free (GF)
Granulocyte monocyte progenitors (GMPs)
Granulocyte colony stimulating factor (G-CSF)
Gut associated lymphoid tissue (GALT)
Hematopoietic stem cell (HSC)
Human immunodeficiency virus (HIV)
Inflammatory bowel disease (IBD)
Interferon gamma (IFNγ)
Interferon regulatory factor 8 (IRF8)
Interleukin-23 receptor (IL-23R)
Immunoreceptor tyrosine-based activation motif (ITAM)
Immunoreceptor tyrosine-based inhibition motif (ITIM)
Δ*invA::tetRA* Δ*spiB::KSAC invA spiB* (Δ*invAspiB*)
Lethal factor (LF)
Lethal Factor N-terminal domain (LFn)
Lineage negative (Lin^-)
$Lineage^-sca\text{-}1^+c\text{-}kit^+$ (LSK)
Lipopolysaccharide (LPS)
Macrophage colony stimulating factor (M-CSF)
Matrix metallopeptidase 9 (MMP9)

Mesenteric lymph nodes (MLNs
Microfold cell (M cell)
Mineral apposition rate (MAR)
Monocyte-dendritic cell progenitors (MDPs)
Myeloid derived suppressor cells (MDSCs)
Myeloid DNAX activation protein 12-associating lectin-1 (MDL-1)
Myeloid differentiation primary response 88 (MyD88)
Natural resistance-associated macrophage protein 1 (NRAMP1)
NLR family apoptosis inhibitory proteins (NAIPs)
NLR family CARD domain containing 4 (NLRC4)
NOD-, LRR-, and pyrin domain-containing protein 3 (NLRP3)
Non-typhoidal *Salmonella* (NTS)
Nuclear factor kappa B (NF-kB)
Nuclear factor of activated T cells 1 (NFATC1)
Nucleotide-binding oligomerization domain 1 (NOD1)
Osteoblast (OB)
Osteoclast (OC)
Osteoclast activating factor (OAF)
Osteoclast associated Ig-like receptor (OSCAR)
Osteoclast precursors (OCPs)
Osteoprotegerin (OPG)
Oxygen consumption rate (OCR)
Paired immunoglobulin receptor A (PIR-A)
Pattern recognition receptors (PRRs)
Protective antigen (PA)
Peripheral blood mononuclear cells (PBMCs)
Quantitative real-time polymerase chain reaction (qRT-PCR)
Quiescent osteoclast precursors (QOPs)
Receptor activator of nuclear factor kappa-B (RANK)
Receptor activator of nuclear factor kappa-B ligand (RANKL)
Recombination activating gene 1 (Rag)
Red blood cells (RBCs)
Region of interest (ROI)
Salmonella-containing vacuole (SCV)
Salmonella enterica subspecies *enterica* serovar Typhimurium (STm)
Salmonella pathogenicity islands 1 (SPI-1)
Salmonella pathogenicity islands 1 (SPI-2)
Severe combined immunodeficiency (scid)
Specific pathogen free (SPF)
Tartrate-resistant acid phosphatase (TRAP)
Total volume (TV)
T helper 1 (Th1)
T helper 1 (Th17)
T helper 2 (Th2)
T cell immunoglobulin and mucin domain-containing protein 3 (TIM-3)
T-regulatory cells (T-regs)

2,4,6-trinitrobenzene sulphonic acid (TNBS)
Tumor necrosis factor (TNF)
Tumor necrosis factor-receptor associated factor 6 (TRAF6)
Tumor necrosis alpha (TNF-α)
TNF-α converting enzyme (TACE)
Triggering receptor expressed on myeloid cells 2 (TREM2)
Type 3 secretion system 1 (T3SS1)
Type 3 secretion systems (T3SS2)
Tyrosine-protein kinase (TEC)
Ulcerative colitis (UC)

CHAPTER I:
INTRODUCTION

Although the gastrointestinal and skeletal systems are spatially distinct, these organ systems share overlapping physiologic and molecular mechanisms to maintain homeostasis. Pathologic conditions that impact one of these organ systems may consequently disrupt homeostasis at distal sites. At the molecular level, signaling through the tumor necrosis factor (TNF) superfamily receptor-ligand pair, receptor activator of nuclear factor kappa-B (RANK) and receptor activator of nuclear factor kappa-B ligand (RANKL) controls intestinal cell development, immune cell-cell interactions, lymphoid organogenesis, and skeletal cell differentiation. However, additional mechanisms that link these interconnected organ systems remain poorly described.

Inflammatory bowel disease (IBD) is a collection of gastrointestinal disorders hallmarked by severe, relapsing-remitting intestinal inflammation. The etiology of IBD is complex and represents a constellation of genetic and environmental factors that aberrantly impact innate and adaptive immune signaling pathways. Remarkably, the inflammatory consequences of intestinal inflammation during IBD are not limited to the gastrointestinal tract. Extra-intestinal disease manifestations impact up to 40% of patients with IBD. Among the various tissue types that IBD impacts, musculoskeletal pathology is the most common and bone loss during IBD ultimately confers a 40% increased fracture risk compared to the general population. Fundamentally, bone loss occurs through dysregulated interactions between bone resorbing osteoclasts (OCs) and bone forming osteoblast (OB) lineage cells.

To better understand the mechanisms of bone loss during IBD, we employed multiple mouse models of intestinal inflammation. These models were driven by either innate, adaptive,

or infectious triggers of intestinal inflammation. Data from these murine models of IBD implicated the expansion and alteration of OC precursors as potential drivers of bone loss during intestinal inflammation. Chapter II will provide background on what is currently understood about bone loss during IBD, introduce OC differentiation and function, and highlight the crosstalk between intestinal inflammation, immunology, and osteoclastogenesis. While studies in Chapter III address how gastrointestinal inflammation impacts skeletal homeostasis, Chapter IV conversely investigates how bone signaling impacts gastrointestinal disease. With an interest in further examining how a specific enteric pathogen impacts skeletal biology, I investigated how *Salmonella enterica* subspecies *enterica* serovar Typhimurium (STm) impacts skeletal cell biology. STm is a Gram-negative pathogen capable of causing a broad spectrum of diseases across an impressive range of host species. In humans, Nontyphoidal *Salmonella* (NTS) infection leads to significant morbidity and mortality worldwide. While NTS infection typically occurs in the gastrointestinal tract, it can lead to systemic infection and is one of a few pathogens that can successfully persist in the bone microenvironment. We utilized *Salmonella enterica* subspecies *enterica* serovar Typhimurium (STm) as a model of NTS infection. At the cellular and molecular levels, one route of STm infection is through infection of microfold (M) cells. The development of M cells is crucially dependent upon RANK/RANKL signaling. Therefore, I investigated the role of RANK/RANKL signaling on STm infection as well as direct interactions between STm and RANKL-treated monocytes. Chapter II will further introduce *Salmonella* as a pathogen and the host response to STm infection, with an emphasis on overlapping features with skeletal biology.

The goal of Chapter II is to provide sufficient information for the rationale for studies in Chapters III and IV, which are based on original research. Chapter III focuses on the innate and

adaptive immune contributions to bone loss during intestinal inflammation. The central hypothesis tested in Chapter III is that *alterations to osteoclast precursors contribute to bone loss during intestinal inflammation*. To test this hypothesis, I used chemical, T cell driven, and infectious models of intestinal inflammation and evaluated changes in the osteoclast progenitors during the course of colitis. I directly tested the impact of cytokines associated with intestinal inflammation on OC progenitor populations, evaluated the osteoclastogenic potential of these cells from mice with and without colitis, and measured the expression of several key surface receptors involved in osteoclast differentiation and function. Data from these studies revealed increased surface expression of an important co-receptor involved in osteoclast formation, myeloid DNAX activation protein 12-associating lectin-1 (MDL-1) on a specific subset of OC progenitors during chemically induced colitis. I found that anti-MDL-1 treatment ameliorates colitis-associated bone loss during a chemical injury model of colitis.

Chapter IV focuses on direct interactions between STm and OCs and the impact of RANK/RANKL signaling on STm infection. The central hypothesis tested in Chapter IV is that *RANK/RANKL signaling enhances STm survival within monocytes and that STm promotes osteoclastogenesis*. This hypothesis was tested *in vitro* using osteoclast formation culture systems, *in vitro* infections, and cells derived from mice lacking genes important for host defense. Data that I generated from these studies indicate that STm enhances OC formation, and that RANKL promotes STm survival while dampening anti-bacterial responses.

As stated above, Chapters III and IV are based upon original research. Chapter V summarizes these findings and proposes future directions for this work. Finally, a two-part appendix describing additional studies related to this work is provided following Chapter V.

CHAPTER II:
BACKGROUND

Inflammatory bowel disease associated bone loss

IBD, which impacts upwards of 3 million Americans, is characterized by chronic, relapsing-remitting, intestinal inflammation (1, 2). There are several subtypes of IBD, including Crohn's disease and ulcerative colitis (UC) (2). Although important differences exist between Crohn's disease and UC that influence treatment decisions, there are several unifying features among IBD subtypes. These shared features include alterations to innate and adaptive signaling pathways, impaired mucosal barrier function, and alterations to the microbiota. Importantly, the inflammation that patients with both Crohn's disease and UC experience is not restricted to the gut. Up to 40% of patients with IBD experience an extra-intestinal disease (3). Extra-intestinal disease manifestations can impact distal sites such as the skin, eyes, oral mucosa, and, most commonly, the skeleton (3–6). Musculoskeletal pathologies that occur with IBD include osteopenia/osteoporosis, inflammatory arthritis, and ankylosing spondylitis (5). Intriguingly, bone loss during IBD can present prior to, concurrent with, or after evidence of intestinal inflammation (7, 8). Evidence of osteopenia or osteoporosis has been documented in a broad range of patients with IBD across different ages (pediatric and adult populations), IBD subtypes (Crohn's disease and UC), in multiple skeletal locations (*e.g.*, femoral neck and spine), as well as concurrent with and after diagnosis (7–13). Bernstein, *et al*., determined that bone loss associated with IBD ultimately confers a 40% increased risk of fracture compared to the general population and contributes to the morbidity that patients with IBD experience (14).

Bone loss during IBD is a complex and multifactorial process. Sex and IBD subtype do not appear to impact bone loss or fracture risk, as males, females, and patients with either Crohn's disease or UC are at similar risk for these outcomes (15). Serum and tissue markers of

increased bone turnover are elevated in patients with IBD, reflecting both increased osteoclast activity and impaired osteoblast function have been reported in patients with IBD-associated bone loss (9, 11, 12, 16, 17). Corticosteroids, which are frequently used to manage acute IBD flares, are strongly associated with bone loss during IBD (15, 18). However, steroid-naïve patients are still susceptible to IBD-associated bone loss (7–9, 12). Frequent corticosteroid usage may also reflect a higher disease severity, thus making it difficult to disentangle the independent contributions of disease severity and medication use on driving bone loss during IBD. In addition to medication use, altered nutritional status during IBD undoubtedly contributes the bone loss during IBD. Absorption of vitamin D and calcium, two important mineral determinants of bone health, is often dysregulated in patients with IBD due to malabsorptive malnutrition (19). However, repleting vitamin D and calcium did not protect against osteopenia in IBD patients (20, 21). Additionally, previous reports have observed osteopenia in IBD patients demonstrating normal vitamin D and calcium levels (9, 10). These observations point towards alternative drivers of bone loss during IBD in addition to medication use and nutritional status.

Emerging evidence in both clinical and pre-clinical studies has highlighted a prominent role of systemic inflammatory responses as key mediators of IBD-associated bone loss. In patients with IBD, anti-TNF-α therapy led to a partial protection of bone loss during IBD and improved serum markers of bone formation (16, 17, 22). Animal models of IBD are required to better understand the mechanisms of bone loss during IBD. There are over 60 animal models of IBD, each with a unique set of advantages and limitations (reviewed by Mizoguchi (23)). Generally, these models induce intestinal inflammation through either chemical, genetic (including genetic knockout or genetic knock-in), cellular transfer, or infectious modalities.

Chemical irritants, such as dextran sulfate sodium (DSS) and 2,4,6-trinitrobenzene sulphonic acid (TNBS) are frequently used to induce colitis given their cost effectiveness, consistency, and ability to synchronize inflammation (24, 25). While these models have the advantage of studying colitis in the context of a wildtype immune system, they are largely skewed towards inducing inflammation through innate-driven pathways and therefore may underestimate contributions of the adaptive immune system during intestinal inflammation. Several murine models of IBD were developed to better study contributions of the adaptive immune system, and more specifically, T cells. Knockout of *IL-10* removes the important effector cytokine of T-regulatory cells (T-regs) that restrains T cell activation. *IL-10*$^{-/-}$ mice subsequently spontaneously develop a wasting disease characterized by colitis (26). Similarly, adoptive transfer of naïve T cells into immunodeficient mice (*e.g.*, C.B.17 *scid/scid* [severe combined immunodeficiency] or *Rag1*$^{-/-}$ [recombination activating gene 1]), without co-transfer of T-regs, leads to T cell activation and a spontaneous wasting disease associated with intestinal inflammation (27–30). Both models are microbiota dependent, as germ-free *IL-10*$^{-/-}$ mice or recipient germ-free *Rag1*$^{-/-}$ mice do not develop disease (26, 31). These genetic and cellular models have the advantage of manipulating T cell intrinsic factors, altering host genetic factors, and modeling the heterogeneity in timing and severity of colitis that patients with IBD experience. However, one drawback of these genetic or adoptive transfer models of IBD is the baseline systemic alterations to the immune system.

Enteric infections are often associated with IBD flares and contribute to perturbations of the microbiome, reduce epithelial barrier function, and require the coordinated signaling of innate and adaptive immune response to successfully clear the infection. In a genetically susceptible host, enteric infections may be sufficient to alter the host microbiota and trigger

chronic maladaptive immune responses leading to IBD (32, 33). In animal models, several enteric pathogens (*e.g.*, *Citrobacter rodentium*, *Helicobacter hepaticus*, and STm) lead to inflammatory responses and pathological changes in the inflamed intestine that resemble those observed in patients with IBD (31, 34–37). Infectious models of colitis have the advantage of manipulating host genetic background, altering pathogen-associated virulence factors, reducing cost, and inducing consistent, synchronized colitis. However, infectious models of colitis may overestimate the role of pathogen-associated factors in promoting intestinal inflammation, as patient with IBD may not experience enteric infection.

While the mechanisms of intestinal inflammation in these animal models of IBD have been studied for many years, examining skeletal pathology in these experimental systems has only occurred in the past three decades (**Table 1**). In total, these studies highlight contributions from altered OB function, OC formation, nutritional status, TNF-α, and OC interactions with inflammatory T cells as important contributors to bone loss during intestinal inflammation (**Table 1**). Discrepancies in murine models of intestinal inflammation as well as host factors such as age, sex, and gender, make it difficult to compare findings across studies. Despite these differences, several themes emerge. First, several studies have highlighted that bone loss during colitis can occur in the absence of weight loss and without changes to indicators of nutritional status such as vitamin D, parathyroid hormone, and urinary calcium (38–40). Second, these works also highlight the central role of TNF-α as an important contributor to bone loss (41–44). However, most studies to date have focused on cytokines produced within the inflamed intestine or in co-culture models of intestinal explants with skeletal cells. Because bone loss occurs within the skeleton and not the gastrointestinal tract, defining the skeletal cellular composition and cytokine milieu in this tissue compartment remains an outstanding area of investigation to further

delineate the mechanisms of bone loss during IBD. Third, it appears that reduced OB function occurs later in colitis, while changes in OCs or their precursors occur more acutely. Differences in both the kinetics and severity of colitis likely contribute to discrepancies in reported changes to OB or OC differentiation or function. There remains a gap in knowledge of the acute changes that trigger pathologic bone remodeling during intestinal inflammation. Because of the inherent differences in murine models of colitis that appropriately recapitulate some aspects of human IBD but inappropriately model other features, studies employing multiple disease models to confirm mechanisms of bone loss during colitis are greatly needed. To gain a better appreciation of how bone loss occurs during intestinal inflammation, the next section will detail the cellular and molecular mechanisms of physiologic bone turnover.

Table 1 Summary of findings from rodent models investigating bone loss during intestinal inflammation.

Studies examining skeletal phenotypes during rodent experimental colitis are summarized and listed chronologically.

Model	Rodent strain, age, sex	OC findings	OB findings	Comments	Reference
TNBS (3 weeks)	Sprague-Dawley rats Age not specified ♂	None reported	None reported	↓ Bone ash weight, specific density, and calcium content ↑ Urinary calcium excretion	(45)
TNBS (1, 2, 3, 6, and 12 weeks)	Wistar rats 13 weeks ♂ ♀	Increase in eroded surface (ES) / bone surface (BS) at 3 weeks following TNBS treatment	↓ Bone formation rate (BFR) (6 weeks) followed by ↑ BFR (12 weeks)	↓ Trabecular bone volume (BV) per total volume (TV) (6 weeks)	(46)
***IL-2*$^{-/-}$ mice** **Adoptive transfer of *IL-2*$^{-/-}$ T cells into *Rag1*$^{-/-}$ mice**	C57BL/6 4, 7, 9 weeks ♂ ♀	↑ OC number 7 weeks (*IL-2*$^{-/-}$ colitis) and 6-8 weeks (adoptive T cell transfer) following colitis	↓ Calcein double labelling (7 weeks) in *IL-2*$^{-/-}$ mice	↑ RANKL expressing $CD4^+$ T cells Fc-Osteoprotegerin (OPG) treatment ameliorated osteopenia in both colitis models	(47)
***IL-10*$^{-/-}$**	129 Sv/Ev *IL-10*$^{-/-}$ 13 weeks ♂ ♀	None reported	None reported	↓ Bone mineral density (BMD) and indices of bone quality	(48)
***IL-10*$^{-/-}$**	C57BL/J 8 and 12 weeks ♂	No difference in OC number or serum markers of bone resorption	↓ OB differentiation *ex vivo* in primary cultures from *IL-10*$^{-/-}$ mice	↓ Bone ash weight and indices of bone quality No change in indicators of nutritional status (serum 25-OH vitamin D_3 and parathyroid hormone levels)	(38)
Adoptive transfer of $CD4^+CD45RB^{hi}$ T cells into C.B.17 *scid/scid* mice	C.B.17 *scid/scid* 14-16 weeks ♀	↑ OC number serum TRAP 5 weeks post-transfer	↓ OB number and alkaline phosphatase levels (serum)	Fc-OPG treatment prevented bone loss during colitis without impacting severity of colitis No change in serum calcium or phosphorus	(39)
TNBS	Balb/c 4-5 weeks ♂	None reported	↓ OB expression of *Phex* during colitis that was phenocopied with TNF-α injection and abrogated with	Establishes a link between TNF-α during colitis and maintaining nutritional homeostasis	(41)

			anti-TNF-α treatment ↓OB *Phex* expression corresponded with reduced OB mineralization		
Acute: 3% DSS 7d **Chronic: 3% DSS 5d → 3 weeks H_20**	C57BL/6 9 weeks ♀	None reported	Reduced osteocalcin levels in chronic colitis	No difference in BMD between controls and acute colitis model	(49)
5% DSS (7d) → 2.5% DSS (7d)	Balb/c 9 weeks ♂	↑ OC number	↓ Calcein double labelling, mineral apposition rate (MAR), and BFR	32% ↓ BV/TV No change in cortical bone	(50)
5% DSS (5d) → H_20	C57BL/6 4 weeks ♂	↓ OC gene expression, OC surface, and serum markers of bone resorption 1- and 2-weeks following colitis	↓ Expression OB differentiation markers at 1 and 2 weeks following DSS treatment	Recovery of BV/TV by 7 weeks after colitis Cortical differences noted 2 and 4 weeks after colitis ↓ Growth plate thickness and expression of chondrocyte markers	(51)
TNBS ***IL-10*$^{-/-}$** **Adoptive T cell transfer of CD4^{+}CD45RB^{hi} T cells into *Rag2*$^{-/-}$ mice**	TNBS: Balb/c *IL-10*$^{-/-}$: 129Sv/EV Adoptive transfer: C57BL/6 *Rag2*$^{-/-}$ Sex of mice not indicated	None reported	None reported	Three models of colitis ↓ *Klotho* expression in the distal convoluted tubules of kidneys. Klotho plays a critical role in calcium homeostasis, reduction of oxidative stress, and inhibition of TNF-α induced inflammation	(42)
1% DSS (15d)	C57BL/6 6 weeks ♂	None reported	None reported	Altered hematopoiesis and cellular composition of the bone marrow as evidenced by ↑ granulocytic and monocytic cells and ↓ lymphocytes and erythrocytes	(52)
***H. hepaticus* infected *IL-10*$^{-/-}$ mice**	C57BL/6 14 weeks ♂♀	↓ OPG in male mice, no difference in OC number or surface	No difference in OB surface area or MAR	Trabecular bone loss only observed in male mice, which also demonstrated increased colitis severity	(53)
1% DSS (15d) → H_20	C57BL/6 5-6 weeks	No difference on OC number	↓ BFR and MAR	Trabecular bone loss occurred in the absence	(40)

	♂	or gene expression (d15)		of detectable changes in baseline weight	
Adoptive T cell transfer of $CD4^+CD45RB^{hi}$ T cells into *Rag1*$^{-/-}$ mice	C57BL/6 *Rag1*$^{-/-}$ Age and sex of mice not stated	Co-culture of *ex vivo* generated OCs from mice with colitis and $CD4^+$ T cells ↑ TNF-α and IL-17 production and ↓ FoxP3 expression	None reported	Observed increase in CX_3CR1 OCs during colitis linked with dendritic cell origin	(43)
***IL-10*$^{-/-}$** **Adoptive T cell transfer of $CD4^+CD45RB^{hi}$ T cells into *Rag1*$^{-/-}$ mice**	C57BL/6, Balb/c *IL-10*$^{-/-}$, 4months ♂ ♀ C57BL/6 *Rag1*$^{-/-}$ Age and sex of *Rag1*$^{-/-}$ not stated	↑ *Ex vivo* OC formation in co-culture with colitis-derived T cells ↑ $Cd11b^{-/lo}Ly6C^{hi}$ and $CD11b^{hi}Ly6C^{hi}$ cells in bone marrow of mice with colitis	None reported	Report murine and human patient colitis-associated TNF-α IL-17 producing $CD4^+$ T cells linked with enhanced OC formation	(44)
3% DSS (3d) → 1d H_20 → 3% DSS (3d) → 2d H_20	C57BL/6 8 weeks Sex of mice not indicated	↑ *Ex vivo* OC formation in whole bone marrow culture ↑ Lineage negative $sca\text{-}1^+$ $c\text{-}kit^+$ (LSK) cells during DSS colitis	↓ BFR and MAR	Link bone loss to intra-epithelial cell NF-kB activation	(54)

Physiologic bone turnover

Bone is a dynamic tissue that requires coordinated actions between bone building OB-lineage cells and bone resorbing OCs to maintain homeostasis. Mesenchymal stems cells (MSCs) give rise to osteoblast-lineage cells. OBs produce and mineralize the inorganic components of the skeleton, and, upon maturation, are embedded within the skeleton as mature osteocytes. On the other hand, OCs are derived from hematopoietic stem cells (HSCs) and are the only cells capable of resorbing bone. Macrophage colony stimulating factor (M-CSF) and RANKL are necessary for OC differentiation and survival (55–57). Genetic inactivation of M-CSF or RANKL leas to severe osteopetrosis that is rescued by administration of soluble cytokine (58–62). Genetic knockout of the receptors that recognize M-CSF or RANKL, CSF1R or RANK, also results in severe osteopetrosis in mice (58–62). Under physiologic conditions, OB-lineage cells are the primary regulators of OC differentiation, primarily through the production of RANKL and the RANKL soluble decoy receptor, OPG (56, 57, 63, 64). Elegant conditional knockout studies have demonstrated specifically that osteocyte membrane-bound RANKL is the primary contributor to physiologic OC differentiation and function in adult mice (65).

The actions of OCs and OB-lineage cells do not occur agnostically from one another. Rather, OB-lineage cells and OCs are closely tied together through secreted and membrane-bound coupling factors that allow for the staggered processes of bone resorption followed by bone formation (66–73). The coupling of OCs and OBs has led to the conceptual framework of bone remodeling as driven by the concerted effort of the "bone multicellular unit" (BMU) comprising of the coordinated actions of OCs and OBs. Intriguingly, recent work suggests that RANK/RANKL signaling may function as a bidirectional positive coupling factor (74). In this

study, mature OCs were shown to secrete vesicular RANK, which activated OB differentiation cells through OB-membrane-bound RANKL and led to subsequent bone formation (74).

Fundamentally, bone homeostasis is maintained by balancing dynamic bone formation with bone resorption. Defects in either of these processes will result in osteoporosis (bone resorption > bone formation) or osteopetrosis (bone formation > bone resorption). Consequently, the differentiation of bone forming OB-lineage cells and bone resorbing OCs represents an important regulatory step to maintain skeletal homeostasis. The current understanding of both OB and OC differentiation is evolving and complex. The next section will provide additional information centered on OC differentiation and function that is necessary for a complete understanding of the experiments described in this thesis.

Osteoclast ontogeny, trafficking, signaling, and function

Ontogeny

OCs are highly specialized, multinucleated cells capable of resorbing bone. Parabiosis and transplant experiments unequivocally demonstrated OCs are haematopoietically derived (75–79). This discovery led to intense research into delineating the precise cellular origin of OCs. Cells within the lineage negative sca-1^+ c-kit^+ (LSK) compartment contain HSCs capable of reconstituting hematopoiesis in lethally irradiated mice (80). Many cell types have been demonstrated as capable of OC formation downstream of LSK HSCs. These cell types include common myeloid progenitors (CMPs), monocyte-dendritic cell progenitors (MDPs), monocytes, macrophages, myeloid derived suppressor cells (MDSCs), dendritic cells, $Cd11b^{-/lo}Ly6C^{hi}$ osteoclast precursors (OCPs), and quiescent osteoclast precursors (QOPs) (**Figure 1**) (81–86). In addition to the array of cell subtypes capable of forming OCs, myeloid cells derived from

heterogenous tissues can also form OCs when cultured *ex vivo* in the presence of M-CSF and RANKL including blood, bone marrow, and spleen (56, 57, 87–90). Recent work has demonstrated the kinetics of circulating pre-OC populations fusing with existing OCs, demonstrating that pre-OC populations exit the bone marrow space prior to trafficking back to the bone to mature into OCs, or fuse into an existing OC syncytium (90, 91). Until recently, the origin of the initial seeding OC populations was unclear. Recent findings utilizing cutting-edge reporter mice have shown that that yolk-sac derived erythromyeloid precursors form the first OCs during development and are gradually replaced as haematopoietically derived precursors fuse into existing OCs (90, 91). Pathologic conditions, such as bone fractures, can induce OC formation from these erythromyeloid OC precursors from distal reservoirs such as the spleen (90). To add more complexity to the fate mapping of OCs, exciting new studies have shown that OCs *in vitro* and *in vivo* can undergo fission to yield cells called osteomorphs, which are capable of recycling back into mature OCs (92). As much is being uncovered about the OC ontogeny at baseline, there remains a gap in knowledge in how pathologic conditions alter pre-osteoclast populations.

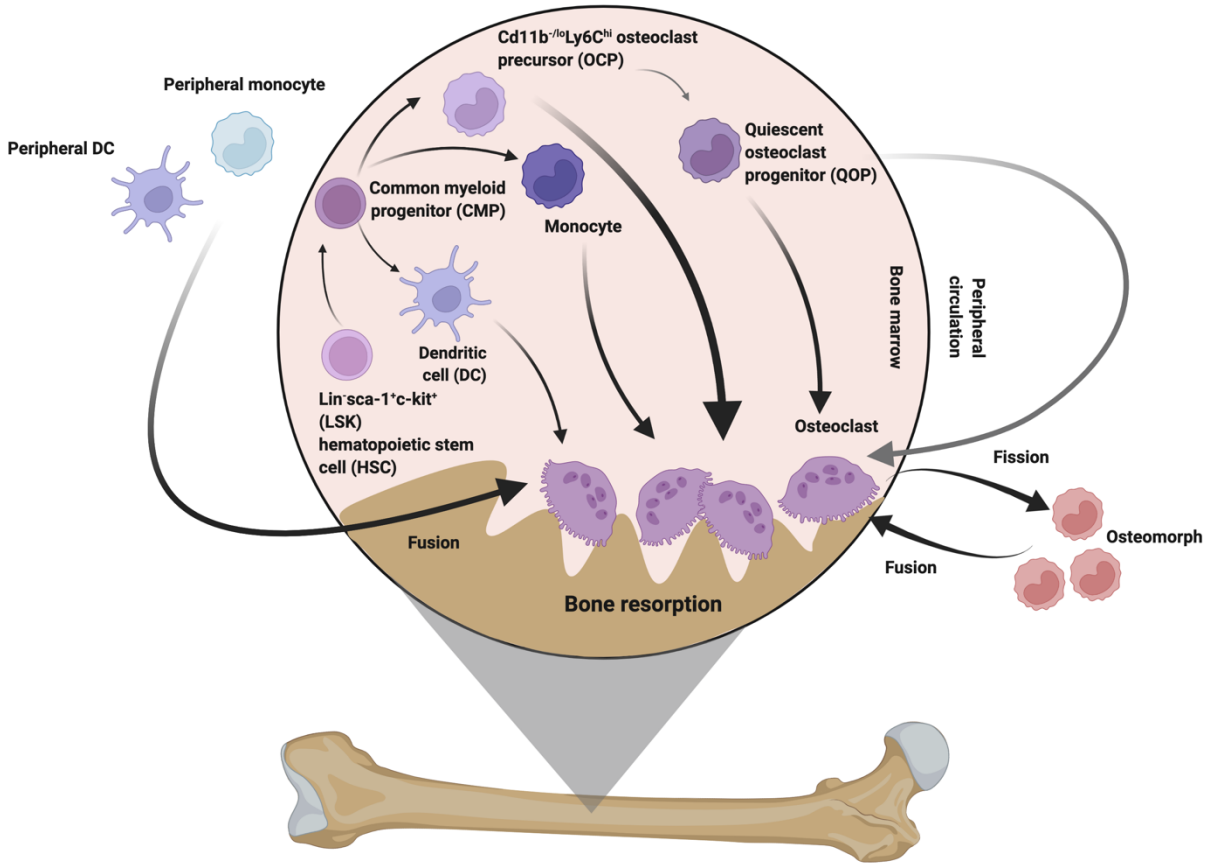

Figure 1 Ontogeny of an osteoclast.

Osteoclasts (OCs) are haematopoietically derived cells. Lineage negative sca-1^{+} c-kit^{+} (LSK) hematopoietic stem cells (HSCs) give rise to multipotent common myeloid progenitors (CMPs), which, in turn, differentiate into several populations capable of undergoing osteoclastogenesis. These populations include monocytes, dendritic cells (DCs), and Cd11b$^{-/lo}$Ly6C^{hi} osteoclast precursors (OCPs), all of which can directly differentiate into mature OCs. OCPs are proposed to differentiate into quiescent osteoclast precursors (QOPs). Some cells, including monocytes and QOPs, may exit the bone marrow into the peripheral circulation before trafficking back to the bone marrow space to differentiate into mature OCs or fuse into existing OCs. Mature OCs have been demonstrated to undergo fission into osteomorphs, exit the bone marrow, and subsequently re-enter the bone marrow and form OCs. Black arrows represent differentiation steps that have

been previously demonstrated, while grey arrows represent hypothesized routes of differentiation or trafficking. Created with Biorender.com.

Trafficking

OCs, by definition, are closely associated to bone. However, the molecular mechanisms controlling the trafficking of OCs and their precursors to the bone are poorly understood. Supernatants from rodent bone cultures serve as chemoattractants to human monocytes but not neutrophils or lymphocytes, suggesting that active bone resorption generates soluble factors that recruit monocytes (93). Recent work utilizing *in vivo* two-photon microscopy and parabiosis experiments with fluorescent reporter mice have begun to illuminate this process. From these studies, it is apparent that several signaling molecules, including CX_3CL1 and S1P regulate the movement of OCs and their precursors to and from the bone *in vivo* (94–96). Additional *in vitro* work has implicated the involvement of additional chemokines including CCL2/CCR2 signaling in promoting osteoclast precursor chemotaxis to the bone (97–101). While these studies have delineated several important chemotactic molecules that drive OC precursor trafficking during homeostasis, additional studies are needed to investigate how chemoattract signaling changes during disease statues such as gastrointestinal inflammation.

Signaling

The signaling events that result in OC formation are complex (**Figure 2**). RANKL and M-CSF are required for osteoclastogenesis (55–57). RANKL, a TNF super family member cytokine, binds its cognate receptor, RANK (60–62). Both membrane-bound and soluble forms of RANKL are capable of initiating signaling through the RANK receptor (102, 103). RANKL signaling through RANK initiates a cascade of signaling events that reorganizes the metabolic, epigenetic, and cytoskeletal landscape. RANK recruits tumor necrosis factor-receptor associated factor 6 (TRAF6), which, in turn, leads to nuclear factor kappa B (NF-kB) nuclear translocation and transcription of downstream targets (104). The master transcriptional regulator of

osteoclastogenesis, nuclear factor of activated T cells 1 (NFATC1) is among these downstream NF-kB targets (105). Concurrently, RANK signaling promotes spleen tyrosine kinase (Syk)-dependent calcium mobilization (104). Calcium flux in the cell results in nuclear translocation of NFATC1 (104, 105). Activation of NFATC1 results in the transcription of OC identity genes and repression of anti-osteoclastogenic factors (104, 105). Additionally, RANKL leads to pro-survival signaling by activating Src and mitogen-activated protein kinases (MAPKs), inducing anti-apoptotic factors, and downregulating apoptosis machinery (106). M-CSF binds to its cognate receptor, colony stimulating factor 1 receptor (CSF1R), and further reinforces pro-survival signaling through Src (107).

While both RANKL and M-CSF are essential for proper OC survival and function, signaling through these cytokines alone without co-stimulatory factors is not sufficient to promote *in vivo* or *in vitro* OC formation (108, 109). Both positive and negative co-stimulatory receptors are expressed on pre-OC populations that contribute to the intricate regulation of osteoclastogenesis (110). These receptors are conserved amongst many innate immune cells, such as natural killer cells, macrophages, and neutrophils (110). Pro-osteoclastogenic co-receptors promote Syk signaling and calcium flux by associating with intracellular receptors with immunoreceptor tyrosine-based activation motifs (ITAMs). Conversely, anti-osteoclastogenic co-receptors inhibit calcium mobilization and subsequent OC formation through associating with intracellular receptors harboring immunoreceptor tyrosine-based inhibition motif (ITIM) domains (110).

Pro-osteoclastogenic receptors associate with either DNAX activating protein of 12 kDa (DAP12) or FcεR1 gamma chain (FcRγ). Examples of DAP-12 associating activating receptors include myeloid DNAX activation protein 12-associating lectin-1 (MDL-1) and triggering

receptor expressed on myeloid cells 2 (TREM2) (110). Examples of FcRγ associating receptors include osteoclast associated Ig-like receptor (OSCAR) and paired immunoglobulin receptor A (PIR-A) (110). *DAP-12$^{-/-}$FcRγ$^{-/-}$* demonstrate severe osteopetrosis *in vivo* with few osteoclasts despite maintaining intact RANKL and M-CSF signaling (108, 109). Co-culture of *DAP-12$^{-/-}$*, but not *FcRγ$^{-/}$* or *DAP-12$^{-/-}$FcRγ$^{-/-}$*, with OB-lineage cells rescues osteoclastogenesis (108, 109). These data suggest that OBs can ligate FcRγ associated co-receptors but not DAP-12 associated receptors. While some ligands for OC co-receptors have been described, many remain undiscovered. Signaling through pro-osteoclastogenic co-receptors amplifies calcium signaling through Syk dependent phosphorylation and further potentiates NFATC1 activation (110). NFATC1 activation ultimately leads to transcription of pro-osteoclastogenic genes associated with bone resorption while simultaneously downregulating genes known to inhibit OC formation (104, 105). As the precise molecular mechanisms of OC formation are still being uncovered, additional work is needed to understand how pathologic conditions may alter the specific mechanisms of OC formation.

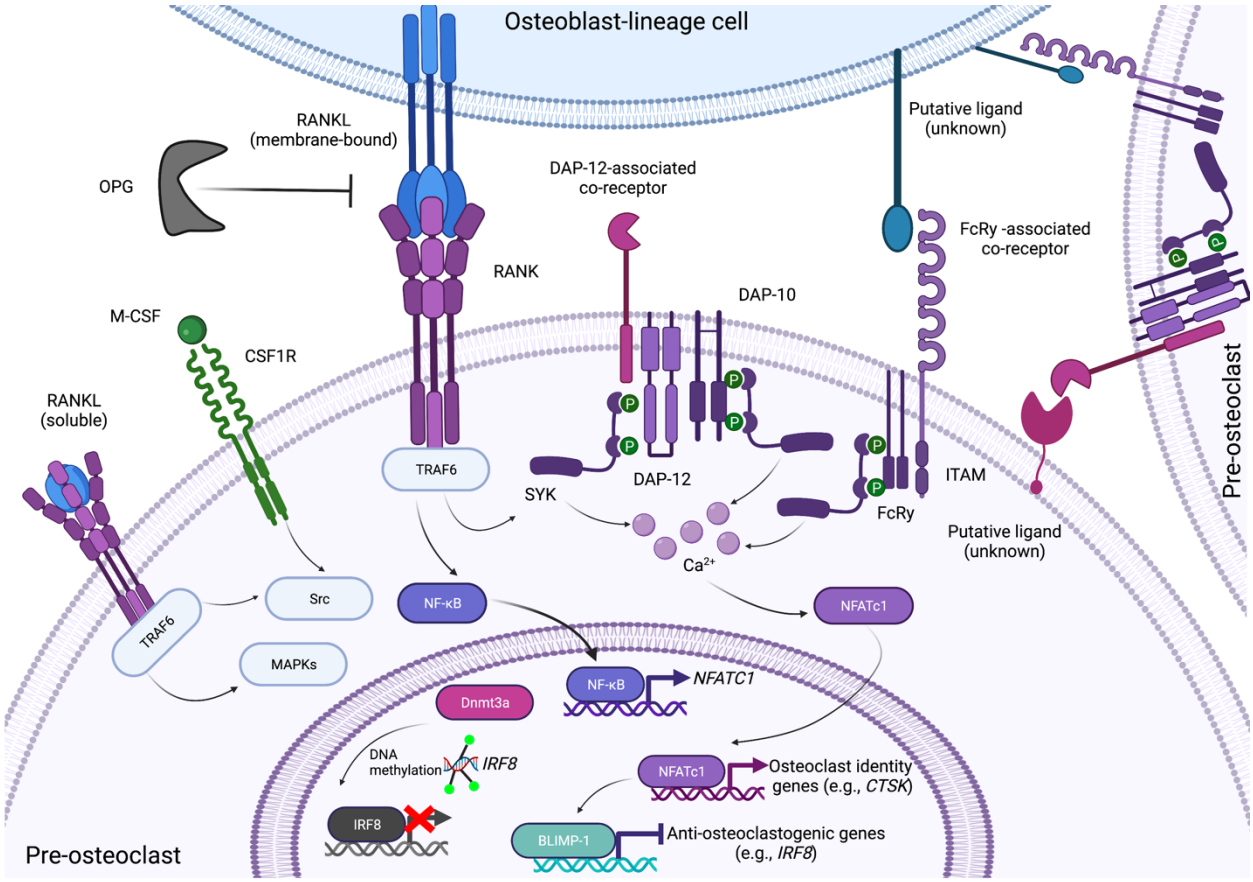

Figure 2. Osteoclastogenic signaling.

Simplified schematic of complex signaling events that promote osteoclast (OC) formation. Membrane-bound receptor activator of nuclear factor kappa-B (RANKL) expressed on osteoblast (OB)-lineage cells binds to receptor activator of nuclear factor kappa-B (RANK) on pre-osteoclasts. OB-lineage cells also produce soluble RANKL capable of binding RANK as well as the soluble RANKL decoy receptor, osteoprotegerin (OPG), which inhibits RANK/RANKL interactions. RANKL binding RANK leads to the recruitment of tumor necrosis factor-receptor associated factor 6 (TRAF6), which results in nuclear factor kappa-B (NF-kB) nuclear translocation, cell survival through mitogen-activated protein kinases (MAPKs) and Src, and calcium release through spleen tyrosine kinase (SYK). NF-kB activation results in *NFATC1* expression. Calcium release facilitates nuclear translocation of nuclear factor of activated T cells

1 (NFATC1) and downstream expression of OC identify gene. Downstream targets of NFATC1 also include transcription factors, such as B lymphocyte-induced maturation protein-1 (BLIMP-1), which is a transcriptional repressor that represses negative regulators of osteoclastogenesis (*e.g.*, interferon regulatory factor 8 [IRF8]). Signaling through RANK leads to additional cellular changes including cytoskeletal rearrangement, metabolic changes, and alterations to the epigenetic landscape (*e.g.*, methylation of IRF8 through DNA methyltransferase 3 alpha [DNMT3A]). Macrophage colony stimulating factor (M-CSF) binds its cognate receptor, colony stimulating factor 1 receptor (CSF1R) and promotes cell survival through Src. OC activating co-receptors pair with intracellular receptors (*e.g.*, DNAX activating protein of 12 kDa [DAP12] or FcεR1 gamma chain [FcRγ]) that possess immunoreceptor tyrosine-based activation motifs (ITAMs). FcRγ OC co-receptors are capable of binding ligands expressed on OB-lineage cells while DAP12 OC co-receptors bind ligands on pre-osteoclast cells. Signaling through activating OC co-receptors results in calcium release through SYK and amplifies NFATC1 translocation to the nucleus. NFATC1 activation ultimately drives the expression of OC-identity genes (*e.g.*, *CTSK*). Created with Biorender.com.

Function

The primary biological function of an OC is to resorb bone. Bone is a complex tissue with both organic and inorganic components. Accordingly, OCs must secrete proteases, hydrolases, and acids capable of degrading this substrate while simultaneously restricting the activity of these enzymes to the exact location of bone resorption. To accomplish this goal, OCs specifically secrete protons and chloride that form hydrochloric acid, cathepsin k, matrix metallopeptidase 9 (MMP9), and tartrate-resistant acid phosphatase (TRAP) that ultimately break down the hydroxyapatite and organic components of bone (103, 111). To prevent off-target cytotoxic effects of these enzymes, mature OCs form a tight sealing zone around the site of bone resorption, mediated in part, by a characteristic F-actin ring as part of an organelle structure known as the "sealing zone" (111). OCs are also capable of removing debris from resorption pits via transcytosis from the basolateral to apical side of the cell (111, 112).

Bone resorption is critical for many physiologic functions. First, removing damaged, structurally unstable bone to allow for new bone formation is a critical and necessary process for homeostatic bone turnover (113, 114). Second, bone resorption is critically linked to nutrient homeostasis, as degrading bone leads to the systemic and rapid release of calcium and phosphate (19). Third, during infectious or inflammatory conditions, the proteases secreted by OCs not only degrade bone, but also tethering factors that retain cells within the bone marrow (115). Cleavage of these tethering factors leads to stem cell mobilization and cell egress from the bone marrow. Finally, OC activity appears to be intimately linked with host immune function during local bone infections. Understanding the two-way interactions between the skeletal and immune systems has led to the burgeoning field of osteoimmunology. The next section will provide background

on the cross talk between the skeletal and immune systems, as well as how these organ systems interface with the gastrointestinal system.

Osteo-immunologic-intestinal cross talk

The skeletal, immune, and gastrointestinal systems are intricately connected organ systems. In addition to providing structural support to vertebrates, the skeletal system houses the developing immune system. The intestinal tract, in addition to absorbing vitamins and minerals key in maintaining bone structure, harbors the most immune cells in the body. Cellular and molecular mechanisms further tie these organ systems together. Genetically inactivating RANK or RANKL results in severe osteopetrosis due to a lack of OC development (58–62). In addition to this skeletal phenotype, RANKL deficient mice lack lymph nodes and have compromised secondary lymphoid structures (60, 62). The remainder of this section will summarize what is currently understood about how immune and intestinal biology influence osteoclastogenesis.

Innate immunity

OCs and their precursors are capable of directly responding to infection through the expression of cytokine pattern recognition receptors (PRRs) (116, 117). Importantly, the timing of exposure of pathogen associated molecular patterns (PAMPs) relative to the timing of RANKL exposure has profound effects on OC formation. RANKL naïve cells that encounter PAMPs prior to or concurrent with RANKL exposure commit to a macrophage fate in what is thought to be a relatively irreversible step (118–120). Conversely, myeloid lineage cells that ligate RANKL prior to sensing PAMPs demonstrate enhanced osteoclastogenesis compared to RANKL-experienced cells not exposed to PAMPs (117, 118). In addition to PRRs, ITAM OC co-receptors can further interact with PRR signaling (121, 122). While this cross-regulation of ITAM receptors and signaling through PRRs is complex, it appears that the strength of ITAM

signaling contributes towards OC differentiation and function (121, 122). Future work is needed to understand if leukocytes from the intestine are capable of trafficking back to the bone marrow to contribute to osteoclastogenesis.

Adaptive immunity

Accumulating evidence suggests that OCs interact with the lymphocytes in a bidirectional manner. Effector T cell subsets, such as T helper 1 (Th1) or T helper 17 (Th17) cells have been shown to express membrane-bound RANKL and cytokines that can directly promote OC formation (44, 123–129). However, the net impact of Th1 cells on OC differentiation and function is complex, as the canonical Th1 effector cytokine, interferon gamma (IFNγ), appears to inhibit osteoclastogenesis, thereby dampening the pro-osteoclastogenic effects of Th1 derived RANKL (124, 130, 131). Th17 cells have also been shown to enhance OC formation through contact dependent and independent mechanisms (44, 123, 125, 129, 132). New studies utilizing cutting edge photo-convertible reporter mice has demonstrated that T cells can migrate from the intestine to the bone to subsequently promote OC formation (125). T-regs have been shown to promote bone formation through interactions with OBs, a phenotype that has also been linked to alterations in the microbiome and intestinal permeability (133, 134). Both mature OCs and their precursors are induced during inflammatory conditions such as inflammatory arthritis (44, 82). Prior work has demonstrated the ability of these OC precursors to suppress the activity of inflammatory T cells in a manner reminiscent of myeloid derived suppressor cells (MDSCs) (82). Furthermore, inhibiting osteoclastogenesis by administering OPG, the soluble decoy receptor of RANKL, ameliorated bone loss in two T cell-dependent models of intestinal inflammation (39, 47). These findings demonstrate that osteoclasts and adaptive immune cells interact in a bidirectional manner.

Cytokines

OCs and their precursors are exquisitely responsive to the surrounding cytokine milieu. Cytokines associated with both innate and adaptive immune function can alter OC fate and function. There has been extensive research conducted to determine how cytokines impact osteoclastogenesis. Low concentrations of some cytokines, such as TNF-α and IL-1ß, can induce OC formation *in vitro* in RANKL-primed cells (135–138). In fact, IL-1ß was originally referred to as "osteoclast activating factor" (OAF) due to its potent osteoclastogenic effects, further highlighting the cross talk between the immune and skeletal systems (137). Many inflammatory cytokines have been shown to impact OC differentiation and function, either through direct interactions with receptors expressed on OCs, or alternatively, indirectly through the downstream effectors these cytokines elicit from OC-interacting cells. The cellular sources of these cytokines are varied, and include OC-intrinsically derived cytokines, as well cell extrinsically derived cytokines from OBs, T cells, B cells, neutrophils, macrophages/monocytes, stromal cells, and fibroblasts.

Moreover, cytokine signaling in OCs and their precursors can cross-regulate other facets that contribute to osteoclastogenesis. For example, the expression of several co-receptors, including MDL-1, PIR-A, and OSCAR, are induced by TNF-α, suggesting that the relative role of co-receptors in driving osteoclastogenesis may increase during inflammation (121, 122, 139, 140). Prior research has described positive feedback loops whereby cytokines, such as TNF-α, enhance RANK expression and subsequently feed-forward into OC formation (141). Although many studies have carefully defined the direct actions of single cytokines on OC differentiation and function, there remains a gap in understanding how more physiologically relevant, complex cytokine environments like those induced during pathologic conditions impact

osteoclastogenesis. Furthermore, much of the existing work has focused on systemically circulating cytokines, with few studies investigating how inflammatory conditions alter cytokine production at the site of bone loss.

Hematopoiesis

The bone marrow is a complex environment that not only contains trabecular bone integral to skeletal health, but also houses the precursors to all haematopoietically derived cells. Regulating the ontogeny of red blood cells and leukocytes during homeostasis and disease requires a delicate dance of regulatory steps. Hematopoiesis is thought to take place in specific locations, known as the hematopoietic niche. Within the skeleton, early fractionation studies discovered that areas near the endosteal bone marrow were enriched for HSCs (142). While bone marrow is the primary site of hematopoiesis, organs such as the spleen are capable of extramedullary hematopoiesis under certain conditions. The hematopoietic niche is defined as the intimate association of HSCs, endothelial cells, periarteriolar cells, and surrounding stromal and vascular components within the bone marrow or spleen (143). However, accumulating evidence indicates that OCs also participate in the regulation of hematopoiesis (115, 144–146). Previous work has shown that proteases secreted by mature OCs, specifically cathepsin K, can degrade the tethering factors and endosteal components (*e.g.*, osteopontin) that retain HSCs within the bone marrow (144, 146). Mice deficient in OCs have been demonstrated to have a dramatic reduction in bone marrow LSK HSCs (145). RANKL administration leads to LSK HSC mobilization while treatment with an anti-RANKL antibody inhibits this process, even in the presence of conditions that would otherwise lead to emergency hematopoiesis such as LPS administration or blood loss (144). Furthermore, the signaling factors that regulate hematopoiesis, such as granulocyte colony stimulating factor (G-CSF), have been shown to

enhance osteoclastogenesis (144, 146, 147). While the precise mechanisms of G-CSF enhanced osteoclastogenesis are unclear, G-CSF has been demonstrated to potently increase the expression of the pro-osteoclastogenic co-receptor, MDL-1, on immature myeloid cells (139, 148).

Recently, there has been an increased appreciation for how inflammatory conditions impact hematopoiesis (149). Several studies have highlighted how intestinal inflammation can skew the bone marrow environment towards increased production of monocytic and granulocytic precursors while decreasing the production of lymphocyte precursors (52, 150). Although it has long been appreciated that the microbiota contributes to regulating hematopoiesis, few studies have mechanistically evaluated how inflammatory conditions of the gastrointestinal tract alter the cytokine signals or surface receptors on pre-osteoclast populations (151–154). Such studies are important given how OCs themselves likely contribute to shaping the hematopoietic niche.

Intestinal microbiota

Recent work has highlighted how alterations to the microbiota impact skeletal biology. The impact of the microbiota on skeletal homeostasis is hypothesized to involve a combination of alterations to epithelial barrier function, changes to intestinal immune cells that subsequently traffic to the bone, induction of cytokines within the intestine that circulate to the skeleton, and detection of bacterial derived products (*e.g.*, metabolites or PAMPs). Administering low dose antibiotics has been shown to increase bone mass in mice (155). Germ-free (GF) mice demonstrate aberrantly enhanced trabecular bone compared to mice housed in specific pathogen free (SPF) conditions (156, 157). Importantly, the generalizability of these findings may be restricted to the specific microbial communities and host genetic backgrounds, as conflicting reports have reported limited impacts of GF microbial reconstitution on skeletal health (158). To address these conflicting findings, microbiota transfer studies elucidated the microbiota to be a

transmissible determinant of skeletal health (159). Taken together, it appears that some level of tonic signaling through the intestinal microbiota is necessary for the proper maintenance of skeletal homeostasis.

Several studies have highlighted that manipulating the microbiota through probiotics can impact the skeleton during pathologic conditions (160–163). However, it is currently unclear whether these bone-protective effects are specific to the skeleton or secondary to treating the underlying pathology driving bone loss. Models of estrogen-induced and PTH-induced bone loss have demonstrated a clear role for T cells in contributing to disease in a microbiota dependent manner (123, 125, 133, 164). Microbial metabolites such as butyrate and propionate, have also been demonstrated to stimulate bone formation (134, 165). While there have been many exciting recent findings in this expanding field, future work is needed to delineate how intestinal pathologies lead to microbiota changes that impact specific skeletal cells.

In summary, it is clear that OCs and their precursors directly participate in a diverse set of functions and commonly interact with immune cells and microbes. Some groups have theorized that the immune function of OCs is specifically linked to pathogen defense (103, 126). To better understand how RANK/RANKL signaling impacts a specific enteric pathogen, the next sections will introduce this pathogen and describe the host response to infection with an emphasis on highlighting overlapping features with skeletal biology.

Salmonella enterica **subspecies** ***enterica*** **serovar Typhimurium**

Salmonella enterica subspecies *enterica* serovar Typhimurium (STm) is a Gram-negative, intracellular pathogen capable of causing a spectrum of disease amongst a broad range of host species. While there are only two *Salmonella* species, there are thousands of serovars (166). In humans, an important serovar distinction is between typhoidal and non-typhoidal

strains of *Salmonella*. Typhoidal strains lead to a systemic disease characterized by high fever and general signs of sickness (also referred to as "typhoid fever") and are host-restricted to humans (167). Non-typhoidal *Salmonella* (NTS) strains are more commonly associated with contaminated food products, and therefore commonly result in enteric infections hallmarked by bloody diarrhea (166). NTS enteric infection is the leading cause of hospitalization and death among food borne diseases in the United States (168). While NTS usually leads to localized intestinal infection in immunocompetent individuals, immunosuppressed individuals and infants are susceptible to invasive disease (166). *Salmonella* demonstrates a proclivity for bone infection in patients with either human immunodeficiency virus (HIV) or hemoglobinopathies (*e.g.*, sickle cell disease), and can survive in bone marrow during system infection (169, 170). Furthermore, bone marrow culture demonstrates enhanced sensitivity in detecting salmonellosis compared to blood culture (171). The mechanisms that dictate tissue tropism, especially to bone, during *Salmonella* infection are complex and poorly described.

In addition to causing several discrete clinical syndromes in humans, *Salmonella* can infect a broad range of mammals including many livestock, pets, and rodents (167). The broad range of animals susceptible to *Salmonella* infection has led to the use of a number of animal models to study disease pathogenesis. In mice, the development of these infection models has led not only to important discoveries in bacterial pathogenesis, but also the discovery of important host-restriction factors, as different strains of mice demonstrate marked differences in susceptibility to *Salmonella* infection. Systemic infection with STm in genetically susceptible strains of mice (*e.g.*, C57BL/6) leads to bacteremia and death, similar to salmonellosis in an immunodeficient person (167, 172). However, in genetically resistant strains of mice (*e.g.*, CBA/J), infection leads to self-limiting disease with dissemination and colonization and various

organ sites (including the intestine), but ultimately results in pathogen clearance, a process thought to resemble features of human typhoid fever (167, 172). Seminal studies in the field determined through backcrossing different strains of mice that the host restriction factor, natural resistance-associated macrophage protein 1 (NRAMP1), was a major contributor of differential outcomes during *Salmonella* infection in mice (173). Until recently, models of *Salmonella* acute gastrointestinal disease have been lacking. Treating mice with a single dose of antibiotics was sufficient to enable robust *Salmonella* colonization in mice that were previously resistant to *Salmonella* colonization via orogastric infection (174). Now, this model of *Salmonella* infection is widely used to study acute NTS gastroenteritis.

Pathophysiology and host response to gastrointestinal *Salmonella enterica* infection

The pathophysiology of STm infection is complex (**Figure 3**). Following ingestion, STm must outcompete resident microbiota species to establish a replicative niche within the intestine and traverse the intestinal epithelium to spread systemically (174). One route of infection that STm commonly exploits is by bypassing the intestinal epithelium through uptake by microfold (M) cells. M cells are specialized cells within the intestinal epithelium that transport antigens from the intestinal lumen into the lamina propria. These antigens are subsequently taken up by antigen presenting cells (APCs) and presented to lymphocytes. M cells allow STm a portal of entry to the lamina propria, upon which STm replicates within cells in the lamina propria and Peyer's patch. Upon entry into a cell, *Salmonella* replicates and eventually leads to cell death through either apoptosis, pyroptosis, or necroptosis, which subsequently leads to further dissemination (175). Simultaneously, STm is capable of invading and replicating within epithelial cells and can lead to an epithelial intrinsic inflammasome response leading to cell

expulsion, thereby providing additional points of entry for STm to invade the lamina propria (176–178).

STm infects and persists within host cells by employing two separate type 3 secretion systems (T3SS1 and T3SS2) that are encoded on *Salmonella* pathogenicity islands 1 (SPI-1) and 2 (SPI-2) (175, 179, 180). T3SS1 facilitates invasion of host cells in part by coordinating cytoskeletal rearrangements (179, 180). SPI-1 effectors result in endocytosis or phagocytosis of STm. To avoid lysosomal degradation and promote intracellular survival, T3SS2 effectors promote replication in a modified phagolysosome known as the *Salmonella*-containing vacuole (SCV). Replication in this niche helps shield PAMPs from host recognition. T3SS2 is in part triggered by a reduction in pH that occurs during endosomal-lysosomal trafficking (179, 180). Additionally, signaling through toll like receptors further regulates the switch from transcribing T3SS1 to T3SS2 effectors (181).

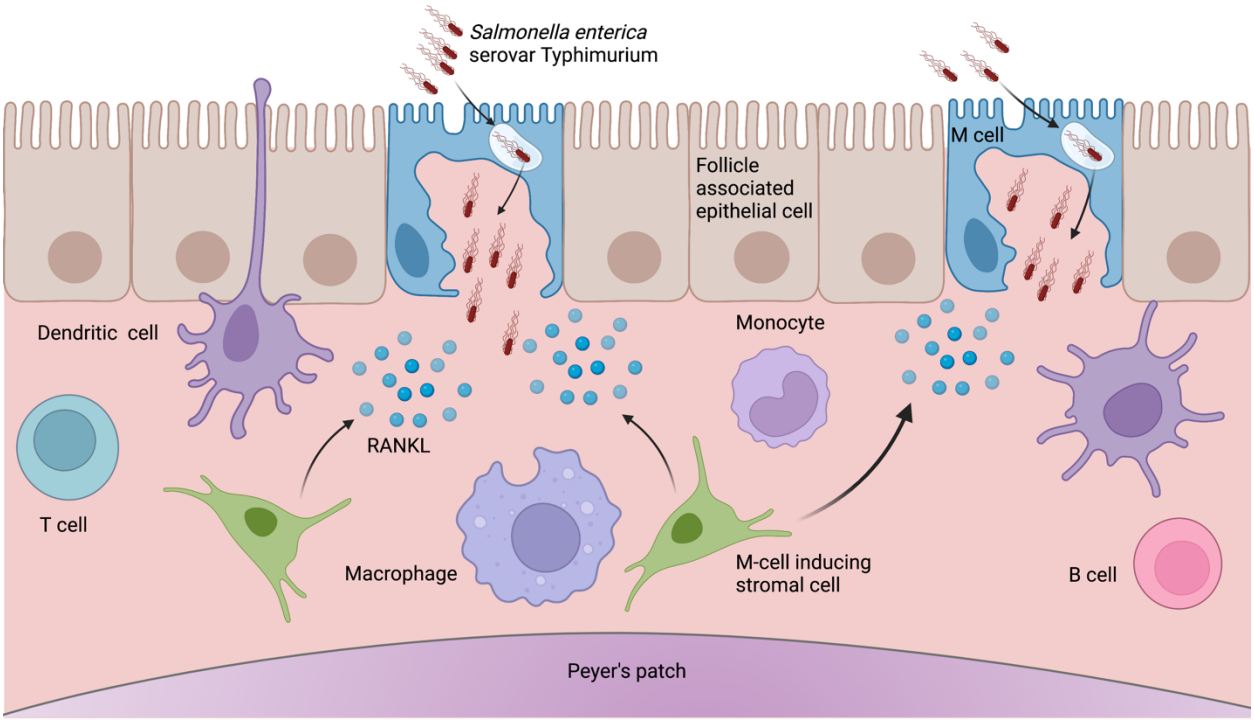

Figure 3. Pathogenesis of *Salmonella enterica* subspecies *enterica* serovar Typhimurium enteric infection.

Salmonella enterica subspecies *enterica* serovar Typhimurium (STm) can invade microfold (M) cells that sit atop Peyer's patches in the intestinal epithelium. M cells are induced by RANKL production from M-cell inducing stromal cells. Once STm enters the lamina propria, it encounters a range of immune cells including macrophages, monocytes, dendritic cells, monocytes, and lymphocytes. STm can cause systemic disease through intracellular infection of these cells and subsequent hitch-hiking to extra-intestinal locations, as well as dissemination through the bloodstream or lymphatic systems.

STm engages and evades many aspects of the host immune response (**Figure 4**). Recognition of PAMPs by PRRs is essential for host defense against STm infection. *Salmonella* lipopolysaccharide (LPS), flagellin, and components of the T3SSs are the major PAMPs that drive PRR recognition during infection. Intracellular PRRs, such as NOD1 and NOD2, also play a crucial role in recognizing and responding to infection with STm. Engaging inflammasomes are critical to host defense against *Salmonella*. STm has been shown to directly engage the NOD-, LRR-, and pyrin domain-containing protein 3 (NLRP3) and NLR family CARD domain containing 4 (NLRC4) inflammasomes (176, 182–185). STm LPS binds TLR4, which activates NLRP3, while STm needle, rod, and flagellar components activate NLR family apoptosis inhibitory proteins (NAIPs), which in turn, activate the NLRC4 inflammasome (176, 183–186). Noncanonical inflammasome activation can also occur through intracellular LPS direct binding of caspase 11 (187). Engagement of the NLRP3 and NLRC4 inflammasomes results in IL-1ß and IL-18 release and pyroptosis (176, 183, 184, 186) (**Figure 4**).

Recent studies have begun to explore the cross talk between RANK/RANKL signaling and STm pathogenesis. Mice lacking OPG, the soluble decoy receptor for RANKL, demonstrated increased abundance of M cells and enhanced STm bacterial burdens (188). Administration of soluble RANKL phenocopied these results (188). However, the precise cellular and molecular mechanisms underlying these findings are not currently understood and are ripe for future investigation. These findings are especially intriguing when placed in the context of additional work demonstrating that RANKL silences transcriptional regulators of inflammasome components that are crucial for STm inflammasome responses (183, 189–191) (**Figure 4**). Specifically, RANKL epigenetically silences a transcriptional regulator of NAIPs, *IRF8*, through DNMT3a and EZH2 (183, 189, 191). Therefore, it is unclear how modulating

RANKL may impact anti-bacterial, inflammatory, and cell fate outcomes during STm infection. Studies described in Chapter IV will further test the impact of RANKL signaling on these outcomes.

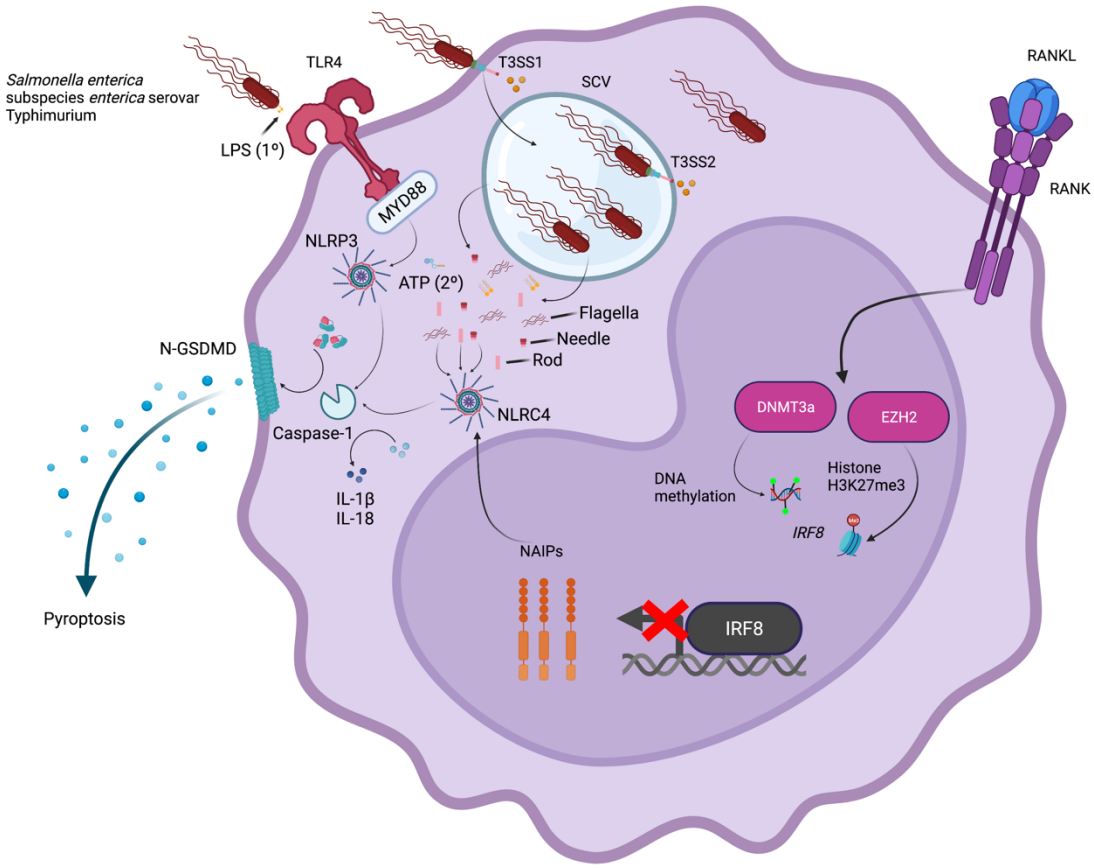

Figure 4. Crosstalk between RANKL signaling and *Salmonella* engagement of the innate immune system.

Salmonella enterica subspecies *enterica* serovar Typhimurium (STm) engages multiple aspects of the innate immune system. Pathogen associated molecular patterns (PAMPs), such as toll-like receptor 4 (TLR4) can lead to downstream inflammatory responses through the adaptor protein, myeloid differentiation primary response 88 (MyD88). STm can enter a host cell through a type 3 secretion system one (T3SS1) dependent mechanism. Once intracellular, STm replicates inside the *Salmonella* containing vacuole (SCV), which is maintained by effectors secreted by the type 3 secretion system two (T3SS2). Some STm are also capable of replicating cytoplasmically, outside of the SCV. During replication, STm associated PAMPs, including lipopolysaccharide (LPS), flagella, and components of the T3SSs (*e.g.*, rod and needle proteins) induce

inflammasomes that ultimately lead to a pyroptotic cell death. Extracellular LPS leads to inflammasome priming and transcription of key inflammasome components such as *NRLP3* and *IL1ß*. A second signal (*e.g.*, adenosine triphosphate [ATP]) subsequently activates and promotes assembly of the NOD- LRR- and pyrin-containing protein 3 (NLRP3) inflammasome. Intracellular LPS can activate the non-canonical inflammasome by directly binding caspase 11 (not depicted). STm intracellular rod, needle, and flagella activate the NLR family CARD domain containing 4 (NLRC4) inflammasome. NLR family apoptosis inhibitor proteins (NAIPs) sense cytosolic intracellular STm PAMPs including STm flagella, needle, and rod proteins. *IRF8* transcriptionally regulates the expression of NAIPs. RANKL silences *IRF8* expression through DNA methylation mediated by DNMT3A and histone H3K27 tri-methylation mediated by Enhancer of Zeste Homolog 2 (EZH2). Inflammasome activation results in cleavage of pro-IL-1ß and IL-18 to their mature forms as well as cleavage of gasdermin-D (GSDMD) to generate the N-terminal fragment, N-GSDMD, which subsequently forms pores in the host cell membrane leading to cell death by pyroptosis.

Conclusions

In summary, the cellular and molecular mechanisms governing interactions between the skeletal and intestinal organ systems are still being uncovered. Prior studies have highlighted a crucial role of RANK/RANKL signaling in maintaining homeostasis in each of these sites (60, 62). Interactions between the intestinal and skeletal systems are apparent in pathologic conditions that impact either of these organ systems. Bone loss during IBD represents an important clinical manifestation linking intestinal inflammation to skeletal pathology. Dysregulated interactions between OCs and OBs drive bone loss. OCs are haematopoietically-derived multinucleated cells capable of bone resorption. Emerging studies have begun to highlight the interface between skeletal biology and immunology, referred to as osteoimmunology. OCs play in important role in the bidirectional regulation of the skeletal and immune systems through both innate and adaptive immune cells as well as through cytokines and regulating hematopoiesis. However, the precise mechanisms that impact osteoclastogenesis during intestinal inflammation are still being uncovered.

Work described in this thesis also takes a complementary approach to investigate how modulating RANK/RANKL signaling impacts responses to a specific enteric pathogen. STm is an important cause of intestinal inflammation. One route of STm infection occurs through M cells, which are dependent upon RANKL signaling. However, the impact of RANK/RANKL signaling on STm survival within monocytes and the subsequent immune response remains unclear. RANKL is predicated to dampen the NLRC4 inflammasome responses to STm, however, this hypothesis has not been previously examined.

This thesis seeks to address critical gaps in knowledge in these fields, such as delineating the specific shifts in cellular populations and inflammatory signals that occur within the skeletal

environment during intestinal inflammation. Identifying these alterations may lead to the discovery of potential therapeutic targets to ameliorate bone loss during IBD. Furthermore, studying how tissue-specific homeostatic signaling, such as RANKL, alters the immune response to pathogens is an important area of research to better study infectious diseases. In total, this work seeks to add to what is currently understood about the crosstalk between the skeletal and intestinal systems.

CHAPTER III: INTESTINAL INFLAMMATION DRIVES MDL-1^{+} OSTEOCLAST PRECURSOR EXPANSION AND ENHANCED OSTEOCLASTOGENESIS TO PROMOTE COLITIS-ASSOCIATED BONE LOSS

Introduction

Inflammatory bowel disease (IBD) is hallmarked by severe gastrointestinal inflammation that is mediated, in part, by aberrant innate and adaptive immune responses. Additionally, the inflammation that patients with Crohn's disease and UC experience frequently impacts extra-intestinal sites. Up to 40% of patients with IBD experience extra-intestinal symptoms, which can occur in nearly every tissue type before, concurrent with, or after the onset of colitis (4, 5, 12). Musculoskeletal disease during IBD is among the most common extra-intestinal manifestations and ultimately confers a 40% increased risk of osteoporotic fracture compared to the general population (192). While nutritional status and medication use are potential contributors to colitis-associated bone loss, accumulating evidence supports a primary role for inflammation in driving bone loss during IBD. Patients with normal vitamin D and calcium levels are still susceptible to IBD-associated bone loss, as are patients who have not yet started IBD anti-inflammatory treatments (12, 21, 193). Moreover, TNF-α blocking therapy partially prevents bone loss in patients with IBD and correlates with improved serum markers of bone resorption (16, 17). These findings suggest that systemic inflammation is an important driver of bone loss during IBD. One potential mechanism by which IBD-associated inflammation triggers bone loss is through the actions of inflammatory cytokines on skeletal cells.

The goal of studies described in this Chapter was to further define how gastrointestinal inflammation leads to bone loss by focusing on osteoclasts. Osteoclasts are multi-nucleated, myeloid lineage cells capable of resorbing bone. Osteoclast differentiation and survival require receptor activator of nuclear factor kappa-B ligand (RANKL) and macrophage colony

stimulating factor (M-CSF) signaling and are further regulated by the RANKL decoy receptor, osteoprotegerin (OPG). Multiple myeloid cell types across various tissue sources can differentiate into osteoclasts in the presence of M-CSF and RANKL. Cells capable of differentiating into osteoclasts include LSK (lineage negative, SCA-1^+, C-KIT^+) hematopoietic stem cells (HSCs), monocytes, and dendritic cells (81, 83, 85, 88). Patients with IBD-associated bone loss exhibit altered RANKL/OPG levels and elevated serum markers of bone turnover, suggesting that osteoclast differentiation and activity are increased in this patient population (17, 194).

Importantly, the isolated binding of M-CSF and RANKL to their cognate receptors is insufficient to induce osteoclast formation *in vivo* or *in vitro* without the coordinated signaling of several osteoclast co-receptors (108). Activating co-receptors promote osteoclast formation through intracellular immunoreceptor tyrosine-based activation motif (ITAM)-signaling adaptors (108). Intracellular ITAM-signaling adaptors, such as DNAX activation protein 12 (DAP-12) or FcεR1 gamma chain (FcRγ), pair with receptors capable of binding membrane-bound and extracellular ligands to transduce ITAM activation and trigger calcium fluxes that initiate osteoclast formation (110). Myeloid DAP-12-associating lectin-1 (MDL-1; also known as C-type lectin domain family 5, member A or CLEC5A) and triggering receptor expressed on myeloid cells 2 (TREM2) are examples of DAP-12-associating osteoclast co-receptors, while FcRγ-associated co-receptors include osteoclast activating receptor (OSCAR) and paired-immunoglobulin-like receptor A (PIR-A). Although some ligand-receptor pairs have been identified for these osteoclast co-receptors, many remain poorly described.

Osteoclasts and their precursors are exquisitely sensitive to inflammatory cytokines (*e.g.*, IL-1 and TNF-α), chemokines (*e.g.*, sphingosine-1-phosphate and CCL-2), and colony

stimulating factors (*e.g.*, G-CSF) that can further modulate osteoclast differentiation and function (95, 97, 101, 135, 136, 138). The sensitivity of osteoclasts to the surrounding cytokine milieu is, in part, driven by cross regulation of ITAM-associated osteoclast co-receptors. G-CSF, IL-23, and TNF-α have been previously reported to enhance MDL-1 expression on myeloid cells and increase osteoclast formation *in vitro* and *in vivo* (139, 148, 195). Activation of MDL-1 on myeloid cells results in the robust release of RANTES/CCL-5, CXCL-10, TNF-α, and G-CSF (139, 148, 196, 197). Several of these osteoclastogenic cytokines are crucial to both the intestinal and extra-intestinal pathogenesis of IBD (198–200).

Previous studies have examined bone loss in murine models of colitis, including chemical injury, genetic, T cell mediated, and infection models (19, 39, 40, 43, 44, 46–48, 50–52, 54, 201–203) (**Table 1**). However, the mechanisms by which gastrointestinal inflammation promotes bone loss through effects on skeletal cells are still being uncovered. We hypothesized that changes in OC progenitor populations during colitis contribute to IBD-associated bone loss. Using chemical injury, infectious, and adoptive T cell transfer models of gastrointestinal inflammation, we discovered that an increase in the surface expression of the osteoclast co-receptor MDL-1 on $Cd11b^{-/lo}Ly6C^{hi}$ osteoclast precursors (OCPs) is associated with enhanced osteoclastogenesis and significant bone loss during colitis. Moreover, anti-MDL-1 treatment was sufficient to blunt the enhanced *ex vivo* osteoclast formation observed in OCPs derived from mice with chemical colitis. Importantly, *in vivo*, anti-MDL-1 was efficacious in limiting bone loss during DSS colitis.

Materials and methods

Animal use

Male and female 7 to 9-week-old C57BL/6J (Stock # 000664), CBA/J (Stock # 000656), and *Rag1*$^{-/-}$ (Stock # 002216) mice were purchased through The Jackson Laboratory and maintained in our colony for at least one week prior to experimentation. C57BL/6J and *Rag1*$^{-/-}$ mice were bred homozygously. C57BL/6J and CBA/J mice were maintained in specific pathogen free (SPF) conditions. *Rag1*$^{-/-}$ mice were maintained in sterile conditions with autoclaved food and bedding prior to adoptive T cell transfer, after which they were switched to SPF conditions.

Mouse models of colitis

For experiments involving DSS colitis, 3% DSS (TdB Labs) was administered *ad libitum* in the sterile drinking water of 7-week-old male or female WT or *Rag1*$^{-/-}$ mice for one week, after which time mice were switched back to sterile drinking water. Mice were euthanized at days 1, 3, 7, or 14 following the initiation of DSS treatment. Where indicated, mice were treated with 50 μg of either anti-MDL-1 (R&D, clone 226402) or IgG2a isotype control (R&D clone 54447) at day 3 following DSS-treatment. Mice were monitored for signs of clinical disease and weighed daily. For experiments involving adoptive T cell transfer mediated colitis, colitis was induced in male or female *Rag1*$^{-/-}$ mice by adoptive transfer of sorted $CD4^+CD25^-CD45RB^{hi}$ cells. $CD4^+$ T cells were isolated from the splenocytes of WT 8–12-week-old sex-matched C57BL/6J mice using negative selection magnetic enrichment (Stem Cell Technologies) per the manufacturer's instructions. Enriched $CD4^+$ T cells were stained with a surface staining cocktail including CD4-APC-Cy7 (Biolegend, clone GK1.5), CD25-APC (Biolegend, clone PC6.1), and CD45RB-BV711 (BD Optibuild, clone 16A), as well as a live/dead stain (eBioscience Fixable Viability Dye eFluor 506). Live $CD4^+CD25^-CD45RB^{hi}$ (Tnaive) and live $CD4^+CD25^+CD45RB^-$

(Treg) cells were sorted by FACS using either 4- or 5-laser FACS Aria III systems. Naïve T cells were gated to include the $CD4^+$ T cells demonstrating the top 30-40% expression of CD45RB. $5.0x10^5$ Tnaive or a combination of $5.0x10^5$ Tnaive and $1.0x10^5$ Treg cells (non-colitis control) were adoptively transferred into sex-matched 8-10-week-old C57BL/6J *Rag1*$^{-/-}$ recipient mice by intraperitoneal (i.p.) injection. Post-sort viability of Tnaive and Treg cells was routinely observed to be >85%. Mice were weighed weekly, monitored for disease progression, and euthanized at weeks 5 or 8 post-transfer. For experiments involving *Citrobacter rodentium* colitis, infection was achieved as previously described (204, 205). Briefly, male C57BL/6J mice were infected by oral gavage with $5.0x10^8$ colony forming units (CFUs) of *C. rodentium* or mock-infected with Luria broth. Mice were weighed and monitored for disease progression. Colon tissue was homogenized, serially diluted, and plated on MacConkey Agar for enumeration of bacterial CFUs per gram of stool. For experiments involving *Salmonella enterica* serovar Typhimurium (STm) CBA/J mice were infected as previously described (206). 8-week-old CBA/J female mice were infected with $1.0x10^9$ CFUs STm strain IR715 via oral gavage or an isogenic mutant lacking functional T3SS1 and T3SS2 (Δ*invA::tetRA* Δ*spiB::KSAC invA spiB*). Mice were weighed and monitored for disease progression. Stool was collected throughout the course of infection and at the experimental endpoint, snap frozen, homogenized, serially diluted, and plated on MacConkey Agar for enumeration of bacterial CFUs per gram of stool.

Colitis scoring

Colons from mice with or without colitis were harvested at the indicated experimental time point, Swiss-rolled, fixed in 10% neutral buffered formalin for 24 h, and subsequently processed for paraffin embedding, sectioning, and staining with hematoxylin and eosin (H&E). For STm infections, ceca were harvested at the indicated time point and processed as stated

above for colons. H&E-stained colon sections were scored in a blinded manner by a gastrointestinal pathologist using previously published scoring criteria for DSS colitis (207), adoptive T cell transfer colitis (208), and *C. rodentium* induced colitis (204, 205). H&E-stained cecal sections were scored in a blinded manner by a veterinary pathologist using previously published scoring criteria (206).

Micro-computed tomography of trabecular bone

Femurs were harvested at the indicated time point and fixed with 10% neutral buffered formalin for 48 h at 4ºC and then placed in 70% ethanol. Trabecular bone was analyzed using a μCT40 (Scanco Medical, AG Bassersdorf, Switzerland) and Scanco software. Images were acquired at 55 kVp and 145 mA with an isotropic voxel size of 12 μm and an integration time of 250 ms with 1000 projections collected per 360º rotation. Images were reconstructed, filtered (sigma = 0.8, support = 1.0), and thresholded at 200 mg HA/ccm. Trabecular bone at the distal femur was manually contoured every 10 slices starting 30 slices proximal to the growth plate and advancing proximally for 100 slices such that trabeculae were included, and cortical bone was excluded in accordance with ASBMR guidelines (209). Sections between manual contours were automatically contoured.

Bone histology and histomorphometry

Following micro CT imaging, femurs were decalcified for 3 days in 20% EDTA (pH 7.4) at 4ºC. Samples were then dehydrated, embedded in paraffin blocks, and sectioned longitudinally at 4 μm thickness through the medullary cavity with a Leica RM2255 microtome. Tissue sections were mounted onto Leica Superfrost glass slides and then stained with tartrate-resistant acid phosphatase (TRAP) stain with hematoxylin counterstain. Bioquant software (Nashville, TN) was used to perform quantitative histomorphometry (osteoclast number, osteoclast surface,

and bone perimeter) on the distal femoral metaphysis (region of interest determined between the growth plate and central sinus) in accordance with ASBMR guidelines using 10x images generated from a Cytation 5 imaging system (Biotek) (210).

Flow cytometry and cell sorting

Bone marrow from femurs and tibias was flushed with cold alpha-minimal essential media (α-MEM). Red blood cells were lysed for 5 minutes with ammonium chloride potassium (ACK) lysing buffer, pelleted, resuspended in PBS, and passed through a 70 μm filter. Single cell suspensions were washed with PBS, enumerated, and 1 million bone marrow cells per sample were pelleted in PBS prior to live/dead staining per the manufacturer's protocol (Zombie Violet, Biolegend). Cells were then washed with FACS buffer (PBS containing 3% FBS and 0.1% sodium azide). Non-specific antibody staining was blocked with anti-CD16/32 (Biolegend, clone 93) for 15 minutes at room temperature. Single cell bone marrow suspensions were stained with a cocktail of surface-staining antibodies to identify specific myeloid populations. Unless otherwise indicated, all antibodies were purchased from Biolegend. For OCPs and monocytes, the following anti-mouse antibodies were used: Anti-CD45-AlexaFluor700 (clone 30-F11), anti-Cd11b-BV605 (clone M1/70), anti-Ly6G-PE or anti-Ly6G-PE-Dazzle (clone 1A8), anti-Ly6C-FITC (clone HK1.4), anti-TER119-Pacific Blue (clone TER-119), anti-B220-Pacific Blue (clone RA3-6B2), anti-CD3-Pacific Blue (clone 145-2C11). For LSK cells, the following antibodies were used: Anti-mouse lineage cocktail-FITC (clones 145-2C11, RB6-8C5, RA3-6B2, Ter-119, M1/70), anti-Sca-1-APC (clone D7), and anti-c-kit-PE (clone QA17A09). Additional surface markers were evaluated on monocytes and OCPs by staining with anti-CXCR4-BV-711 (clone L276F12), anti-MDL-1-APC (Miltenyi, clone REA582), anti-CX_3CR1-APC (clone SA011F11), anti-CCR2-APC/Fire-750 (clone SA203G11), anti-RANK-PE (clone R12-31), and anti-CSF1R-

PerCP/Cy5.5 (clone AFS98). Osteoclast co-receptors antibodies specific for OSCAR (Novus Biologicals, clone 5B8), PIR-A/B (clone 6C1), and TREM2 (R&D, clone 237920) were conjugated to APC using the APC conjugation kit – lightning link (Abcam) per the manufacturer's instructions. Surface staining was accomplished by incubating single cell suspensions with a given antibody cocktail at 4ºC for 30 minutes. For intracellular staining, cells were fixed and permeabilized overnight at 4ºC using the Foxp3 / transcription factor staining buffer set (eBioscience) per manufacturer's instructions followed by intracellular staining for Ki67-APC (clone 16A8). Cells were washed twice in FACS buffer and fixed in PBS with 2% paraformaldehyde and analyzed using a 3- or 4-Laser Fortessa analytical flow-cytometer. Single cells were gated using successive gates including side scatter-area by forward scatter-area (SSC-A x FSC-A), side scatter-height by area (SSC-H x SSC-A), and forward scatter-height by area (FSC-H x FSC-A). Gating for the indicated populations was done as described in **Figure 5** and **Figure 13A**. For cell sorting, single cell bone marrow suspensions were obtained as described above, live-dead stained, and blocked as described above. Cells were stained with Anti-CD45-AlexaFluor700 (clone 30-F11), anti-Cd11b-BV605 (clone M1/70), anti-Ly6G-PE (clone 1A8), anti-Ly6C-FITC (clone HK1.4), anti-TER119-Pacific Blue (clone TER-119), anti-B220-Pacific Blue (clone RA3-6B2), and anti-CD3-Pacific Blue (clone 145-2C11). Monocytes (live $CD3^{-}B220^{-}Ter119^{-}Ly6G^{-}CD45^{+}Cd11b^{+}Ly6C^{+}$) OCPs (live $CD3^{-}B220^{-}Ter119^{-}Ly6G^{-}CD45^{+}Cd11b^{-/lo}Ly6C^{hi}$) or $Cd11b^{-}Ly6C^{-}$ double negative ($CD3^{-}B220^{-}Ter119^{-}Ly6G^{-}CD45^{+}Cd11b^{-}Ly6C^{-}$) populations and sorted using either 4- or 5-laser FACS Aria III systems. Data were analyzed using FlowJo software (Version 10, Tree Star Inc.). The purity of sorted populations was >90%.

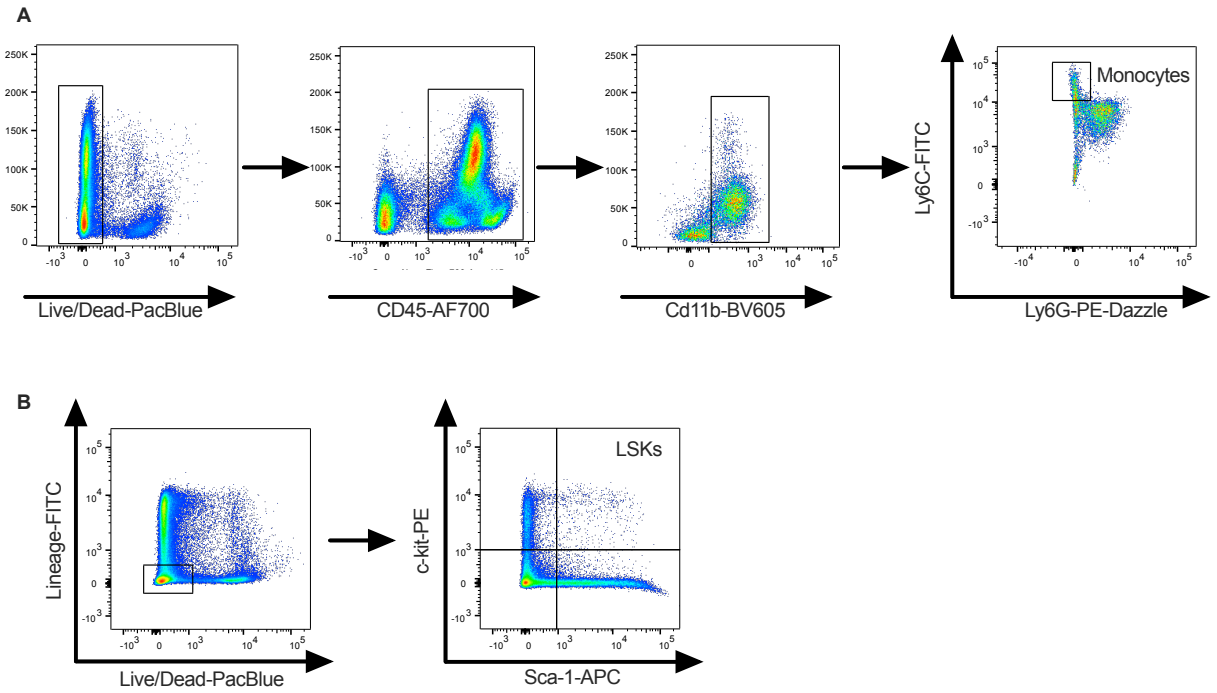

Figure 5. Gating strategy for monocytes and LSK populations.

(A) Single cells were gated using successive gates including side scatter-area by forward scatter-area (SSC-A x FSC-A), side scatter-height by area (SSC-H x SSC-A), and forward scatter-height by area (FSC-H x FSC-A). Monocytes were then gated as live, $CD45^{+}Cd11b^{+}Ly6C^{+}Ly6G^{-}$ cells. (B) Single cells were gated as described above, after which LSK cells were gated as live, $lineage^{-}$ $c\text{-}kit^{+}sca\text{-}1^{+}$ cells.

In vitro osteoclast formation assays

FACS purified populations were used immediately after sorting. $5.0x10^5$ unsorted whole bone marrow or $1.0x10^4$ FACS purified populations were seeded per well into 96 well plates supplemented with 5% v/v CMG14-12 supernatant (as a source of M-CSF) and 35 ng/mL RANKL. Cells were cultured for 4 days, at which point the cells were fixed and stained for TRAP per the manufacturer's instructions (Sigma). Where indicated, cells were treated with 10 μg/mL of either anti-MDL-1 (R&D, clone 226402) or IgG2a isotype control (R&D clone 54447). Fixed cells were stained with DAPI and imaged using a Cytation 5 imaging system (Biotek) prior to manual enumeration of multi-nucleated TRAP+ cells as osteoclasts.

Multiplexed cytokine analysis

Femurs were homogenized in cell lytic buffer at 4ºC in sterile Bullet Blender® Navy Bead Lysis Kit 1.5 mL microcentrifuge tubes (Next Advance, Troy, NY) using a Bullet Blender® BBX24 (Next Advance, Troy, NY). Cell lysates were frozen at -80ºC until use for multiplexed cytokine detection. Thawed cell lysates were centrifuged twice at 4,000 x *g* for 5 minutes at 4ºC to remove debris and then subjected to multiplexed cytokine detection via the Milliplex-MAP magnetic bead-based antibody detection kits (EMD Millipore, Billerica, MA) according to manufacturer's instructions. Specifically, the 32-plex Mouse Cytokine/Chemokine Magnetic Bead Panel (MCYTMAG-70K-PX32) or the Mouse Th17 Magnetic Bead Panel (MTH17MAG-47K) kits were used, and data were collected using the FLEXMAP 3D instrument. Measurements were corrected for total protein input as quantified by the Pierce BCA Protein Assay Kit per manufacturer's instructions and reported as either log2 fold change in pg/mg of cytokine abundances in mice with colitis compared with controls or pg/mg normalized cytokine abundances.

Statistical analysis

Statistical analyses were conducted using GraphPad Prism Software (Version 9). Statistical significance was assessed using 2-tailed Student's t-test, ordinary one-way ANOVA with post-hoc Holm-Šidák multiple comparison's test, or 2-way ANOVA with post-hoc Šidák multiple comparisons test as appropriate and as indicated in the figure legends. Differences were considered significant with a p value ($p< 0.05$). Post-hoc multiple comparisons test for significant differences within groups were only performed following a significant ANOVA p value ($p<0.05$).

Results

Intestinal inflammation results in trabecular bone loss

To investigate bone loss during colitis, we first induced gastrointestinal inflammation via chemical injury with dextran sulfate sodium (DSS). Mice were given 3% DSS orally for one week followed by a one-week recovery period. As expected, DSS treatment led to weight loss and colonic injury (**Figure 6A-B**). We evaluated bone loss using micro-computed tomography (micro CT). DSS-treated mice demonstrated a 37% reduction in trabecular bone volume over total volume (BV/TV) 14 days following DSS treatment compared to controls (**Figure 6C-D**). Trabecular bone loss was associated with a significant reduction in trabecular bone thickness, increased trabecular separation, loss of trabeculae, and reduced connective density (**Figure 6E-H**). To evaluate if this bone loss was associated with changes in the number of osteoclasts, we performed histomorphometry on tartrate-resistant acid phosphatase (TRAP)-stained femur sections. Histologically, we observed a significant increase in osteoclast number per bone surface and but not osteoclast surface per bone surface in DSS-treated mice that occurred at day 7 following DSS administration, prior to the bone loss that was observed at day 14 following DSS

treatment (**Figure 6I-K**). To assess if male mice were differentially susceptible to bone loss during DSS colitis, we confirmed these findings in male mice (**Figure 7**). These results indicate that trabecular bone loss occurs during a chemical injury model of intestinal inflammation, and that an increase in osteoclasts precedes trabecular bone loss.

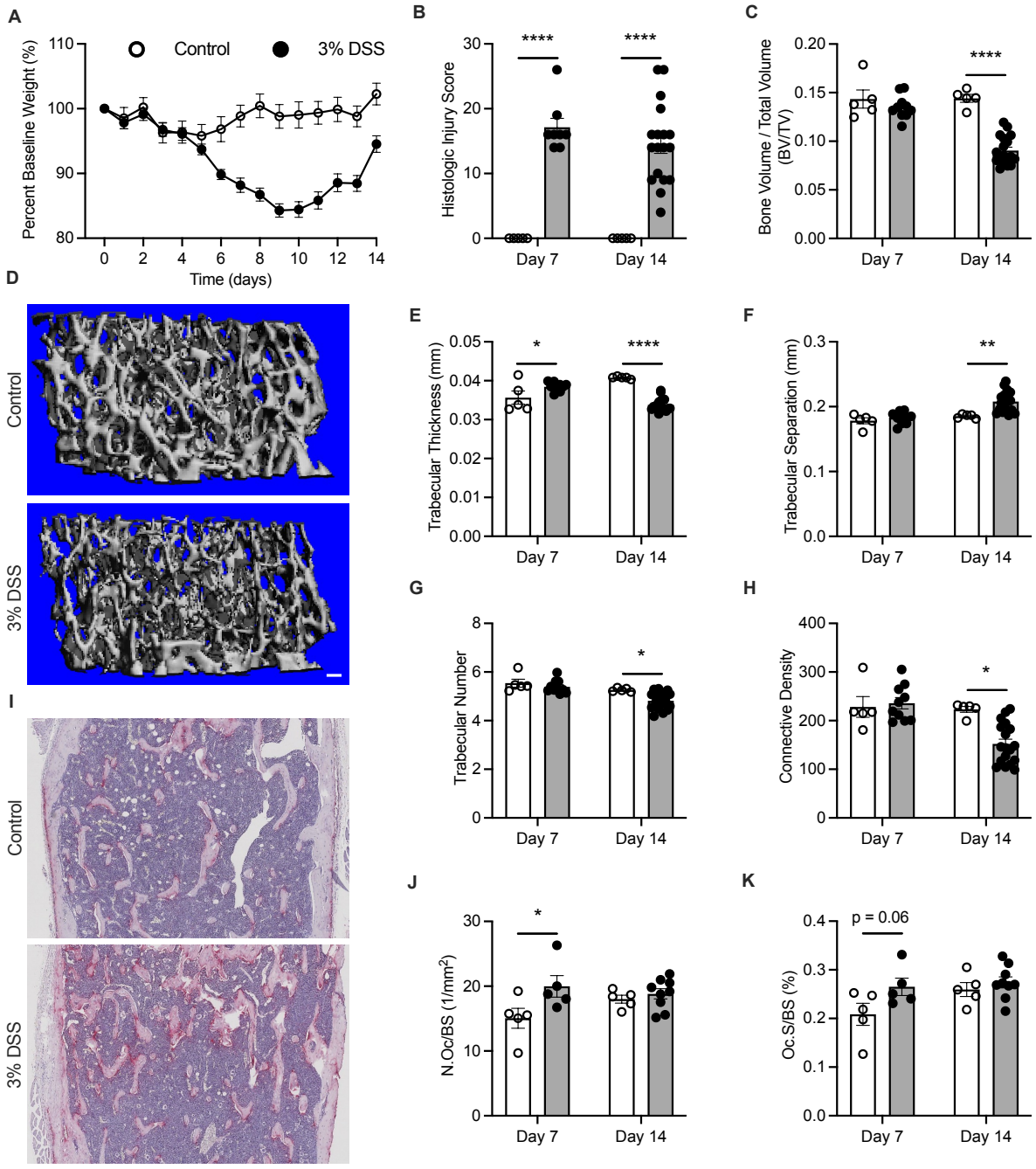

Figure 6. DSS colitis leads to trabecular bone loss.

Mice were administered 3% DSS (closed circles) or water (control, open circles) for 7 days, after which time DSS was switched to water. (A) Percent baseline weight of mice with or without DSS colitis. (B) Histologic injury score of hematoxylin and eosin (H&E) stained colons on days 7 and 14 following DSS administration. (C-H) Micro-computed (micro CT) tomography analysis

of control (open circles) and DSS-treated (closed circles) formalin-fixed femurs for trabecular bone volume per total volume (BV/TV) (C), representative three-dimensional reconstruction of trabecular bone from mice with or without colitis at day 14 (D), trabecular thickness (E), trabecular separation (F), trabecular number (G), and connective density (H) at day 7 or 14 following DSS treatment. Scale bar = 100μm. (I-K) Fixed femurs were paraffin-embedded, sectioned, and stained for tartrate resistant acid-phosphatase (TRAP). (I) Representative image of TRAP-stained femurs from mice with or without colitis at day 7 (original magnification = 10x). (J) Number of osteoclasts per bone surface (N.Oc/BS). (K) Osteoclast surface per bone surface (Oc.BS). Error bars represent mean ± S.E.M. Data analyzed via 2-way ANOVA with Šidák multiple comparisons test. n = 5-18 mice per group. * $p<0.05$, ** $p<0.01$, **** $p<0.0001$.

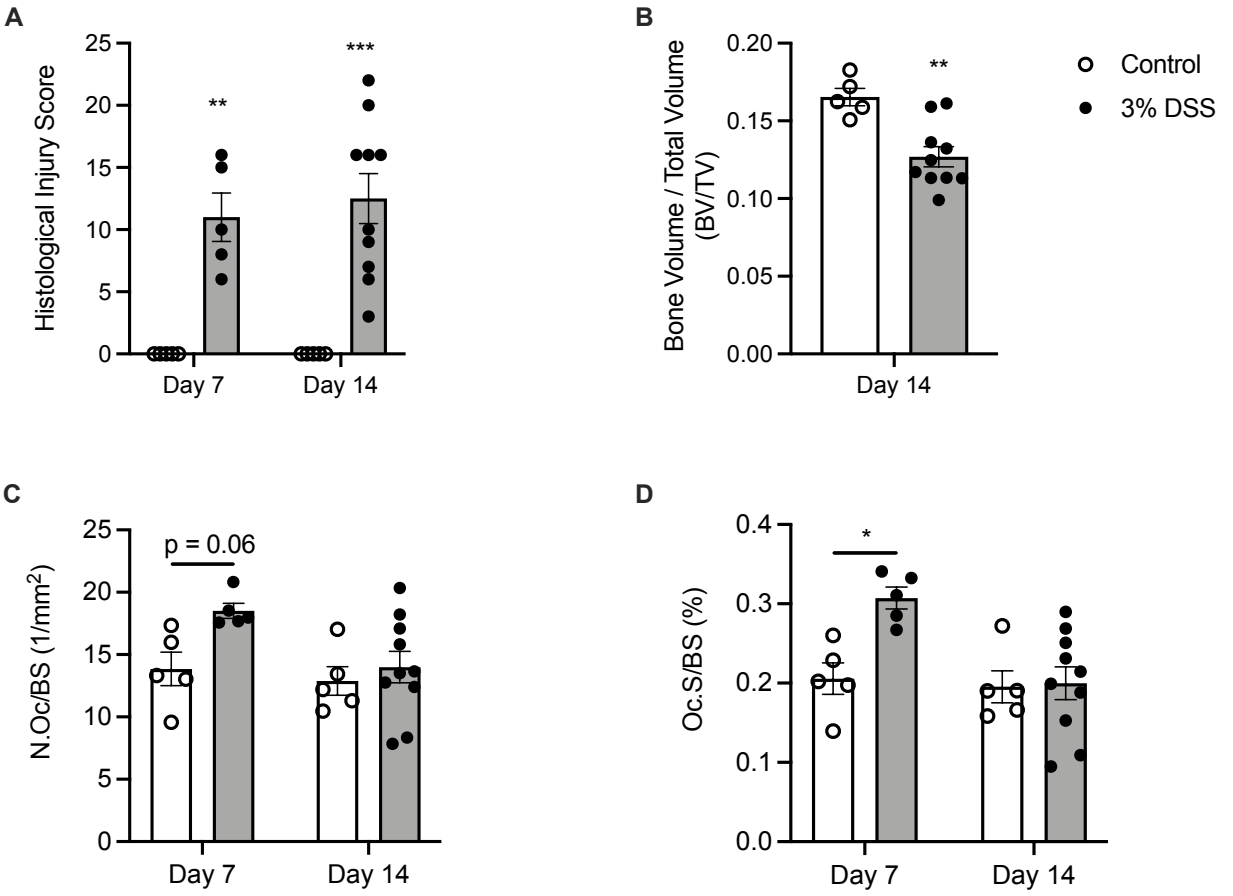

Figure 7. Male mice are susceptible to bone loss during DSS colitis.

Mice were administered 3% DSS (closed circles) or water (control, open circles) for 7 days, after which time DSS was switched to water. (A) Histologic injury score of hematoxylin and eosin (H&E) stained colons on days 7 and 14 following DSS administration. (B) Micro-computed (micro CT) tomography analysis of control (open circles) and DSS-treated (closed circles) formalin-fixed femurs for trabecular bone volume per total volume (BV/TV) at day 14 following DSS treatment. Fixed femurs were paraffin-embedded, sectioned, and stained for tartrate resistant acid-phosphatase (TRAP). (C) Number of osteoclasts per bone surface (N.Oc/BS). (D) Osteoclast surface per bone surface (Oc.S/BS). Error bars represent mean ± S.E.M. Data

analyzed via Student's t-test (B) or 2-way ANOVA with Šidák multiple comparisons test (A, C-D). n = 5-10 mice per group. * $p<0.05$, ** $p<0.01$, *** $p<0.001$.

Next, we tested whether alternative models of intestinal inflammation are associated with bone loss. First, we utilized an adoptive T cell transfer (ACT) model of colitis where *Rag1*$^{-/-}$ mice, injected with naïve $CD4^{+}CD25^{-}CD45RB^{hi}$ T cells, subsequently developed colitis (28). Mice subjected to ACT colitis experienced colonic injury and bone loss, with a 65% reduction in trabecular BV/TV (**Figure 8A** and **Figure 9A**). We subsequently investigated if two infectious models of intestinal inflammation were associated with bone loss. Mice subjected to infectious colitis following inoculation of *Citrobacter rodentium* developed significant trabecular bone loss compared to mock infection (**Figure 9B**). We next infected mice with either wildtype (WT) *Salmonella enterica* subspecies *enterica* serovar Typhimurium (STm), or an attenuated STm mutant, Δ*invA::tetRA* Δ*spiB::KSAC* (*invA spiB*), that lacks functional type III secretion systems 1 and 2 (T3SS1 and T3SS2) and does not induce robust intestinal inflammation (211). We observed that mice infected with WT STm developed significant trabecular bone loss compared to infection with *invA spiB* (**Figure 9C**). Importantly, both *C. rodentium* and WT STm infection led to bacterial colonization, intestinal inflammation, and bone loss in the absence of significant changes in weight over the course of the infection (**Figure 8B-C**). Taken together, these data indicate that trabecular bone loss occurs during T cell driven and infectious models of intestinal inflammation.

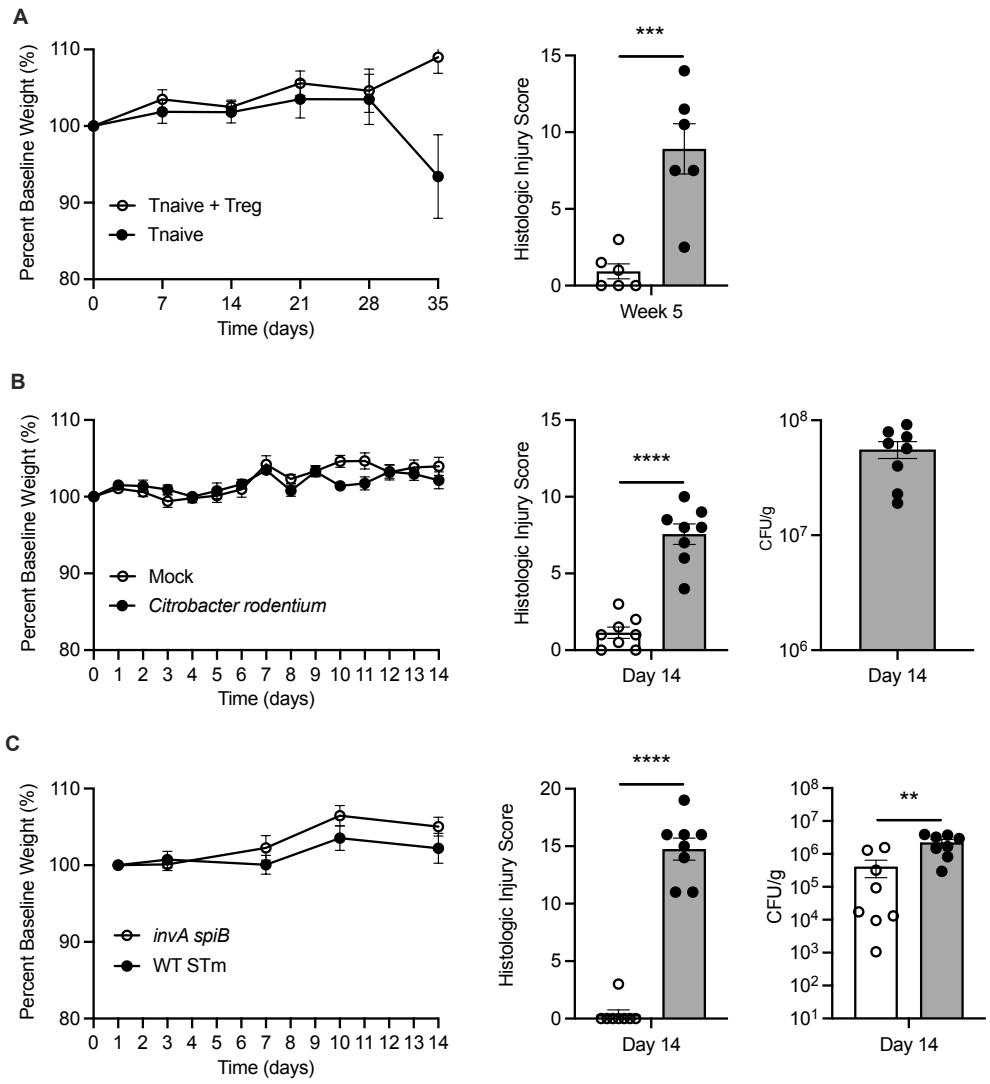

Figure 8. Evidence of histologic injury in mice with adoptive T cell transfer or infection-induced colitis.

(A) *Rag1*$^{-/-}$ mice were injected with 5.0x10^5 CD4$^+$CD25$^-$CD45RB^{hi} T cells (Tnaive) or a non-colitis control of a 5:1 ratio of Tnaive cells with CD4$^+$CD25$^+$ T-regulatory cells (Treg) via intraperitoneal injection. Mice were weighed to monitor disease progression and colons were evaluated for histologic injury at the indicated time point. (B) C57BL/6J mice were mock-infected with Luria broth (mock) or infected with 5.0 x 10^8 colony forming units (CFUs) *Citrobacter rodentium* via oral gavage. Mice were weighed to monitor disease progression.

Colons were harvested at day 14 and evaluated for histologic injury and enumeration of bacterial CFUs. Colon tissue was homogenized, serially diluted, and plated on MaConkey Agar for enumeration of CFUs per gram of tissue. (C) CBA/J mice were infected via oral gavage with either 1.0 x 10^9 CFUs of either a *Salmonella enterica* serovar Typhimurium (STm) T3SS mutant (*invA spiB*) or WT IR715 STm. Ceca were scored for histologic injury in a blinded fashion at the indicated time point. Stool was collected at the experimental endpoint, snap frozen, homogenized, serially diluted, and plated on MacConkey Agar for enumeration of bacterial CFUs per gram of stool. Error bars represent mean ± S.E.M. Data analyzed via Student's t-test. n = 6-8 mice per group. ** $p<0.01$, *** $p<0.001$, *** $p<0.0001$.

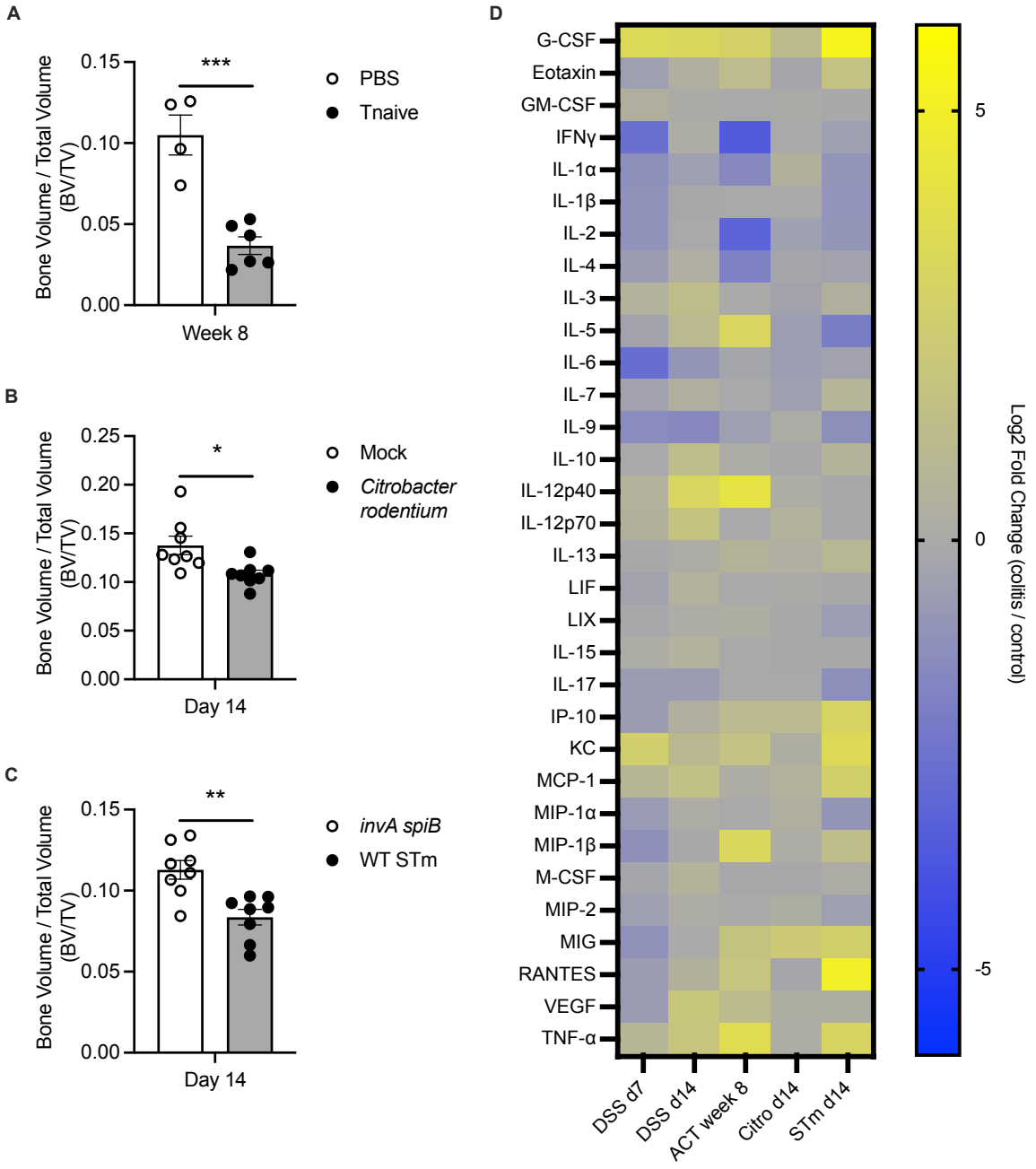

Figure 9. Multiple murine models of intestinal inflammation lead to bone loss and alter the bone marrow cytokine milieu.

Mice were subjected to adoptive T cell transfer (ACT), *C. rodentium* infection, or *S. enterica* serovar Typhimurium (STm) infection prior to harvest of femurs for micro CT analysis. (A) *Rag1*$^{-/-}$ mice were administered 5.0x10^{5} CD4^{+}CD25^{-}CD45RB^{hi} T cells (Tnaive) or PBS via

intraperitoneal injection. (B) C57BL/6J mice were mock-infected with Luria broth (mock) or infected with $5.0x10^8$ colony forming units (CFUs) *Citrobacter rodentium* (Citro) via oral gavage. (C) CBA/J mice were infected with $1.0x10^9$ CFUs of either WT *Salmonella enterica* serovar Typhimurium (STm) strain IR715 (WT) or an *invA spiB* non-colitis control mutant via oral gavage. (D) Femurs from mice with or without intestinal inflammation were homogenized at the indicated time point and assessed for cytokine abundance via Luminex profiling. For DSS colitis, mice were administered 3% DSS for 7 days followed by 7 days of recovery with water. Heatmap of cytokine abundance displayed as Log2 fold change of mice with colitis relative to respective non-colitis controls. Error bars represent mean ± S.E.M. Data analyzed via Student's t-test. n = 4-10 mice per group. * $p<0.05$, ** $p<0.01$, *** $p<0.001$.

Intestinal inflammation alters cytokine abundance within the bone

We hypothesized that bone loss during intestinal inflammation was mediated, in part, by alterations in the cytokine milieu within the bone microenvironment. To test this hypothesis, we performed multiplexed cytokine analysis on homogenized femurs from mice with or without colitis. We observed significant increases in several chemokines and inflammatory cytokines, including G-CSF, TNF-α, IL-12p40, MCP-1/CCL-2, RANTES/CCL-5, and keratinocyte-derived chemokine (KC)/CXCL1 across multiple colitis models (**Figure 9D** and **Figure 10**). Notably, G-CSF, IL-12p40, and TNF-α were among the most significantly increased cytokines across DSS, ACT, *Citrobacter rodentium*, and STm induced colitis (**Figure 9D**). Additional cytokines, including IL-23 and CCL-20, were also significantly elevated during DSS-induced colitis (**Figure 10**). These data suggest that cells within the bone environment of mice with colitis experience an altered cytokine milieu.

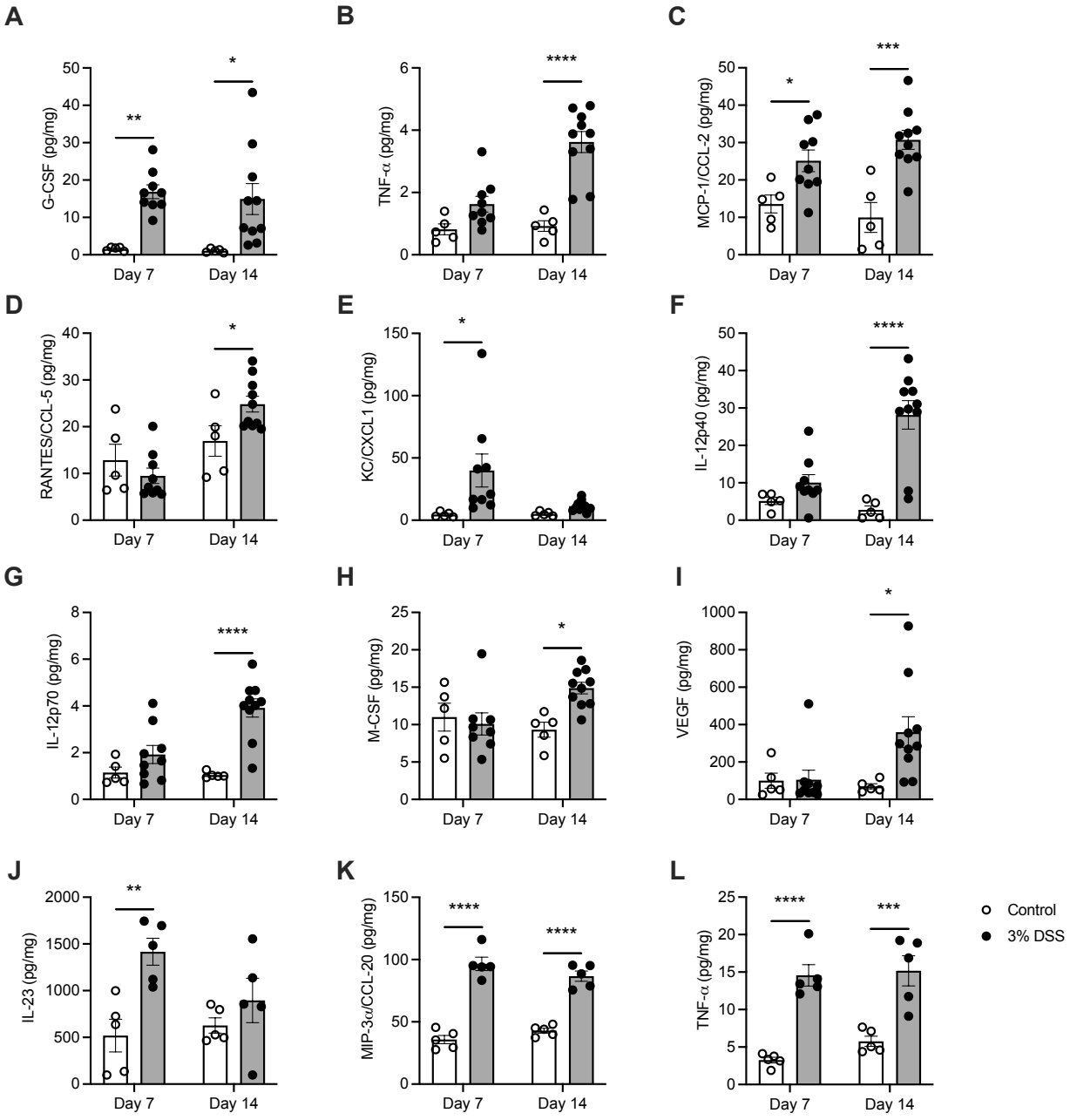

Figure 10. DSS colitis increases the abundance of several MDL-1 associated cytokines.

(A-I) Related to **Figure 9D**. Mice were administered water (control, open circles) or 3% DSS (closed circles) for 7 days followed by 7 days of recovery with water. At the indicated time point, femurs from mice with or without intestinal inflammation were homogenized and assessed for cytokine abundance via Luminex profiling and normalized to total protein as measured by a

Pierce BCA protein assay. Cytokines that were significantly elevated during colitis are shown. (A) G-CSF, (B) TNF-α, (C) MCP-1/CCL-2 (D) RANTES/CCL-5, (E) KC/CXCL1, (F) IL-12p40, (G) IL-12p70, (H) M-CSF, (I) VEGF. (J-L). A separate cohort of mice were administered water (control, open circles) or 3% DSS (closed circles) for 7 days followed by 7 days of recovery with water and assessed for Th17 related cytokine abundance via Luminex profiling and normalized to total protein as measured by a Pierce BCA protein assay. Cytokines that were significantly elevated during colitis are shown. (J) IL-23, (K) MIP-3α/CCL-20, and (L) TNF-α. Error bars represent mean ± S.E.M. Data analyzed via 2-way ANOVA with Šidák multiple comparisons test. n = 5-10 mice per group. * $p<0.05$, ** $p<0.01$, *** $p<0.001$, **** $p<0.0001$.

DSS colitis leads to trabecular bone loss in *Rag1*$^{-/-}$ mice

Previous work has demonstrated that T cells are not only crucial to the pathogenesis of IBD, but also may directly interact with osteoclasts and their precursors to promote pathologic bone loss during colitis (44). We questioned to what extent bone loss was driven by T and B lymphocytes versus myeloid cells following chemical colitis. To determine if mature T and B cells were necessary for bone loss during chemically-induced colitis, we administered DSS to *Rag1*$^{-/-}$ mice. Both the severity of colitis and the magnitude of bone loss in *Rag1*$^{-/-}$ mice were comparable to that of WT mice given DSS (**Figure 11A-B**). These data highlight that although mature T and B cells may contribute to colitis-associated bone loss, they are not required for trabecular bone loss during DSS colitis.

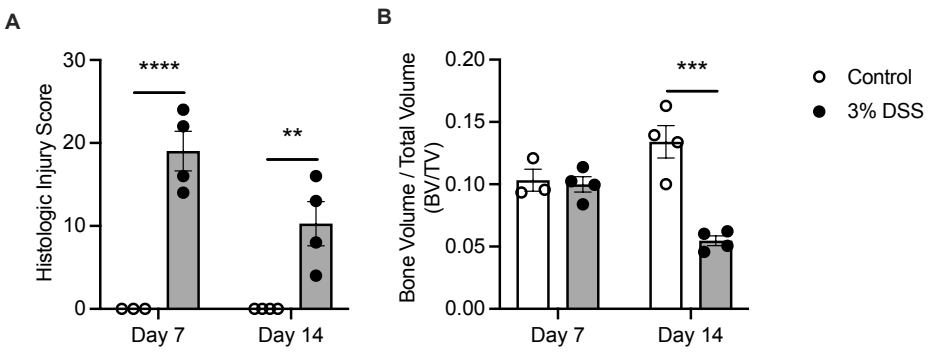

Figure 11. *Rag1*$^{-/-}$ are susceptible to trabecular bone loss during DSS colitis.

Rag1$^{-/-}$ mice were administered either 3% DSS (closed circles) or water (control, open circles) for 7 days, after which time DSS was switched to water. (A) Histologic injury score of hematoxylin and eosin (H&E) stained colons on days 7 and 14 following DSS administration. (B) Micro-computed (micro CT) tomography analysis of control and DSS-treated formalin-fixed femurs for trabecular bone volume per total volume (BV/TV). Fixed femurs were paraffin-embedded, sectioned, and stained for TRAP. Error bars represent mean ± S.E.M. Data analyzed via 2-way ANOVA with Šidák multiple comparisons test. n = 3-4 mice per group. ** $p<0.01$, *** $p<0.001$, **** $p<0.0001$.

Intestinal inflammation leads to expansion of pre-osteoclast populations

Because we observed that multiple models of intestinal inflammation dramatically increased G-CSF, which potently regulates granulopoiesis, we evaluated changes in myeloid-derived osteoclast progenitor populations during colitis. Specifically, we examined LSK HSCs, $Cd11b^{-/lo}Ly6C^{hi}$ OCPs, and monocytes. We observed a significant increase in the relative abundance of monocytes, LSKs, and OCPs within the bone marrow across chemical, infectious, and ACT models of intestinal inflammation (**Figure 12**). Collectively, these data reveal that intestinal inflammation drives an expansion of pre-osteoclast populations.

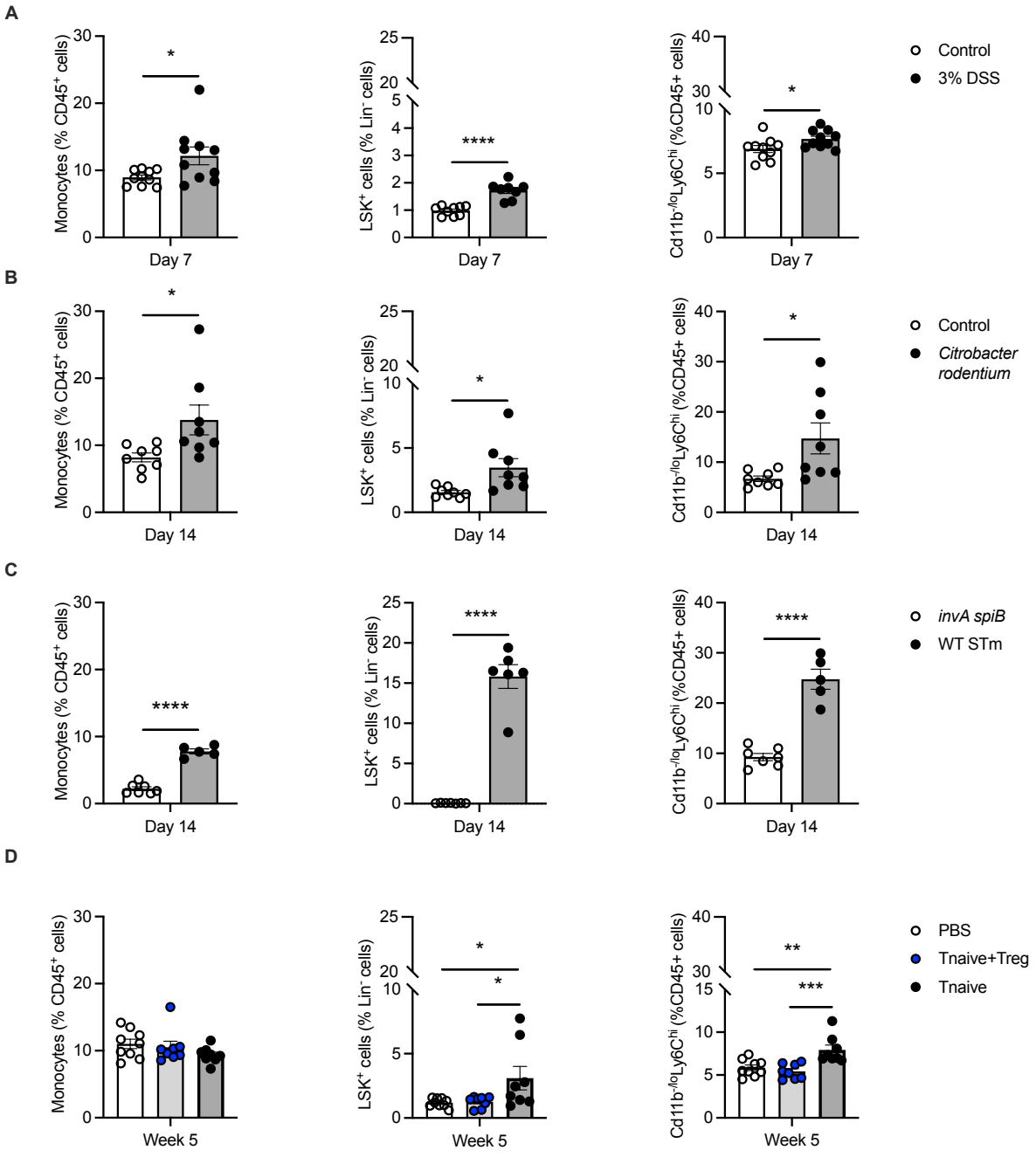

Figure 12. Multiple murine models of colitis alter the relative abundance of osteoclast precursors within the bone marrow.

(A) C57BL/6J mice were administered either water (control, open circles) or 3% DSS (closed circles) for 7 days. (B) C57BL/6J Mice were mock-infected (mock) with Luria broth or infected with *C. rodentium* via oral gavage. (C) CBA/J mice were infected via oral gavage with either a *S.*

enterica serovar Typhimurium (STm) mutant (*invA spiB*) or WT IR715 STm. (D) *Rag1*$^{-/-}$ mice were injected with either 5.0x10^{5} CD4^{+}CD25^{-}CD45RB^{hi} T cells (Tnaive), a non-colitis control of a 5:1 ratio of Tnaive cells with CD4^{+}CD25^{+} T-regulatory cells (Treg), or PBS via intraperitoneal injection. Tibias and femurs were harvested at the indicated time points, and bone marrow was collected for flow cytometry. Bone marrow cells were stained with a panel of antibodies to identify monocytes by lineage (CD45^{+}Ter119^{-}CD3^{-}B220^{-}Cd11b^{+}LyC^{+}Ly6G^{-}), LSK cells (Lin^{-} sca-1^{+}c-kit^{+}), and Cd11b$^{-/lo}$Ly6C^{hi} osteoclast precursors (CD45^{+}Ter119^{-}CD3^{-}B220^{-}Ly6G^{-}Cd11b$^{-/lo}$Ly6C^{hi}). Error bars represent mean ± S.E.M. Data analyzed via Student's t-test (A-C) or one-way ANOVA with Šidák multiple comparisons test (D). n = 5-10 mice per group. * p<0.05, ** p<0.01, *** p<0.001, **** p<0.0001.

Osteoclast precursors display altered surface expression of receptors involved in osteoclast trafficking, differentiation, and function during DSS colitis

Previous work has shown that the $Cd11b^{-/lo}Ly6C^{hi}$ OCP population is highly osteoclastogenic, has distinct surface cytokine receptor expression patterns compared to other myeloid cells, expresses many receptors associated with osteoclast differentiation and function, and suppresses T cells (82). Therefore, we next determined if colitis alters the surface expression of receptors important in osteoclast trafficking, differentiation, and function in OCPs from mice with and without DSS colitis. We focused on early time points after DSS administration given that we observed an increase in OC formation *in vivo* prior to trabecular bone loss (**Figure 6I-K).** Because we observed significant increases in the femoral abundance of MCP-1/CCL-2 in mice treated with DSS prior to bone loss, we first examined the expression of the CCL-2 receptor, CCR2 (**Figure 9D** and **Figure 10C**). We found that OCPs exhibited increased CCR2 expression during DSS colitis compared to controls (**Figure 13B**). Given that CCL-2/CCR2 signaling governs monocyte egress to sites of inflammation, such as the inflamed intestine, we next examined the expression of the tethering factor, CXCR4, which retains $Ly6C^{hi}$ monocytes within the bone marrow (212). OCPs from mice with DSS colitis also demonstrated increased CXCR4 expression compared to control mice (**Figure 13C**). To determine if OCPs from DSS-treated mice express markers associated with immunosuppressive activity, we evaluated the surface expression of CX_3CR1 and observed a significant decrease in CX_3CR1 MFI (**Figure 14**). Next, we measured surface expression of receptors that govern osteoclast differentiation. We detected a significant decrease in RANK expression and a trending decrease in CSF1R (**Figure 13D-E**). Since we observed significant increases in several MDL-1-associated cytokines (*e.g.*, G-CSF, TNF-α, IL-23, and MCP-1/CCL2) in the femurs of mice with colitis, we evaluated MDL-1

expression on OCPs during DSS treatment (**Figure 9D** and **Figure 10**) (139, 148, 195, 197). OCP MDL-1 expression and the percentage of MDL-1^{+} OCPs were significantly increased during DSS colitis (**Figure 13F-H**). MDL-1 expression on OCPs was also significantly increased in *Rag1*$^{-/-}$ mice given DSS (**Figure 13I-K**).

We noted similar, but less dramatic, increases in additional pro-osteoclastogenic co-receptors including OSCAR, PIR-A/B, and TREM2 (**Figure 15A-B**). Increased OCP proliferation may represent one mechanism of increased osteoclast formation *in vivo*, as previous work has demonstrated that OCPs proliferate *ex vivo* in response to M-CSF (82). To test the hypothesis that increased cellular proliferation may contribute to the increased osteoclast formation *in vivo*, we evaluated intracellular Ki67 levels. DSS treatment significantly increased Ki67 MFI but not percent positive Ki67 OCPs during DSS colitis (**Figure 15C-D**). Collectively, these data highlight that OCPs derived from mice subjected to DSS-induced intestinal inflammation demonstrate a unique surface expression pattern of cytokine, chemokine, and osteoclast co-receptors associated with inflammation and enhanced osteoclastogenesis.

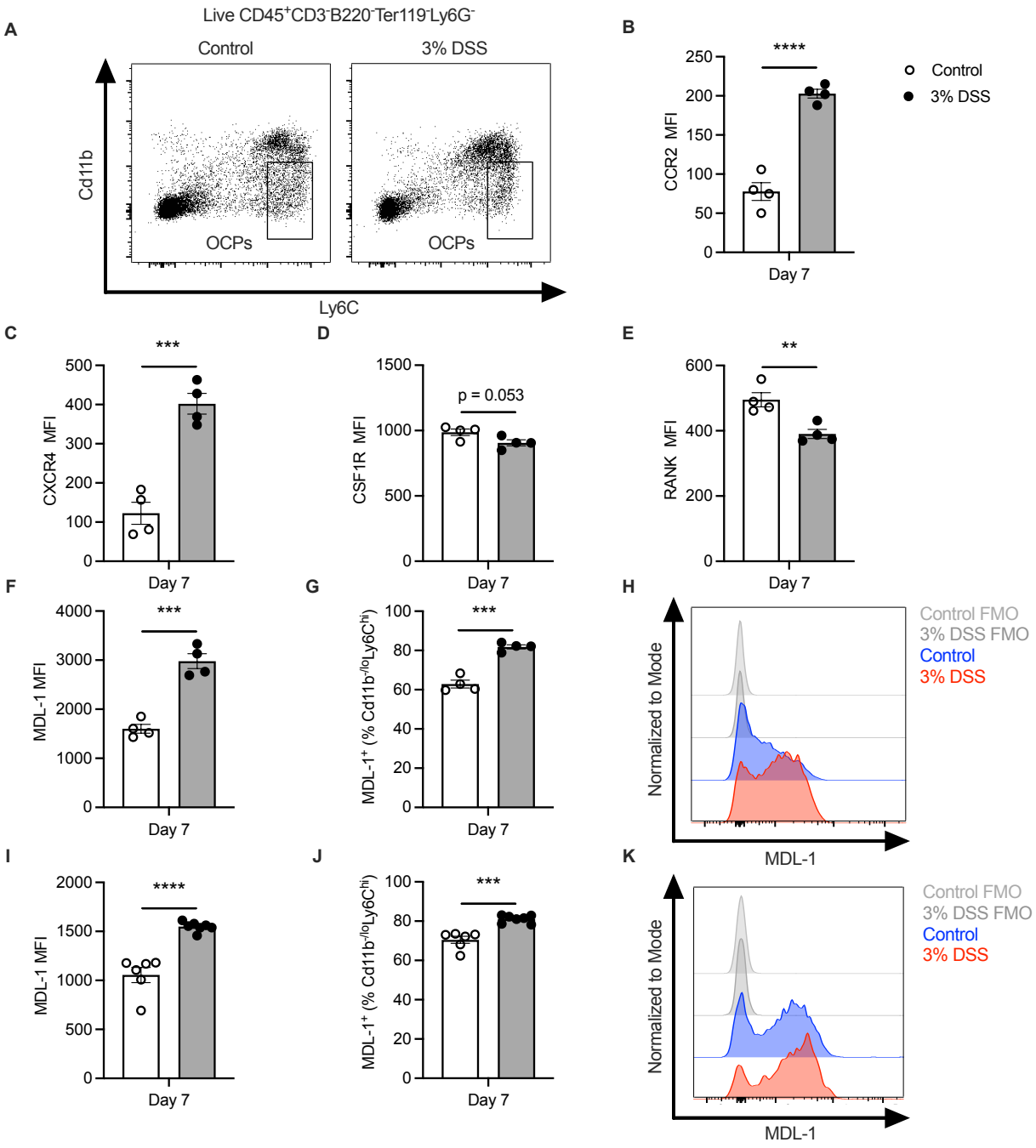

Figure 13. Osteoclast precursors isolated from mice with DSS colitis demonstrate altered expression of receptors involved in osteoclast differentiation and function.

C57BL/6J (A-H) or *Rag1*$^{-/-}$ (I-K) mice were administered 3% DSS or water (control) for 7 days, after which bone marrow was processed for flow cytometry. (A) Gating strategy for Cd11b^{-}

$^{/lo}$Ly6C^{hi} osteoclast precursors (OCPs). (B-F) Mean fluorescence intensity (MFI) of surface markers related to osteoclast differentiation and function from C57BL/6J mice with (filled circles) or without (open circles) colitis including CCR2 (B), CXCR4 (C), colony stimulating factor 1 receptor (CSF1R) (D), receptor activator of nuclear factor kappa-B (RANK) (E), and myeloid DNAX activation protein 12 (DAP-12)-associating lectin-1 (MDL-1) (F). (G) Percent positive MDL-1 OCPs. (H) Representative histogram of MDL-1 distribution among osteoclast precursors. (I) OCP MDL-1 MFI, percent MDL-1^{+} OCPs (J), and representative histogram of MDL-1 staining (K) on OCPs derived from *Rag1*$^{-/-}$ mice with or without colitis. FMO = fluorescence minus one control. Error bars represent mean ± S.E.M. Data analyzed via Student's t-test. n = 4-7 mice per group. ** $p<0.05$, *** $p<0.001$, **** $p<0.0001$.

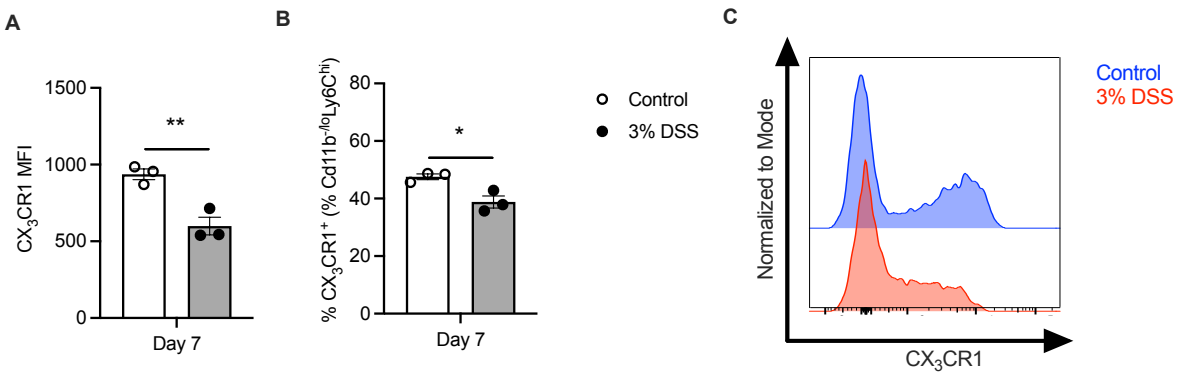

Figure 14. CX_3CR1 expression on OCPs from mice with DSS colitis.

C57BL/6J mice were administered 3% DSS (closed circles) or water (control, open circles) for 7 days, after which time bone marrow was processed for flow cytometry. $Cd11b^{-/lo}Ly6C^{hi}$ osteoclast precursors (OCPs) were stained for CX_3CR1 expression. (A) Mean fluorescence intensity (MFI). (B) Percent positive CX_3CR1 OCPs. (C) Representative histogram of CX_3CR1 distribution among osteoclast precursors. Error bars represent mean ± S.E.M. Data analyzed via Student's t-test. n =3 mice per group. * $p<0.05$, ** $p<0.01$.

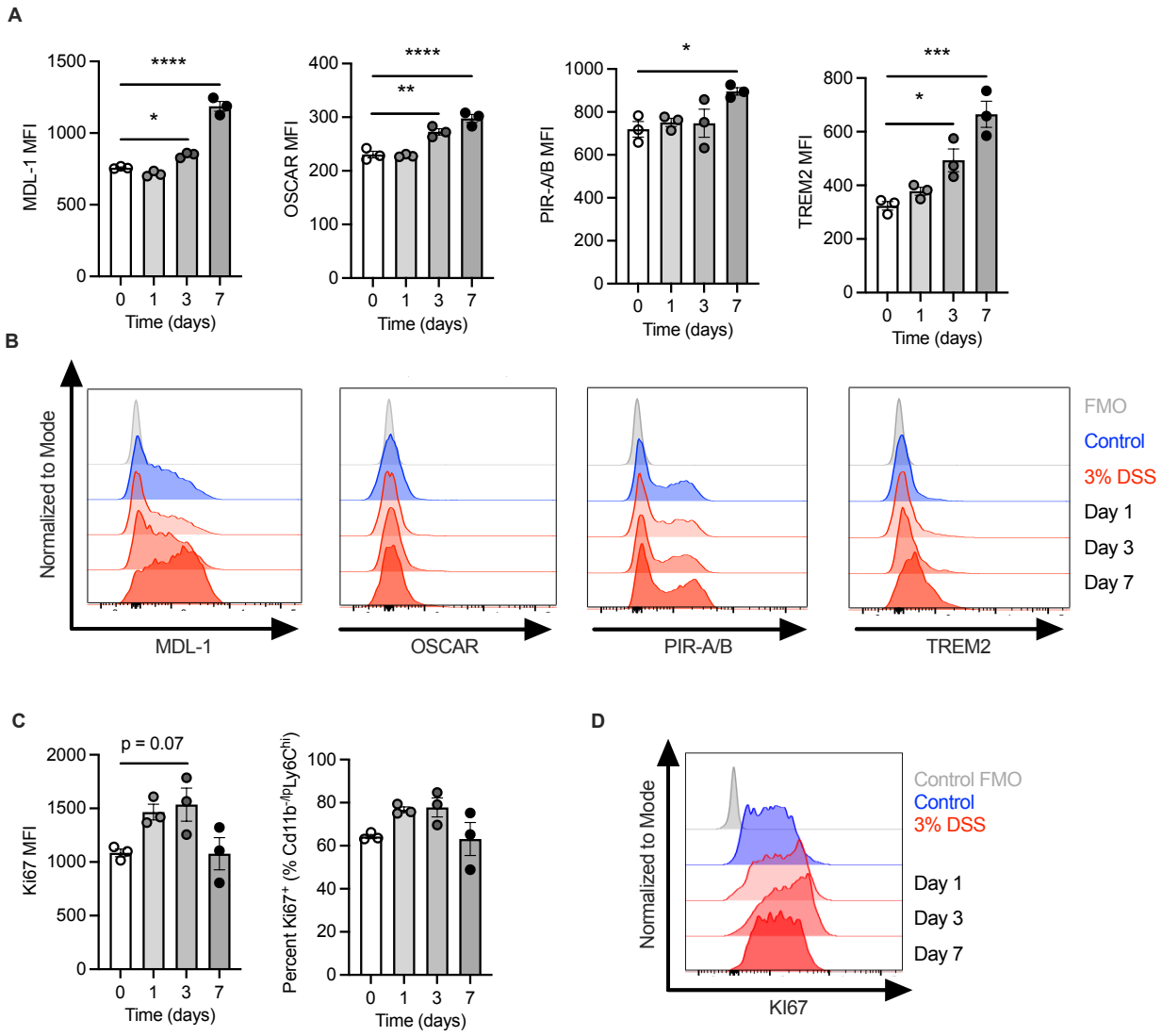

Figure 15. DSS-induced colitis alters osteoclast co-receptor expression within the bone marrow.

C57BL/6J mice were administered either 3% DSS or water (control) for 7 days. Bone marrow was isolated from the long bones of mice with or without colitis on the indicated day and processed for flow cytometry. $Cd11b^{-/lo}Ly6C^{hi}$ osteoclast precursors (OCPs) were stained for either MDL-1, OSCAR, PIR-A/B, TREM2, or intracellular Ki67. (A) Mean fluorescence intensity (MFI) of osteoclast co-receptors at the indicated time point following DSS administration and (B) representative histogram of osteoclast co-receptor staining. (C) MFI of

$Cd11b^{-/lo}Ly6C^{hi}$ OCP intracellular Ki67 staining at the indicated time point following 3% DSS administration and (D) representative histogram of Ki67 staining. Error bars represent mean ± S.E.M. Data analyzed via one-way ANOVA with Šidák multiple comparisons test. n = 3 mice per group. * $p<0.05$, ** $p<0.01$, *** $p<0.001$, **** $p<0.0001$.

Anti-MDL-1 treatment blunts the osteoclastogenic potential of OCPs from mice with colitis and ameliorates colitis-associated bone loss

Given the increase in surface receptors associated with osteoclast differentiation and function, we next tested whether OCPs from mice with colitis are more prone to forming OCs than those derived from healthy controls. To test this hypothesis, we sorted purified $Cd11b^{-/lo}Ly6C^{hi}$ OCPs, $Cd11b^{hi}Ly6C^{+}$ monocytes, or $Cd11b^{-}Ly6C^{-}$ double negative cells from the bone marrow of mice with or without DSS colitis and cultured these cells in the presence of exogenous M-CSF and RANKL. We observed that DSS treatment increased the *ex vivo* osteoclastogenic potential of purified monocytes, OCPs, and unsorted whole bone marrow (**Figure 16A**). OCPs displayed the highest osteoclastogenic potential (**Figure 16A**). Given the increased surface expression of the pro-osteoclastogenic coreceptor MDL-1 on DSS-derived OCPs, we assessed whether *ex vivo* anti-MDL-1 treatment could blunt the enhanced osteoclast formation potential of these cells. Anti-MDL-1 treatment abrogated the increased osteoclast formation in DSS-derived OCPs, as sorted OCPs from DSS-treated mice exhibited a marked reduction in osteoclast formation *ex vivo* when treated with anti-MDL-1 antibody compared to isotype control-treated cells (**Figure 16A**). Anti-MDL-1 treatment also reduced the number of osteoclasts *ex vivo* in OCPs from control mice (**Figure 16A**). We next evaluated whether *in vivo* anti-MDL-1 treatment can prevent bone loss during DSS colitis *in vivo*. Given that we observed an increase in OCP MDL-1 expression as early as day 3 following DSS administration (**Figure 15A-B**) we administered monoclonal anti-MDL-1 antibody or IgG isotype control treatment to DSS-treated mice at day 3 following colitis induction (**Figure 16B**). Anti-MDL-1 treated mice demonstrated no significant differences in histologic injury and demonstrated similar weight changes compared to IgG control treated mice during colitis (**Figure 16C-D**). Mice treated with

anti-MDL-1 demonstrated a 27% increase in BV/TV compared to mice treated with isotype control, which was associated increased trabecular thickness and connective density but not trabecular separation or number (**Figure 16E-J**). One important remaining question of this work is if baseline bone architecture is altered during anti-MDL-1 treatment. To this end, I treated mice with 50 μg of either IgG isotype or anti-MDL-1 four days after acquiring baseline weight measurements and monitored mice for weight loss for an additional ten days to mirror experimental scheme in (**Figure 16**). Following 14 days, I harvested femurs for micro CT analysis of trabecular bone. I did not detect differences in baseline weight or trabecular bone parameters between IgG isotype or anti-MDL-1 treated mice without colitis (**Figure 17**). These findings suggest that anti-MDL-1 does not impact baseline trabecular architecture. Collectively, these data reveal that OCPs derived from mice with intestinal inflammation have enhanced osteoclastogenesis *ex vivo*, that this increased osteoclast formation is associated with increased MDL-1 surface expression on OCPs, and that *in vivo* anti-MDL-1 treatment ameliorates bone loss during DSS colitis. In total, this study showed that multiple murine models of intestinal inflammation resulted in trabecular bone loss via an altered bone marrow cytokine environment that promotes enhanced osteoclast formation through an expansion of MDL-1^{+} OCPs.

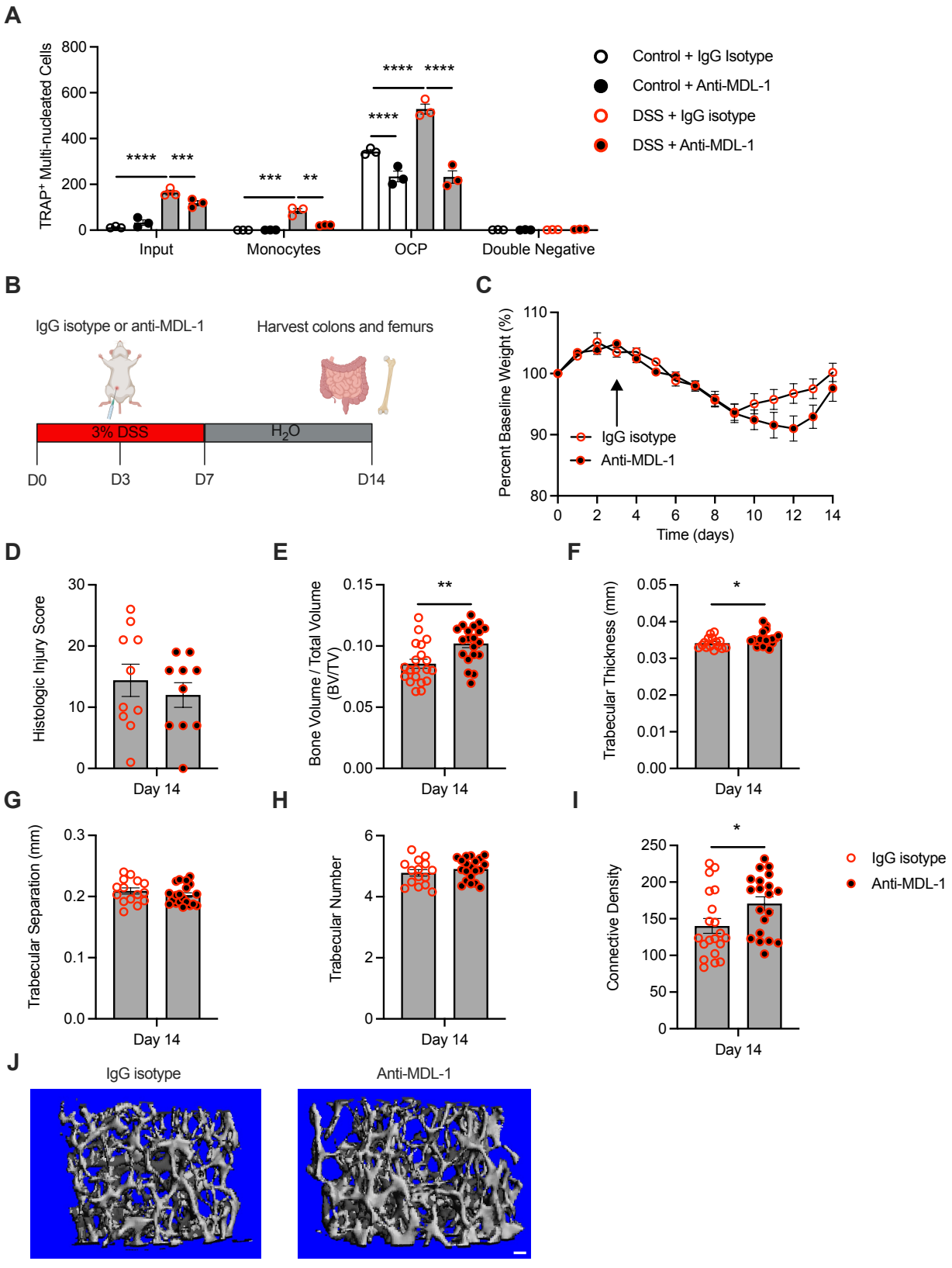
A
TRAP⁺ Multi-nucleated Cells
800
600
400
200
0
Input
Monocytes
OCP
Double Negative
Control + IgG Isotype
Control + Anti-MDL-1
DSS + IgG isotype
DSS + Anti-MDL-1
B
IgG isotype or anti-MDL-1
Harvest colons and femurs
3% DSS
H2O
D0
D3
D7
D14
C
Percent Baseline Weight (%)
Time (days)
IgG isotype
Anti-MDL-1
D
Histologic Injury Score
Day 14
E
Bone Volume / Total Volume (BV/TV)
Day 14
F
Trabecular Thickness (mm)
Day 14
G
Trabecular Separation (mm)
Day 14
H
Trabecular Number
Day 14
I
Connective Density
Day 14
IgG isotype
Anti-MDL-1
J
IgG isotype
Anti-MDL-1

Figure 16. Anti-MDL-1 treatment blunts *ex vivo* osteoclastogenesis and protects against colitis-associated bone loss *in vivo*.

(A) C57BL/6J mice were administered either 3% DSS or water (control) for 7 days. Bone marrow was isolated on day 7 following DSS treatment from the long bones of mice with or without colitis and processed for fluorescent automated cell sorting (FACS). Unsorted whole bone marrow (input), $Cd11b^{+}Ly6C^{+}$ monocytes, $Cd11b^{-/lo}Ly6C^{hi}$ osteoclasts precursors (OCPs), or $Cd11b^{-}Ly6C^{-}$ (double negative) cells were seeded at either $5.0x10^{4}$ (input) or 1.0×10^{4} cells/mL (sorted), differentiated for 4 days with 5% v/v CMG14-12 supernatant and 35 ng/mL RANKL in the presence or absence of 10 μg/mL IgG isotype control or anti-MDL-1 antibody. After 4 days, cells were stained for TRAP and multi-nucleated $TRAP^{+}$ cells were manually enumerated. (B) Experimental design for *in vivo* anti-MDL-1 antibody treatment. C57BL/6J mice were administered 3% DSS for 7 days, after which time mice were switched to water. At day 3 following DSS administration, mice received a single dose of 50 μg of either IgG isotype control or anti-MDL-1 antibody via intraperitoneal injection. Colons and femurs were harvested at day 14 following DSS administration. Created with BioRender.com. (C) Percent baseline weight of DSS-treated mice receiving either isotype control or anti-MDL-1 antibody. Arrow indicates time of IgG isotype or anti-MDL-1 antibody. (D) Histologic injury score of hematoxylin and eosin (H&E) colons from DSS-treated mice receiving either isotype control or anti-MDL-1 antibody. (E-J) Micro-computed tomography (micro CT) analysis of formalin-fixed femurs from DSS-treated mice receiving either isotype or anti-MDL-1 antibody for trabecular bone volume per total volume (BV/TV) (E), trabecular thickness (F), trabecular separation (G), trabecular number (H), connective density (I), and representative three-dimensional reconstruction of trabecular bone from mice treated with either isotype or anti-MDL-1 antibody

(J). Scale bar = 100μm. Error bars represent mean ± S.E.M. Data analyzed via 2-way ANOVA with Šidák multiple comparisons test for comparisons within each sorted population (A) or Student's t-test. (D-I). n = 3 independent cultures (A) or 10-20 mice per group (C-I). * $p<0.05$, ** $p<0.01$, *** $p<0.001$, **** $p<0.0001$.

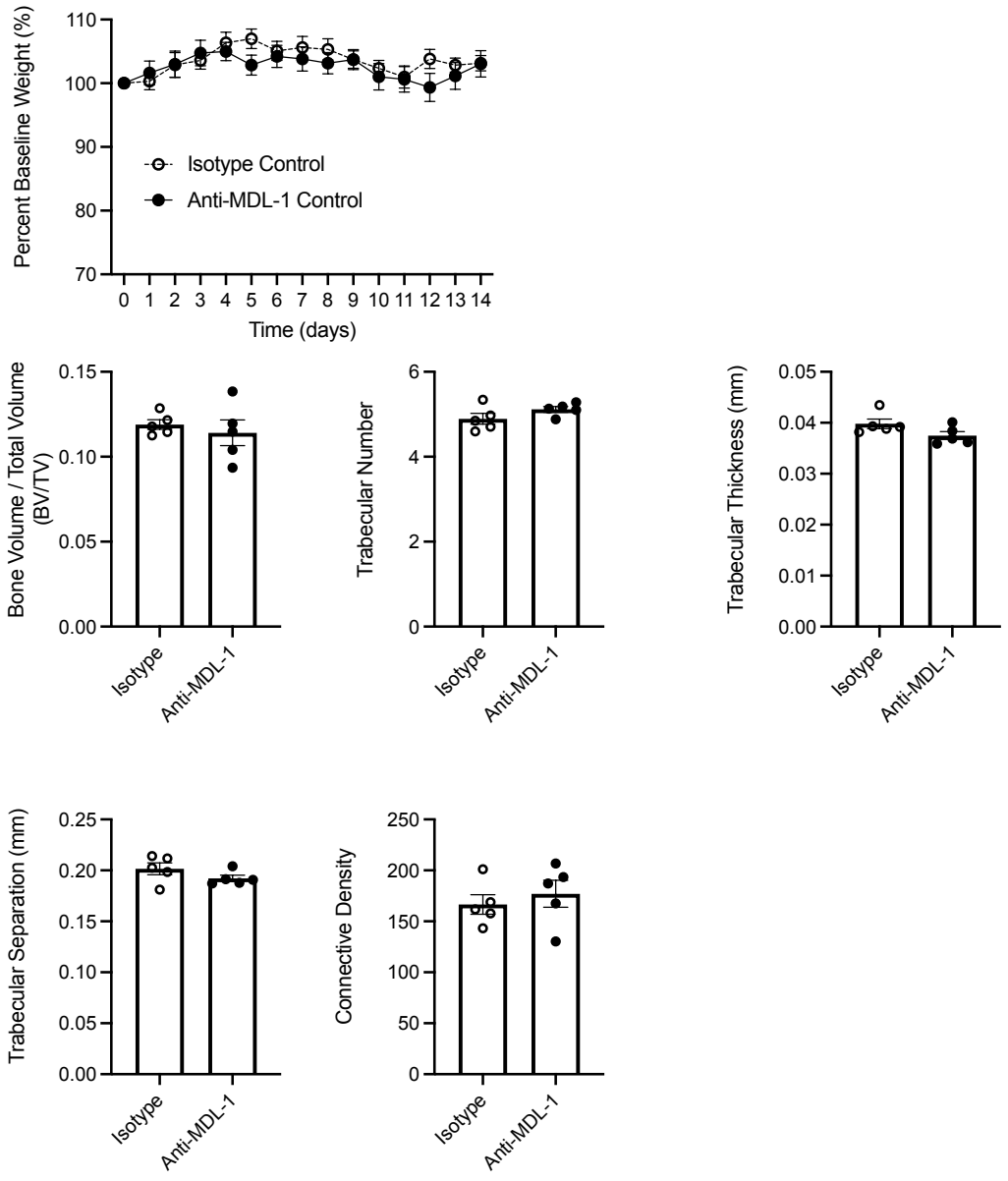

Figure 17. Anti-MDL-1 treatment does not alter baseline trabecular bone architecture.

Mice without colitis (7-week-old C57BL/6J females) were weighed daily for 14 days. On day 3, mice were administered 50 μg IgG isotype or anti-MDL-1 antibody. Femurs were harvest and evaluated for trabecular bone architecture at day 14. Error bars represent mean ± S.E.M. Data analyzed via Student's t-test.

Discussion

The data from this study demonstrate that multiple murine models of IBD result in concomitant bone loss. Significant increases in the relative abundance of a highly osteoclastogenic pre-osteoclast population were observed across four models of intestinal inflammation. Furthermore, this study reveals that during DSS colitis, OCPs demonstrate altered cytokine-, chemokine-, and osteoclast-associated receptors, as compared to OCPs from control mice. The changes to OCP surface receptor expression also occurred in *Rag1*$^{-/-}$ mice, suggesting that both the expansion and alteration of OCPs during DSS colitis are not solely dependent on interactions with inflammatory T cells, B cells, or their cytokines. OCPs from mice with colitis demonstrate increased osteoclast formation *ex vivo* when compared to OCPs derived from control mice, and this enhanced osteoclastogenesis is blunted by anti-MDL-1 antibody treatment. *In vivo*, a single dose of anti-MDL-1 antibody protects against bone loss during DSS colitis. In total, these findings suggest a significant role of inflammation-driven pathologic expansion of myeloid-derived MDL-1^{+} OCPs in bone loss during colitis.

We observed marked increases in cytokines and chemokines capable of inducing MDL-1 expression, most notably G-CSF, in the femurs of mice subjected to models of colitis. This increase in MDL-1-associated cytokines corresponded with a robust increase in expression of MDL-1 on OCPs. Recent evidence has linked MDL-1 with IBD pathogenesis, as MDL-1^{+} TNF-α^{+} monocytes have been found to be significantly increased in the lamina propria of patients with IBD (213). Furthermore, MDL-1 (*CLEC5A*) expression has been identified by single-cell RNA-seq as a gene associated with an inflammatory monocyte cytokine module within the Risk Stratification and Identification of Immunogenetic and Microbial Markers of Rapid Disease Progression in Children with Crohn's Disease (RISK) study (214).

In addition to mediating inflammatory responses, MDL-1 plays an important role in osteoclast formation and triggers osteoclastogenesis by forming a trimolecular complex with DAP-10 and DAP-12 (215). Previous work has demonstrated that OCPs express MDL-1, but studies to date have not examined how MDL-1 or other co-receptors involved in osteoclast differentiation and function change during intestinal inflammation (82). MDL-1 has been reported to form a complex with the IL-23R in human monocytes, and IL-23 treatment of human monocytes leads to both osteoclast differentiation and increased MDL-1 expression (195). Although we did not evaluate OCPs from human bone marrow, these prior studies utilizing human monocytes suggest that MDL-1^+ OCPs could potentiate IBD-associated bone loss in humans. Taken together, these observations suggest a mechanism whereby specific inflammatory cytokines associated with IBD pathogenesis impact the expression of osteoclast coreceptors on OCPs to drive osteoclastogenesis and bone loss.

In addition to increased MDL-1 expression, data from this study also demonstrate that OCPs exhibit increased expression of surface molecules important in osteoclast trafficking (CCR2 and CXCR4) during colitis. Elevated CCR2 may reflect that OCPs during colitis are primed to exit the bone marrow environment and traffic to the inflamed intestine. However, OCPs expressed higher levels of the tethering factor, CXCR4, indicating that these cells might instead be more tightly tethered to the bone marrow environment or contribute to replenishing monocyte pools (212). While G-CSF, which was significantly elevated in the bone across all models of colitis, has been shown to reduce CXCR4 expression in Gr-1^+ myeloid cells as a mechanism of mobilization, it conversely increases CXCR4 expression on HSCs (216, 217). OCPs were originally reported to retain clonogenic potential as measured by colony formation (82). Therefore, G-CSF may induce CXCR4 expression in OCPs in a manner similar to that

previously reported for HSCs. Future studies are needed to investigate how intestinal inflammation alters the tethering and mobilizations properties of OCPs.

While an expansion of OCPs represents one potential mechanism for increased osteoclastogenesis during DSS colitis, this study also demonstrates that colitis alters expression of surface receptors that directly govern osteoclast differentiation and function (RANK, CSF1R, MDL-1, OSCAR, TREM2, and PIR-A/B). OCPs from mice with DSS colitis demonstrated a subtle but statistically significant reduction in RANK expression. The functional consequences of reduced RANK are unclear, but DSS-derived OCPs maintained the ability to form robust osteoclasts *ex vivo* in response to treatment with respective ligands RANKL and M-CSF. TNF-α, which was increased in the femur homogenates across multiple murine models of colitis, has previously been shown to induce both OSCAR and PIR-A in addition to MDL-1 (140, 218). Accordingly, in addition to an increase in abundance of OCPs, enhanced sensitivity to pro-osteoclastogenic signals is likely a complementary mechanism that contributes to increased osteoclastogenesis and bone loss during DSS colitis.

In this Chapter, DSS colitis led to an increase in osteoclast formation in purified monocyte and OCP populations *ex vivo*. Given that OCPs from DSS-treated mice displayed similar Ki67 levels as controls at day 7 following DSS administration, cell cycling prior to exogenous M-CSF and RANKL administration likely does not explain these differences in osteoclast formation *ex vivo*. However, increased cell cycling earlier in colitis at days 1 and 3 following DSS colitis likely contributes to the expansion of OCPs.

There are some limitations of this work that will drive future studies. Because the goal of this study was to evaluate how intestinal inflammation alters osteoclasts and their precursors, we did not examine other important contributors to bone loss during IBD, such as nutrition or

alterations to osteoblast biology. Therefore, these data do not exclude additional complementary mechanisms of IBD-associated bone loss that occur through nutritional deficits or altered osteoblast function, which have been highlighted in previous studies (38, 40, 42, 50, 51, 219, 220). We did observe bone loss in colitis models that were not associated with significant weight loss, which is consistent with previous reports and may point to mechanisms that are independent of nutritional status (40). Future studies should address the relative contributions of OCPs, nutritional status, and osteoblast function in contributing to bone loss during intestinal inflammation. While several important osteoclast precursors were found to expand during colitis, this study did not evaluate alternative cell lineages (*e.g.*, dendritic cells) capable of osteoclastogenesis, and therefore cannot exclude their contribution to bone loss during intestinal inflammation. Anti-MDL-1 antibody treatment reduced osteoclast formation in OCPs isolated from DSS-treated mice *ex vivo*. Moreover, treating mice with a single dose of anti-MDL-1 antibody decreased bone loss *in vivo* during DSS colitis and did not significantly impact the severity of colitis. Previous work has demonstrated that blockade of MDL-1 prevents inflammatory-mediated bone loss in a murine model of inflammatory arthritis without impacting baseline bone formation (139). Yet, endogenous ligands for many osteoclast co-receptors, including MDL-1, remain poorly described. Deciphering the precise ligands that MDL-1 binds and understanding how monoclonal antibodies may disrupt these interactions remains an important area for future research. Ligands for DAP-12 associated receptors, such as MDL-1, are thought to be expressed on the same myeloid OCP populations (108). Future investigations will test if this therapeutic approach ameliorates bone loss in other models of intestinal inflammation. Furthermore, the generation of cell-specific knockouts of MDL-1 will also help to clarify cell-intrinsic versus cell-extrinsic roles of MDL-1 in colitis-associated bone loss. Additional work is

also needed to evaluate MDL-1 expression on OCPs derived from humans with active versus quiescent IBD. Overall, this study demonstrates that intestinal inflammation significantly alters pre-osteoclast populations and implicates the osteoclast co-receptor, MDL-1, as a potential target for the therapeutic amelioration of bone loss during colitis.

CHAPTER IV*: SALMONELLA ENTERICA* SUBSPECIES *ENTERICA* SEROVAR TYPHIMURIUM EXPLOITS RANK/RANKL SIGNALING TO PROMOTE SURVIVAL WITHIN MONOCYTES AND ENHANCE OSTEOCLASTOGENESIS

Introduction

Salmonella enterica subspecies *enterica* serovar Typhimurium (STm) is a Gram-negative intracellular pathogen that leads to a spectrum of diseases across a broad range of mammalian hosts (166, 167). In humans, infection with nontyphoidal *Salmonella* (NTS), such as STm, can lead to distinct clinical entities often linked to the host immune function. In infants or patients with immunodeficiencies and hemoglobinopathies, infection with NTS can lead to life threatening systemic disease, including osteomyelitis (169, 175). In immunocompetent individuals, NTS most commonly results in enteric infection (168). Although NTS enteric infection is self-limiting in most individuals, it is a leading cause of hospitalization and death amongst food borne diseases (168). In order to survive within the host, NTS serovars, such as STm, must successfully invade and replicate in host cells. However, the cellular reservoirs and mechanisms that allow for STm survival within host cells during the distinct clinical phenotypes that STm causes are still being uncovered.

One important route of entry for STm to successfully cause enteric disease is through usurping specialized microfold (M) cells, which are enmeshed within the follicle associated epithelia (FAE) atop lymphoid structures (*e.g.*, Peyer's patches) (**Figure 3**). M cells sample intestinal luminal content so that antigen presenting cells (APCs) can present dietary and microbial antigens to T and B lymphocytes in the underlying Peyer's patches or gut associated lymphoid tissue (GALT). Receptor activator of nuclear factor kappa B-ligand (RANKL) is necessary for driving M cell development (60–62, 221). M-cell inducing stromal cells produce RANKL to regulate M cell development within the intestine, and this process is further regulated

by M cell production of OPG to regulate this process (221, 222). Prior work has demonstrated that STm induces M cell development during infection and can promote the transdifferentiation of FAE cells into M cells (223). Intriguingly, this transdifferentiation was found to be dependent upon a specific STm SP-1 effector, SopB (223). These prior studies establish that RANKL signaling is upregulated during STm infection and that STm can alter a host RANK/RANKL signaling.

RANKL is a potent cytokine with pleotropic effects on many cell types. RANKL biology is most studied in the context of driving monocyte differentiation into bone resorbing osteoclasts (OCs). Within the lamina propria and lymphoid structures within the intestine, STm survives within mononuclear cells such as monocytes. Several mononuclear reservoirs for STm have been identified, although the precise mechanisms that promote STm survival within these cells are unclear (224, 225). Intriguingly, these reservoirs can occur at extra-intestinal sites such as the spleen (224). Furthermore, the impact of systemic, enteric, or skeletal STm infection on bone remodeling and osteoclastogenesis is not well understood. The goal of this study was to determine the impact of RANK/RANKL signaling on STm survival within monocytes and the corresponding host response to infection. Additionally, these experiments investigated the ability of STm to promote OC differentiation as a survival niche.

Materials and methods

Animal use

Male and female 7 to 9-week-old C57BL/6J (Stock # 000664), CBA/J (Stock # 000656), *MyD88*$^{-/-}$ (Stock # 009088), and *TLR4*$^{-/-}$ (Stock # 029015) mice were purchased through The Jackson Laboratory and maintained in our colony for at least one week prior to experimentation. C57BL/6J, CBA/J, *MyD88*$^{-/-}$, and *TLR4*$^{-/-}$ mice were bred homozygously. TdTomato-TRAP

reporter were acquired as a gift from Joseph Lorenzo, originally described and obtained from the laboratory of Masaru Ishii (226). TdTomato-TRAP reporter mice were bred by backcrossing to WT C57BL/6J mice such that one copy of the fluorescent reporter was maintained. C57BL/6J, CBA/J, and TdTomato-TRAP reporter mice were maintained in specific pathogen free (SPF) conditions. *MyD88*$^{-/-}$, and *TLR4*$^{-/-}$ mice were maintained in sterile conditions with autoclaved water, food, and bedding.

Human samples

Where indicated, PBMCs were purchased from Zen-Bio. Samples were collected with informed consent. Consistent with exemption category 4, work with deidentified commercial samples does not require IRB approval. PBMCs were enriched for $CD14^+$ monocytes per negative bead selection per the manufacturer's instructions (Miltenyi). Purity of $CD14^+$ monocytes was confirmed via flow cytometry. Single cell suspensions were washed with PBS, enumerated, and 1 million cells were pelleted in PBS prior to live/dead staining per the manufacturer's protocol (Zombie Violet, Biolegend). Cells were then washed with FACS buffer (PBS containing 3% FBS and 0.1% sodium azide). Non-specific antibody staining was blocked with human TruStain FcX (Biolegend) for 15 minutes at room temperature. The following anti-human antibodies were used: Anti-CD14-APC (clone M5E2) and anti-CD16-PE (clone 3G8). Samples were subsequently analyzed via flow cytometry as described below.

Mouse models of colitis

For experiments involving gastrointestinal-induced disease with STm, C57BL/6J or TdTomato-TRAP reporter mice were infected as previously described (174). Twenty-four hours prior to infection, mice were administered 20 mg streptomycin via oral gavage. Mice were then infected with $1.0x10^9$ CFUs of WT SL1344 STm. Where indicated, mice received 200 μg IgG

isotype (BioXCell, clone 2A3) or anti-RANKL (BioXCell, clone IK22/5) antibody via a single intraperitoneal injection either 48 hr or 24 hr prior to infection. Mice were weighed daily and monitored for disease progression. Organs and stool were collected at the experimental endpoint and either processed for flow cytometry or homogenized, serially diluted, and plated on MacConkey agar for enumeration of bacterial CFU per gram of tissue.

Flow cytometry

Bone marrow from femurs was flushed with cold alpha-minimal essential media (α-MEM). Red blood cells (RBCs) were lysed for 5 minutes with ammonium chloride potassium (ACK) lysing buffer, pelleted, resuspended in PBS, and passed through a 70 μm filter. Spleens were mechanically crushed through a 70 μm filter and processed for single cell suspensions and RBC lysis as described above. Peyer's patches and mesenteric lymph nodes were mechanically dissociated through a 70 μm filter to obtain single cell suspensions. Single cell suspensions were washed with PBS, enumerated, and 1 million bone marrow cells per sample were pelleted in PBS prior to live/dead staining per the manufacturer's protocol (Zombie Violet, Biolegend). Cells were then washed with FACS buffer (PBS containing 3% FBS and 0.1% sodium azide). Non-specific antibody staining was blocked with anti-CD16/32 (Biolegend, clone 93) for 15 minutes at room temperature. Single cell suspensions were stained with a cocktail of surface-staining antibodies to identify specific mononuclear cells. Unless otherwise indicated, all antibodies were purchased from Biolegend. The following anti-mouse antibodies were used: Anti-CD45-AlexaFluor700 (clone 30-F11), anti-Cd11b-BV605 (clone M1/70), anti-Ly6C-APC (eBioscience, clone HK1.4), anti-Ly6G-Pacific Blue (clone 1A8), anti-TER119-Pacific Blue (clone TER-119), anti-B220-Pacific Blue (clone RA3-6B2), and anti-CD3-Pacific Blue (clone 145-2C11). Cells were washed twice in FACS buffer and fixed in PBS with 2%

paraformaldehyde and analyzed using a 4-Laser Fortessa analytical flow-cytometer. Single cells were gated using successive gates including side scatter-area by forward scatter-area (SSC-A x FSC-A), side scatter-height by area (SSC-H x SSC-A), and forward scatter-height by area (FSC-H x FSC-A), followed by identifying live $CD45^+$ lineage negative (Lin^-) as $CD3^-B220^-Ter119^-Ly6G^-$ mononuclear cells. Data were analyzed using FlowJo software (Version 10, Tree Star Inc.).

***In vitro* infections**

In vitro infections were performed as outlined in Wu, *et al*., (227). Murine bone marrow monocytes (BMMs) were derived by flushing tibias and femurs with cold alpha-MEM. Red blood cells were lysed with ACK lysing buffer at room temperature for 10 minutes. Whole bone marrow cells were pelleted and differentiated for four days in alpha-MEM supplemented with 10% FBS, 1x penicillin/streptomycin, and 20% v/v CMG14-12 supernatant (equivalent to 100ng/mL M-CSF). BMMs were harvested by cell scraping and plated into 96-well plates at a density of $5.0x10^4$ cells / well. BMMs were plated for 5 days in the alpha-MEM supplemented with 10% FBS, 1x penicillin/streptomycin, and 5% v/v CMG14-12 (equivalent to 25 ng/mL). RANKL was added at 0, 1, 10, or 100 ng/mL for 1, 2, or 5 days in culture. For infection of human $CD14^+$ monocytes, cells were plated in 96-well plates at a density of $5.0x10^4$ cells / well and cultured for 5 days in alpha-MEM supplemented with 10% FBS, 1x penicillin/streptomycin, and 30 ng/mL human M-CSF. Human RANKL was added at 0, 10, or 100 ng/mL for 1, 2, or 5 days in culture. Two days prior to infection, WT STm IR715, WT STm SL1344, or Δ*invA::tetRA* Δ*spiB::KSAC invA spiB* (isogenic to STm IR715) were struck out onto LB plates and grown overnight at 37ºC. One day prior to infection, a single colony was inoculated from the LB plate into 5mL LB and grown for 14 hrs, shaking, at 37ºC in loosely capped 15mL conical tubes.

Cultures were back-diluted for 4 hrs at a 1:50 dilution prior to infection to normalize bacterial growth to the late logarithmic phase. Optical density 600 nm (OD 600) was used to measure bacterial density, and bacteria were diluted in un-supplemented alpha-MEM to the indicated multiplicity of infection (MOI). Cells were washed once with PBS prior to infection. Following infection, plates were centrifuged at 1,000 x *g* for 10 minutes to facilitate bacterial adherence to the cell monolayer and then cultured for 30 minutes at 37ºC with 5% CO_2 and 37% O_2. Cells were washed again with PBS to remove non-associated bacteria and then incubated in media containing 100 µg/mL gentamicin to eliminate extracellular bacteria for 1 hr at 37ºC with 5% CO_2 and 37% O_2. Cells were then washed again with PBS and switched to media containing 10 µg/mL gentamicin for the remainder of the experiment. At the experimental endpoint, cells were washed once with PBS and then stained with fluorescein diacetate (FDA) and propidium iodide (PI) for 5 minutes at room temperature to visualize live and dead cells. FDA/PI staining media was removed and cells were imaged in PBS on the Cytation 5 Imaging System (Biotek). Gen5 software (Biotek) was used to determine the number of cells per well. Cells were lysed in 0.1% triton X-100, serially diluted, and plated on LB agar for enumeration of bacterial CFUs. Bacterial CFUs were subsequently normalized to cell number.

Dynamic imaging of STm *in vitro* infections

Murine BMMs were differentiated and seeded as described above in Grenier µClear 96-well black plates (catalog # 655096). Cells were infected with STm IR715 containing chromosomally integrated mCherry under control of the P*trc* promoter (*glmS*::P*trc*-*mCherry*::FRT, kindly provided by Dr. Leigh Knodler) at the indicated MOI as described above with the modification that after removal of media containing 100 µg/mL gentamicin, cells were supplemented with alpha-MEM containing 10% FBS, 5% v/v CMG14-12 supernatant

(equivalent to 25 ng/mL M-CSF), and 10 μg/mL gentamicin. Cells were cultured for up to 76 hours following infection in a Cytation 5 imaging system with on-board CO_2 (set to 5.0%) and temperature (set to 37ºC) control. Four regions of interest (ROIs) with ~80% cell confluency were identified prior to kinetic imaging. Images were acquired every 4 hours at 20x magnification using phase contrast and Texas-Red filters. Z-stack images (spanning 5 μm, step size 2.5 μm) were acquired for each ROI. Deconvoluted Z stack projections were generated using in-house functions within the Gen5 software. Automated cell masking was performed using Gen5 software, which further identified infected cells with ≥ one mCherry infectious foci of > 1 μm. Percentage of infected cells, mCherry total and average area per infected cell, mCherry MFI per infected cell, and number of mCherry infectious foci per infected cell were calculated using Gen5 software.

***In vitro* inflammasome activation**

BMMs were differentiated as described above and plated into 96-well plates at a density of $5.0x10^4$ cells / well in alpha-MEM supplemented with 10% FBS, 1x penicillin/streptomycin, and 5% v/v CMG14-12 (equivalent to 25 ng/mL M-CSF) with the indicated dose and duration of RANKL. BMMs were cultured for 5 days before inflammasome activation. Prior to inflammasome activation, cells were either left unprimed or primed with 100 ng/mL ultra-pure *S. enterica* serovar Minnesota LPS (Invivogen) for either 24 hrs or 3.5 hrs. For activation of the NLRP3 inflammasome, cells received 100 ng/mL ultra-pure LPS *S. enterica* serovar Minnesota LPS for 3.5 hrs, followed addition of ATP (final concentration 5 mM) to the culture media for 30 minutes. Vehicle controls received LPS alone. For NLRC4 activation, cells received *B. anthracis* protective antigen (PA) (4 μg/mL) and *B. anthracis* lethal factor (LF) N terminal conjugated to either the PrgJ inner rod protein (200 ng/mL) (Invivogen) or PrgI needle protein (10 ng/mL)

(Invivogen). Vehicle controls received PA alone. Live infection with STm was also used for inflammasome activation, as described above but without the addition of gentamicin. Cell supernatants were collected for IL-1ß ELISA per the manufacturer's instructions (Abcam). Cell supernatants were also collected for detection of lactate dehydrogenase (LDH), per the manufacturer's instructions (Promega) and normalized to condition-matched wells treated with 4 µL 10% triton X-100 for 15 minutes.

***In vitro* osteoclast formation assays**

$5.0x10^4$ BMMs were seeded per well into 96 well plates supplemented with 5% v/v CMG14-12 supernatant (equivalent to 25ng/mL M-CSF) and 35 ng/mL RANKL. Cells were cultured for 2 days, at which point the cells infected with the indicated strain and MOI of STm as described above, with the exception that after the addition of 100 µg/mL gentamicin, the cells were washed with PBS and incubated in alpha-MEM containing 10% FBS, 5% v/v CMG14-12 supernatant (equivalent to 25 ng/mL M-CSF), and 10 µg/mL gentamicin in the presence or absence of 35 ng/mL RANKL for an additional 72 hrs. Cells were fixed and stained for TRAP per the manufacturer's instructions (Sigma). Cells were stained with DAPI and imaged using a Cytation 5 imaging system (Biotek) prior to manual enumeration of multi-nucleated $TRAP^+$ cells as osteoclasts.

Quantitative real-time polymerase chain reaction (qRT-PCR)

RNA was extracted from cell lysates using the RNeasy Mini Kit Plus (Qiagen) according to the manufacturer's instructions. cDNA was synthesized from isolated RNA using the qScript™ cDNA supermix (QuantBio) according to the manufacturer's instruction. cDNA was diluted in RNAse free water and subsequently used for qRT-PCR with the indicated primers (

Table 2), iQ SYBR Green Supermix (Bio-Rad). Samples were run on a Bio-Rad CFX96 Real-Time PCR system (Bio-Rad) for up to 50 cycles with a melting temperature of 55ºC. Data were analyzed using the $2^{-\Delta\Delta CT}$ method.

Micro-computed tomography of trabecular bone

Femurs were harvested at the indicated time point and fixed with 10% neutral buffered formalin for 48 h at 4ºC and then placed in 70% ethanol. Trabecular bone was analyzed using a µCT40 (Scanco Medical, AG Bassersdorf, Switzerland) and Scanco software. Images were acquired at 55 kVp and 145 mA with an isotropic voxel size of 12 µm and an integration time of 250 ms with 1000 projections collected per 360º rotation. Images were reconstructed, filtered (sigma = 0.8, support = 1.0), and thresholded at 200 mg HA/ccm. Trabecular bone at the distal femur was manually contoured every 10 slices starting 30 slices proximal to the growth plate and advancing proximally for 100 slices such that trabeculae were included, and cortical bone was excluded in accordance with ASBMR guidelines (209). Sections between manual contours were automatically contoured.

Table 2. Primer sequences used for qRT-PCR.

Forward and reverse primers were used to determine the expression of the given gene. Harvard PrimerBank ID (https://pga.mgh.harvard.edu/primerbank/index.html) given where applicable.

Gene	Sequence	Reference
ACTB	Forward: 5'-GGCTGTATTCCCCTCCATCG-3'	PrimerBank ID: 6671509a1
	Reverse: 5'-CCAGTTGGTAACAATGCCATGT-3'	
IRF8	Forward: 5'-AAGGTCACCGTGGTCCTTAG-3'	(228)
	Reverse: 5'-GGAAAGCCTTACCTGCTGAC-3'	

Statistical evaluation

Statistical analyses were conducted using GraphPad Prism Software (Version 9). Statistical significance was assessed using 2-tailed Student's t-test, ordinary one-way ANOVA with post- multiple comparison's test, or 2-way ANOVA with post-hoc multiple comparisons test as appropriate and as indicated in the figure legends. Differences were considered significant with a *p* value ($p< 0.05$). Post-hoc multiple comparisons test for significant differences within groups were only performed following a significant ANOVA *p* value ($p<0.05$).

Results

RANKL promotes STm intracellular survival within monocytes

To investigate if RANKL alters STm intracellular survival in monocytes, BMMs derived from C57BL/6J mice were infected in a gentamicin protection assay in the presence or absence of RANKL (**Figure 18**). Monocytes cultured in the presence of 10 or 100 ng/mL RANKL demonstrated significantly increased intracellular STm burdens when infected with WT strains SL1344 or IR715. Bacteria were not recovered in the gentamicin containing fraction. RANKL administration led to a 50-100-fold increase in intracellular bacterial burdens as early as 24 hours after administration (**Figure 18B**). Increasing the duration of RANKL administration sustained the 50-100 increase in STm burdens in both WT SL1344 and IR715 strains (**Figure 18**). To account for differences in cell number, bacterial burdens were normalized to cell number (**Figure 18C-D**). Normalizing to cell number also demonstrated significant increases in bacterial burdens with RANKL treatment (**Figure 18C-D**).

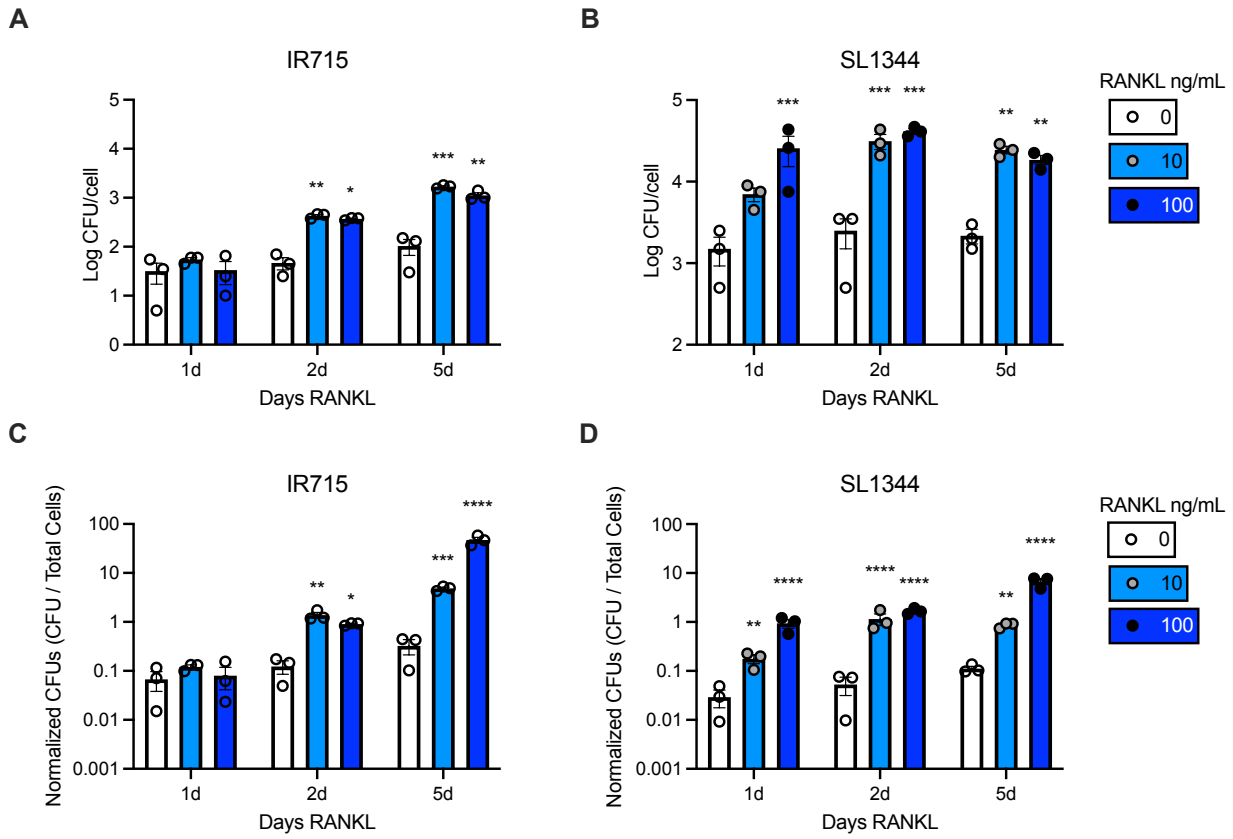

Figure 18. RANKL promotes intracellular STm survival in murine C57BL/6J BMMs.

Bone marrow macrophages (BMMs) were derived from C57BL/6J mice and cultured in the presence of M-CSF (CMG14-12 supernatant 5% v/v) with either 0, 10, or 100 ng/mL RANKL for 1, 2, or 5 days. BMMs were then infected (MOI = 1) with the either WT IR715 (A, C) or WT SL1344 (B, D) in a gentamicin protection assay for 24 hours. Cell lysates were serially diluted and plated for bacterial CFUs (A-B). Prior to lysis, cells were imaged on a Cytation 5 imaging system and counted using Gen 5 software to normalize bacterial burdens to cell number (C-D). Error bars represent mean ± S.E.M. Data representative of 4 independent experiments with similar results. Data analyzed via 2-way ANOVA with Tukey post-hoc test. * $p<0.05$, ** $p<0.01$, *** $p<0.001$, **** $p<0.0001$ compared to 0 ng/mL RANKL for a given time duration of RANKL treatment.

C57BL/6J mice lack the critical host restriction factor, NRAMP1, which has previously been shown to be a crucial determinant of susceptibility to STm infection (173). To determine whether RANKL may also increase the susceptibility of murine BMMs in an $NRAMP^{+}$ background, we performed a gentamicin protection assay in cells derived from $NRAMP^{+/+}$ CBA/J mice. Treatment with 100 ng/mL RANKL for two days and five days significantly increased intracellular STm burdens in CBA/J-derived BMMs infected with either IR715 or SL1344 WT STm (**Figure 19**). To assess if RANKL-mediated enhanced bacterial burdens were dependent on canonical innate-immune signaling pathways, we infected *TLR4*$^{-/-}$and *MyD88*$^{-/-}$ BMMs treated with 0 or 100 ng/mL RANKL for five days with STm. *TLR4*$^{-/-}$and *MyD88*$^{-/-}$ BMMs that were not treated with RANKL restrained intracellular STm burdens similar to WT cells infected with STm (**Figure 20**). RANKL treatment of *TLR4*$^{-/-}$and *MyD88*$^{-/-}$ BMMs led to a 1-2 log increase in intracellular STm burdens as early as one day following 100 ng/mL RANKL treatment, similar to what was observed in WT cells (**Figure 20**).

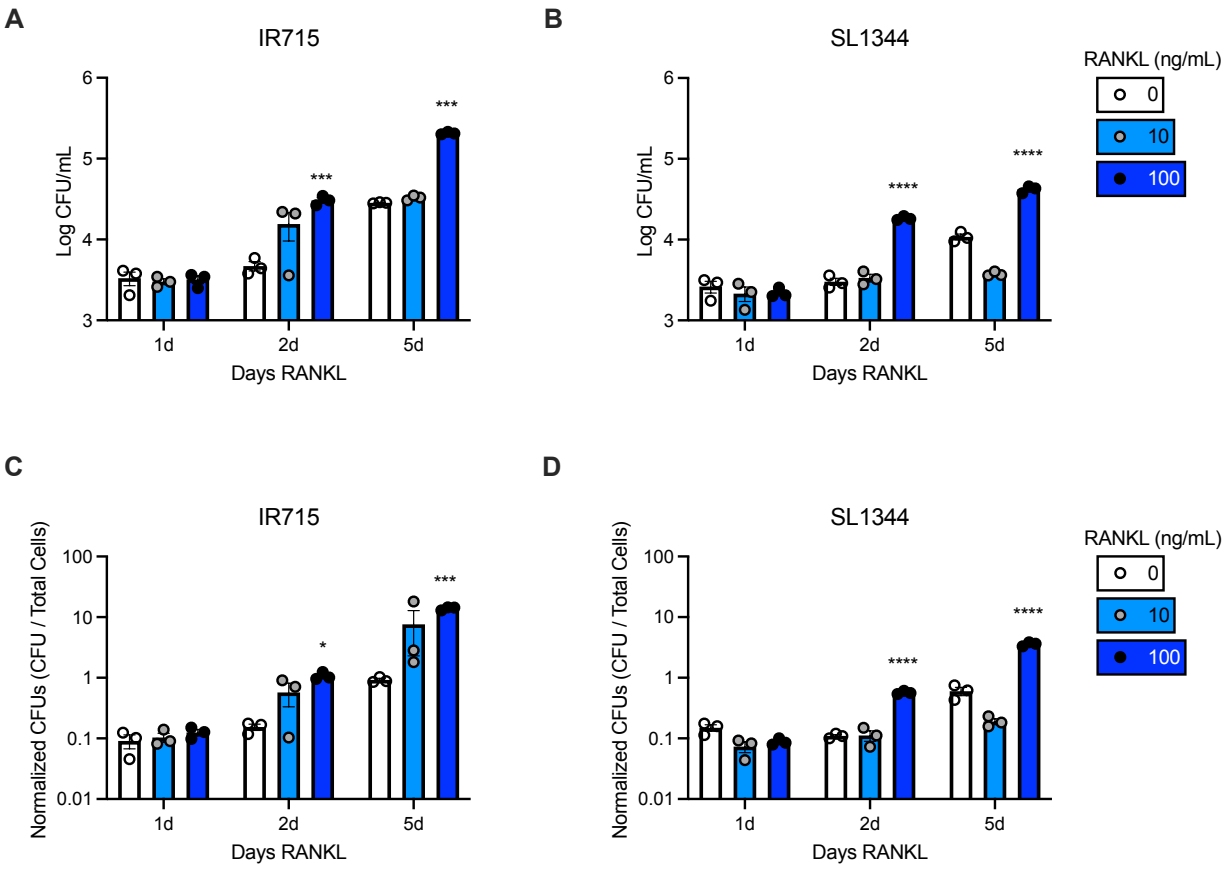

Figure 19. RANKL promotes intracellular STm survival in murine CBA/J BMMs.

Bone marrow macrophages (BMMs) were derived from CBA/J mice and cultured in the presence of M-CSF (CMG14-12 supernatant 5% v/v) with either 0, 10, or 100 ng/mL RANKL for 1, 2, or 5 days. BMMs were then infected (MOI = 1) with the either WT IR715 (A, C) or WT SL1344 (B, D) in a gentamicin protection assay for 24 hours. Cell lysates were serially diluted and plated for bacterial CFUs (A-B). Prior to lysis, cells were imaged on a Cytation 5 imaging system and counted using Gen 5 software to normalize bacterial burdens to cell number (C-D). Error bars represent mean ± S.E.M. Data analyzed via 2-way ANOVA with Tukey post-hoc test. * $p<0.05$, *** $p<0.001$, **** $p<0.0001$ compared to 0 ng/mL RANKL for a given time duration of RANKL treatment.

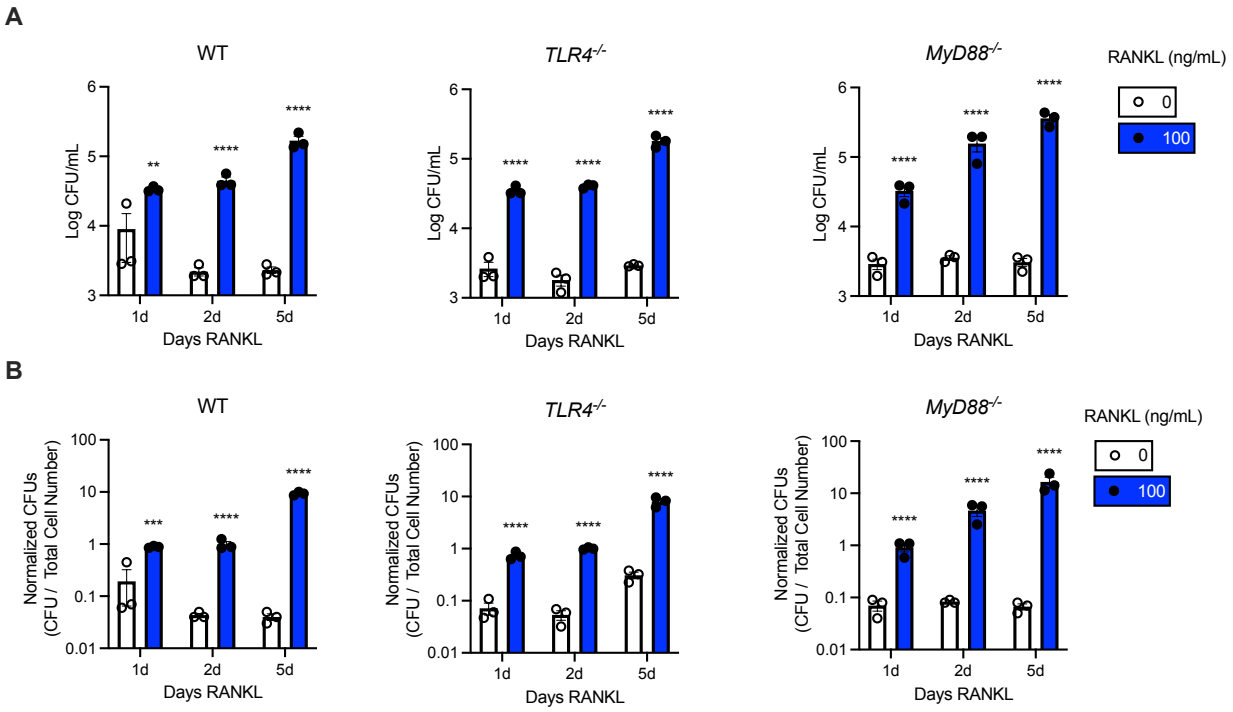

Figure 20. RANKL enhances intracellular STm burdens in *TLR4*$^{-/-}$ and *MyD88*$^{-/-}$ cells.

Bone marrow macrophages (BMMs) were derived from WT C57BL/6J, *TLR4*$^{-/-}$, and *MyD88*$^{-/-}$ mice and cultured in the presence of M-CSF (CMG14-12 supernatant 5% v/v) with either 0 or 100 ng/mL RANKL for 1, 2, or 5 days. BMMs were then infected (MOI = 1) with the WT IR715 in a gentamicin protection assay for 24 hours. Cell lysates were serially diluted and plated for bacterial CFUs (A). Prior to lysis, cells were imaged on a Cytation 5 imaging system and counted using Gen 5 software to normalize bacterial burdens to cell number (B). Error bars represent mean ± S.E.M. Data analyzed via 2-way ANOVA with Tukey post-hoc test. * p<0.05, *** p<0.001, **** p<0.0001 compared to 0 ng/mL RANKL for a given time duration of RANKL treatment.

To extend these findings to humans, we performed similar experiments in $CD14^+$ monocytes from healthy donor peripheral blood mononuclear cells (PBMCs), which express functional NRAMP. $CD14^+$ cells were isolated by magnetic negative selection and routinely isolated at > 95% purity (**Figure 21**). Treatment with two or five days of RANKL led to a 50-100-fold increase in intracellular STm (both IR715 and SL1344) survival across 3 independent donors (**Figure 22**). To complement CFU enumeration after lysing cell monolayers, we utilized a dynamic imaging approach. Here, we infected RANKL-treated monocytes with WT STm IR715 containing chromosomally integrated mCherry under control of the P*trc* promoter (*glmS*::P*trc-mCherry*::FRT, kindly provided by Dr. Leigh Knodler). Treatment with RANKL increased percent infected cells, average mCherry area, total mCherry area, as well as mCherry mean fluorescence intensity (MFI) during the course of infection (**Figure 23**). Additional experiments utilizing dynamic imaging with the *glmS*::P*trc-mCherry*::FRT reporter revealed that RANKL treatment significantly increased the number of mCherry infectious foci per cell over time, beginning at 16 hrs post-infection (**Figure 24**). Collectively, these data demonstrate that RANKL promotes STm survival within murine and human monocytes.

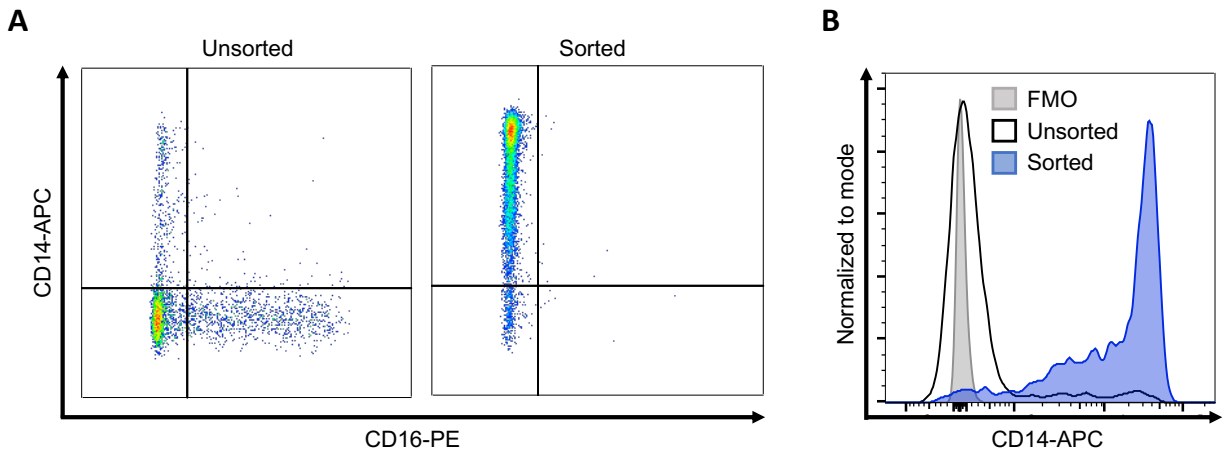

Figure 21. Negative selection enrichment of human CD14$^+$ cells.

Healthy human PBMCs from pooled donors (purchased from Zen-Bio) were enriched for CD14$^+$ cells via negative magnetic selection. (A) Sorted and unsorted fractions cells were assessed for CD14 and CD16 expression after gating for live, single cells. (B) Representative histogram for CD14 expression in live single cells of non-staining fluorescence minus one (FMO) control, unsorted cells, or sorted CD14$^+$ cells.

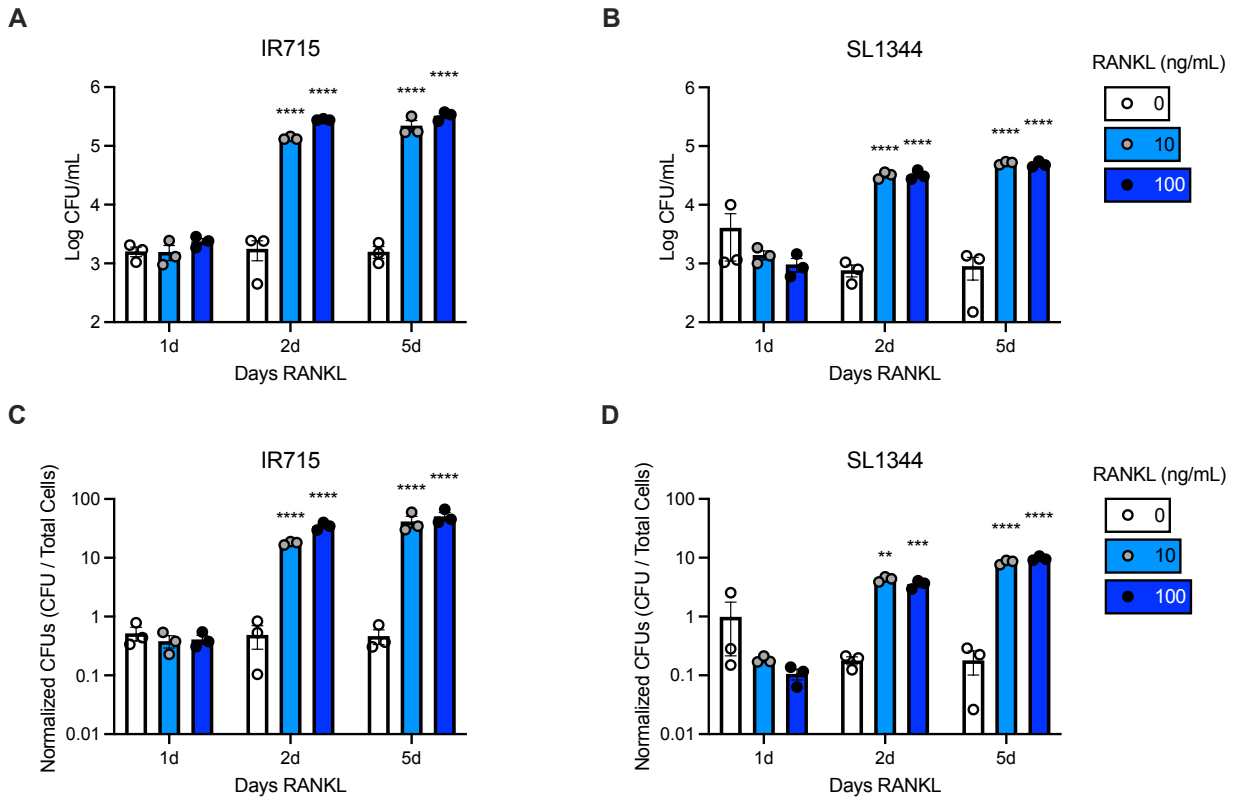

Figure 22. RANKL promotes intracellular STm survival in human CD14$^+$ monocytes. Human CD14$^+$ monocytes were isolated by magnetic negative selection from healthy donor peripheral blood mononuclear cells. CD14$^+$ monocytes were cultured with 30 ng/mL M-CSF with either 0, 10, or 100 ng/mL RANKL for 1, 2, or 5 days. Monocytes were then infected (MOI = 1) with the either WT IR715 (A, C) or WT SL1344 (B, D) in a gentamicin protection assay for 24 hours. Cell lysates were serially diluted and plated for bacterial CFUs (A-B). Prior to lysis, cells were imaged on a Cytation 5 imaging system and counted using Gen 5 software to normalize bacterial burdens to cell number (C-D). Data are representative of 3 independent experiments from 3 separate donors. Error bars represent mean ± S.E.M. Data analyzed via 2-way ANOVA with Tukey post-hoc test. ** p<0.01, *** p<0.001, **** p<0.0001 compared to 0 ng/mL RANKL for a given time duration of RANKL treatment.

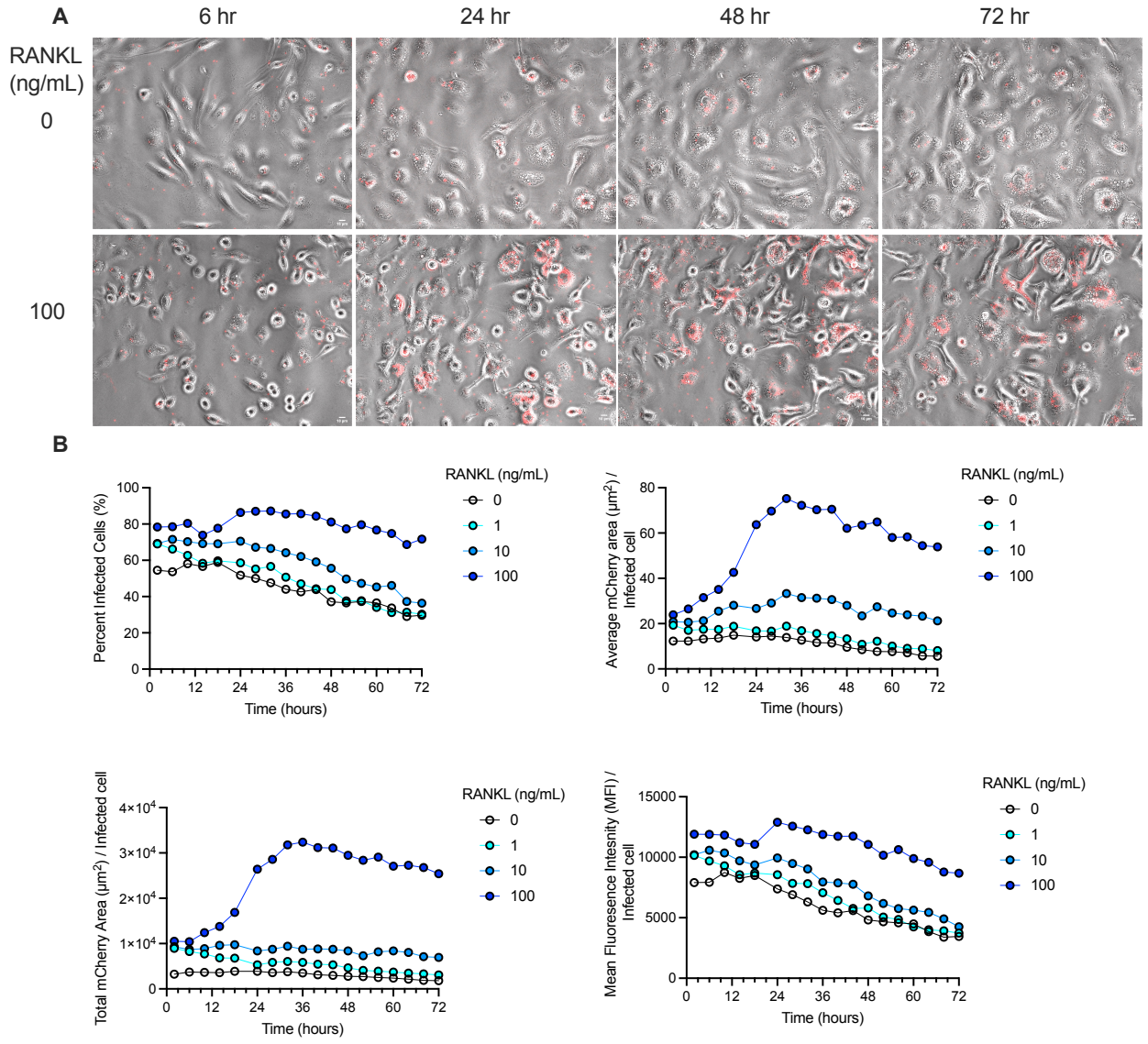

Figure 23. Dynamic imaging of STm-infected BMMs treated with RANKL.

BMMs were treated with 2d of 0, 1, 10, or 100 ng/mL RANKL and subsequently infected in a gentamicin infection assay with mCherry STm (MOI = 5) and imaged every 4 hrs for 72 hrs post-infection utilizing a BioTek Cytation 5 imaging system with on-board temperature (set to 37ºC) and CO_2 (set to 5.0%) control. Four regions of interest were imaged at 20x magnification with phase contrast and Texas-Red filters. (A) Representative images from 6, 24, 48, and 72 hrs post-infection of BMMs treated with either 0 or 100 ng/mL RANKL. (B) Quantification of

percent infected cells, average mCherry area per infected cell, total mCherry area per infected cell, and mean fluorescence intensity (MFI) per cell. Infected cells were determined via automated cell masking using Gen 5 Software.

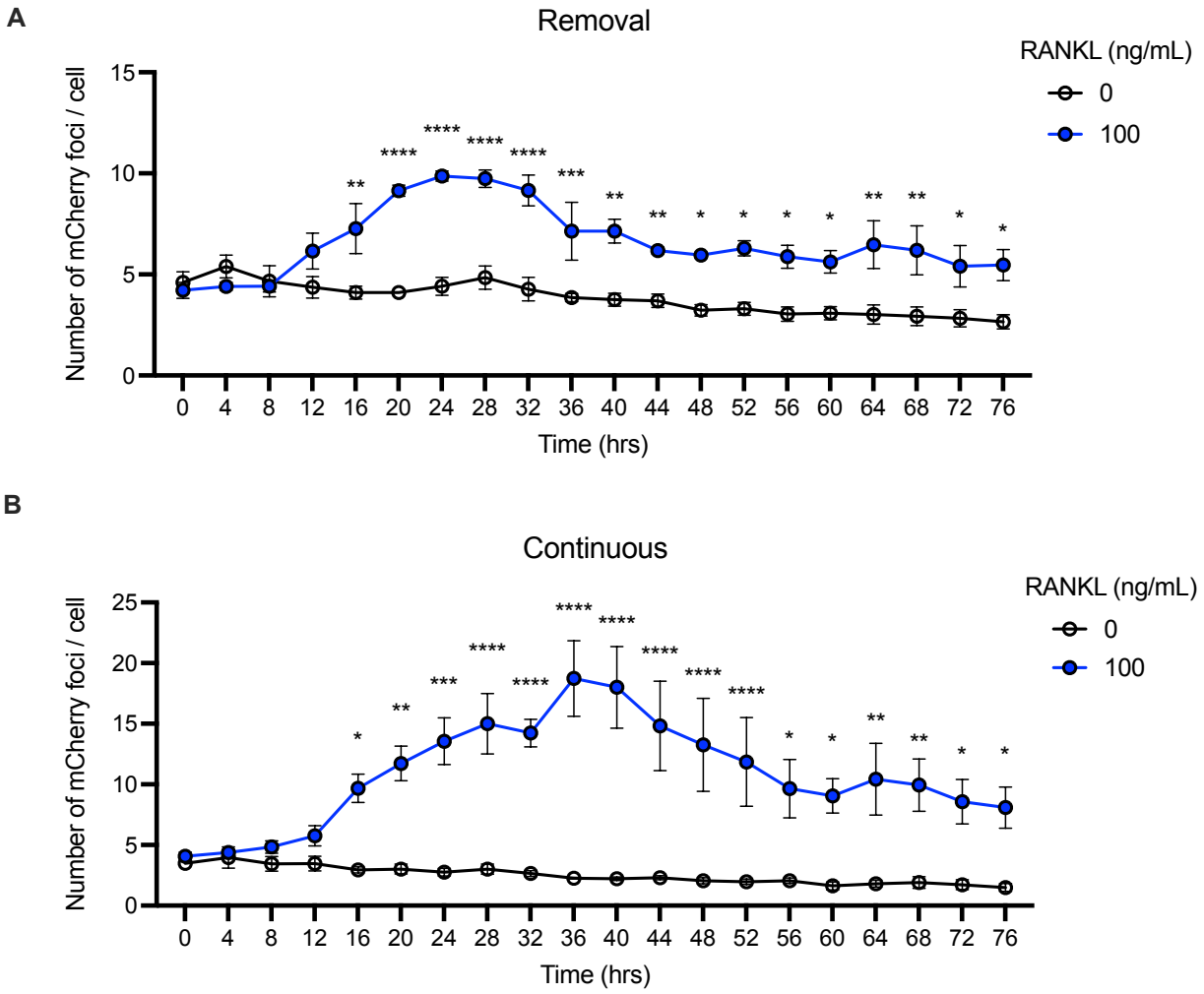

Figure 24. RANKL increases the number of STm infectious foci per cell.

BMMs were treated with 2d of 0 or 100 ng/mL RANKL and subsequently infected in a gentamicin infection assay with mCherry STm (MOI = 5) with either removal (A) or continuation (B) of RANKL treatment. Cells were imaged every 4 hrs for 76 hrs post-infection utilizing a BioTek Cytation 5 imaging system with on-board temperature (set to 37ºC) and CO_2 (set to 5.0%) control. Four regions across of interest across three independent replicates were imaged at 20x magnification with phase contrast and Texas-Red filters. Infected cells were determined via automated cell masking using Gen 5 Software and number of mCherry infectious foci per cell were enumerated. Error bars represent mean ± S.E.M. Data analyzed via multiple t

tests at each timepoint and corrected for multiple comparisons using the Holm-Šidák method. * $p<0.05$, ** $p<0.01$, *** $p<0.001$, **** $p<0.0001$.

RANKL dampens IL-1ß release in response to STm PAMPs

Given that we observed a 50-100-fold increase in intracellular STm during RANKL treatment, we next questioned whether STm infection of RANKL-experienced monocytes would result in increased inflammasome activation. Unexpectedly, monocytes treated with 5 days of either 10 or 100 ng/mL RANKL demonstrated reduced IL-1ß release in cell culture supernatants 4 hr post infection with WT IR715 STm (**Figure 25**). Importantly, RANKL was also able to dampen IL-1ß release from monocytes treated with LPS and ATP, canonical priming and activation signals of the NLRP3 inflammasome (**Figure 25**). A mutant lacking both the T3SS1 and T3SS2 type III secretion systems, Δ*invA::tetRA* Δ*spiB::KSAC invA spiB* (*invAspiB*) was unable to induce IL-1ß release (**Figure 25**). A mutant lacking just the T3SS2 type III secretion system, *sseD*, was able to induce IL-1ß release during infection, which was suppressed during treatment with 10 and 100 ng/mL RANKL (**Figure 25**). Both infection with WT IR715 and NLRP3 induction with LPS and ATP led to robust IL-1ß release in RANKL naïve cells (**Figure 25**). To assess if shorter durations of RANKL treatment were also able to dampen IL-1ß release during STm infection, we performed a similar experiment in murine BMMs treated with two days of 0, 10, or 100 ng/mL RANKL. Treatment with 10 and 100 ng/mL RANKL for two days led to significant reductions in IL-1ß detected in the cell culture supernatant (**Figure 26**).

To extend these findings to human STm infection, we performed similar experiments in human $CD14^+$ monocytes. Similar to murine derived BMMs, RANKL-treated human $CD14^+$ cells infected with STm demonstrated reduced IL-1ß compared to non-RANKL treated controls (**Figure 27**). To assess if reduced IL-1ß was associated with changes in cell death, we measured LDH levels in the cell culture supernatants. Human $CD14^+$ cells treated with 100 ng/mL RANKL for five days release significantly increased LDH compared to non-RANKL controls

(**Figure 28**). In order to determine whether differences in intracellular bacteria at 4 hrs post infection in RANKL vs non-RANKL treated cells may contribute to reduced IL-1ß production, we enumerated STm CFUs at 4 hrs post-infection. We did not detect significant differences in bacterial burdens at this timepoint (**Figure 29**). Taken together, these data indicate that RANKL treated monocytes exhibit a reduced IL-1ß response compared to non-RANKL controls during STm infection, despite demonstrating equivalent intracellular bacterial burdens.

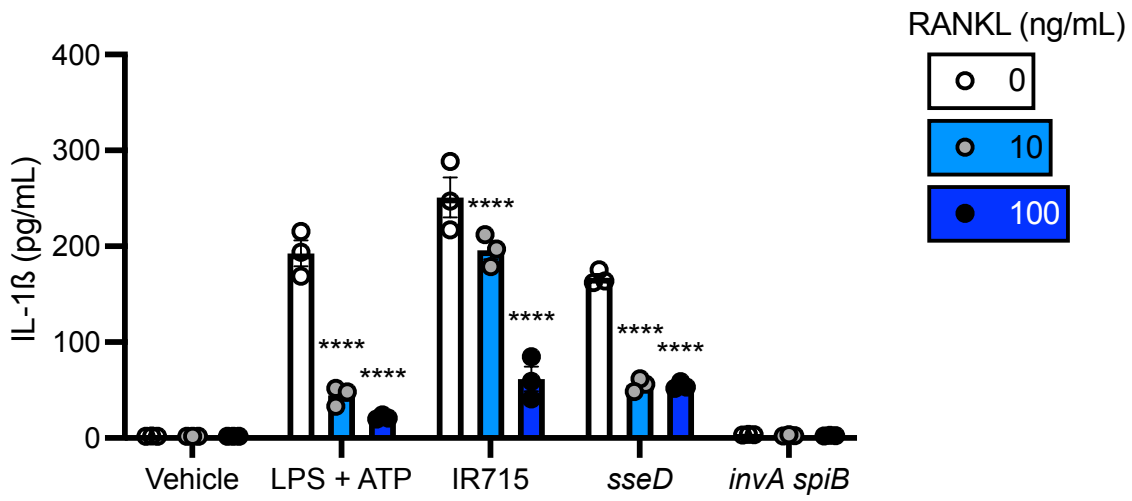

Figure 25. Five days of RANKL treatment blunts IL-1ß release in murine BMMs.

Murine BMMs derived from C57BL/6J mice were cultured for five days in the presence of M-CSF (CMG14-12 supernatant 5% v/v) with either 0, 10, or 100 ng/mL RANKL for 5 days. Cells were either treated with LPS alone (vehicle), infected with the indicated strain of STm (MOI = 1), or treated with LPS for 3.5hr followed by 30 minutes of 5 mM ATP. Cell supernatants were collected 4 hr post-infection and assessed for IL-1ß content via ELISA. Error bars represent mean ± S.E.M. Data analyzed via 2-way ANOVA with Dunnet post-hoc test. **** $p<0.0001$ compared to 0 ng/mL RANKL for a given time condition.

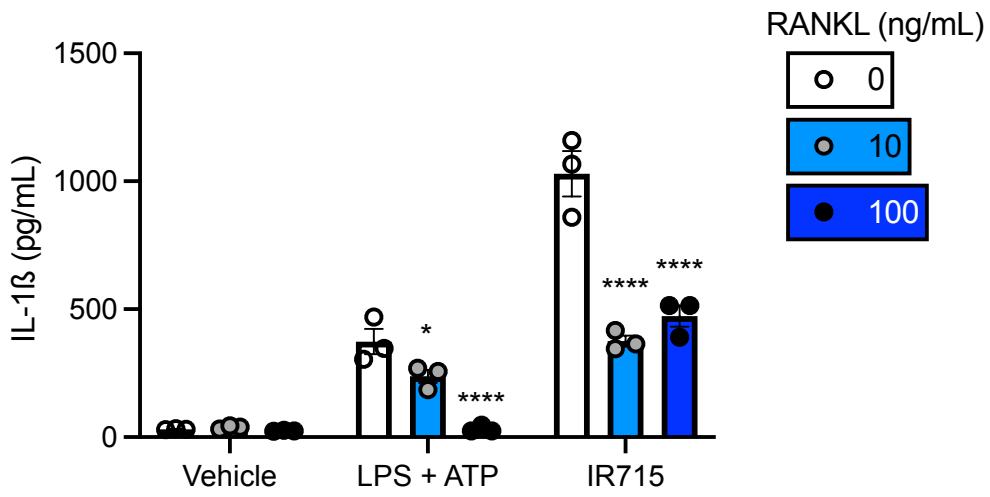

Figure 26. Two days of RANKL treatment blunts IL-1ß release in murine BMMs.

Murine BMMs derived from C57BL/6J mice were cultured for five days in the presence of M-CSF (CMG14-12 supernatant 5% v/v) with either 0, 10, or 100 ng/mL RANKL for the last two days. Cells were either treated with LPS alone (vehicle), infected with IR715 (MOI = 1), or treated with LPS for 3.5 hr followed by 30 minutes of 5 mM ATP. Cell supernatants were collected 4 hr post-infection and assessed for IL-1ß content via ELISA. Error bars represent mean ± S.E.M. Data analyzed via 2-way ANOVA with Dunnet post-hoc test. * $p<0.05$, **** $p<0.0001$ compared to 0 ng/mL RANKL for a given time condition.

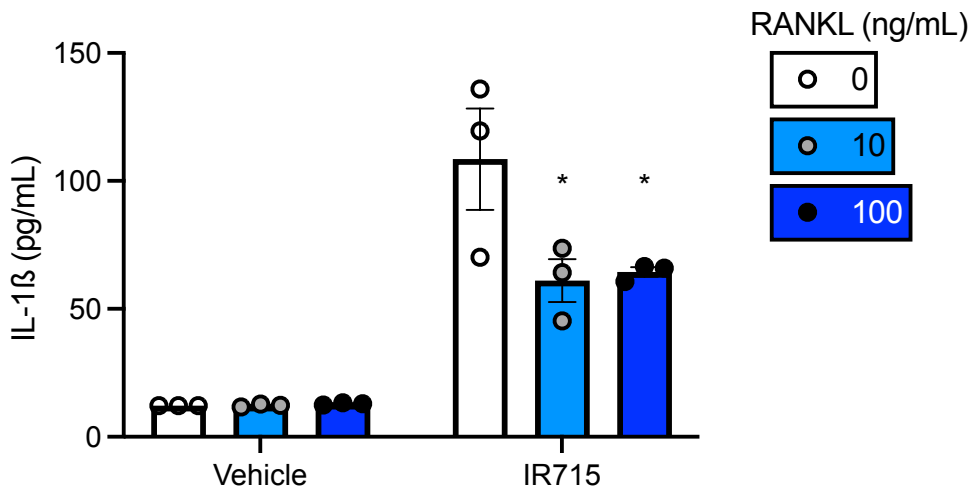

Figure 27. RANKL blunts IL-1ß release from human CD14$^+$ monocytes.

Human CD14$^+$ monocytes were isolated by magnetic negative selection from healthy donor peripheral blood mononuclear cells. CD14$^+$ monocytes were cultured with 30 ng/mL M-CSF with either 0, 10, or 100 ng/mL RANKL for 5 days. Cells were either mock-infected (vehicle) or infected with IR715 (MOI = 1). Cell supernatants were collected 4 hr post-infection and assessed for IL-1ß content via ELISA. Error bars represent mean ± S.E.M. Data analyzed via 2-way ANOVA with Tukey post-hoc test. * $p<0.05$ compared to 0 ng/mL RANKL for a given time condition.

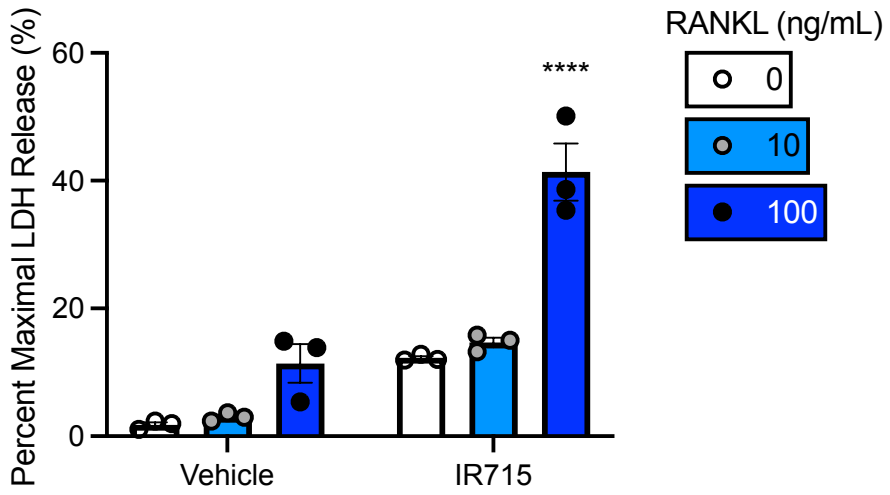

Figure 28. RANKL increases LDH from human CD14$^+$ monocytes.

Human CD14$^+$ monocytes were isolated by magnetic negative selection from healthy donor peripheral blood mononuclear cells. CD14$^+$ monocytes were cultured with 30 ng/mL M-CSF with either 0, 10, or 100 ng/mL RANKL for 5 days. Cells were either mock-infected (vehicle) or infected with IR715 (MOI = 1). Cell supernatants were collected 4 hr post-infection and assessed for LDH levels per the manufacturer's instructions. LDH levels were normalized to RANKL-matched cells treated with Triton-X-100 to determine the theoretical maximal LDH release from detergent-mediated cell lysis. Error bars represent mean ± S.E.M. Data analyzed via 2-way ANOVA with Tukey post-hoc test. **** $p<0.05$ compared to 0 ng/mL RANKL for a given condition.

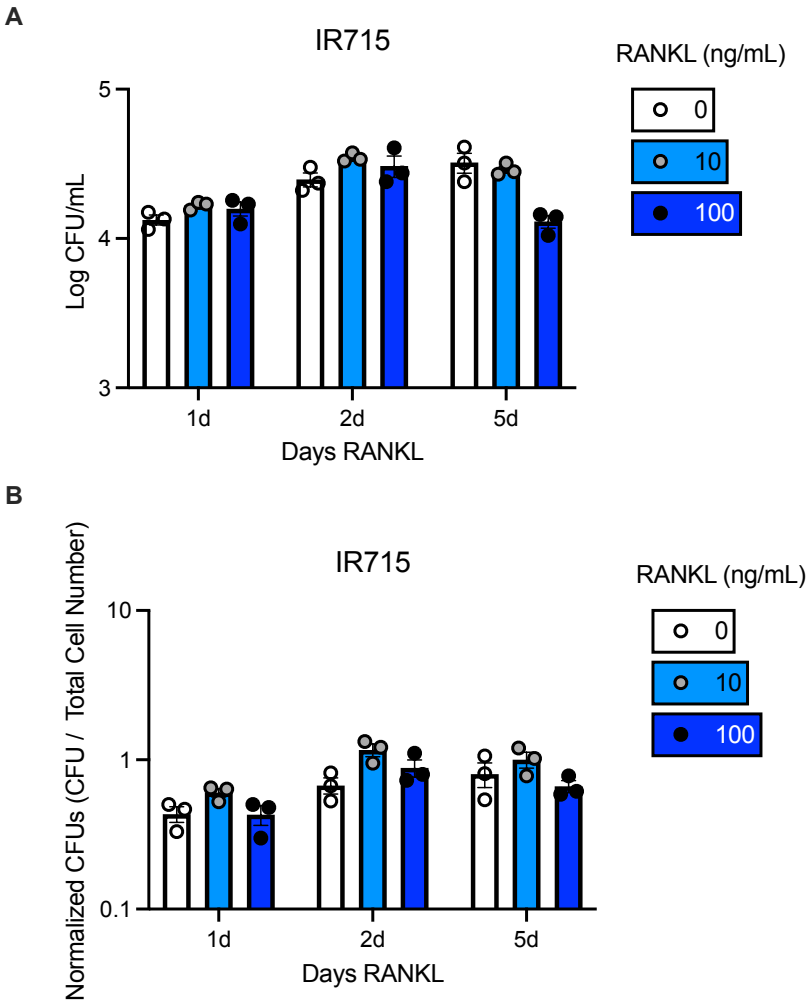

Figure 29. RANKL does not enhance intracellular STm burdens 4 hrs post-infection.

Bone marrow macrophages (BMMs) were derived from C57BL/6J mice and cultured in the presence of M-CSF (CMG14-12 supernatant 5% v/v) with either 0, 10, or 100 ng/mL RANKL for 1, 2, or 5 days. BMMs were then infected (MOI = 1) with the WT IR715 in a gentamicin protection assay for 24 hours. Cell lysates were serially diluted and plated for bacterial CFUs (A). Prior to lysis, cells were imaged on a Cytation 5 imaging system and counted using Gen 5 software to normalize bacterial burdens to cell number (B). Error bars represent mean ± S.E.M. Data analyzed via 2-way ANOVA with Tukey post-hoc test.

In order to link IL-1ß release to specific STm inflammasome inducers, we next evaluated the ability of either the STm Needle or Rod proteins to induce inflammasome activation in RANKL-treated monocytes. We utilized the "Rod-tox" or "Needle-tox" systems, where the Rod or Needle proteins are conjugated to the *B. anthracis* Lethal Factor N-terminal domain (LFn) (229, 230). Delivery of LFn-Rod or LFn-Needle in conjunction with the *B. anthracis* protective antigen (PA) results in cytosolic delivery and specific activation of the NLRC4 inflammasome (229, 230). Treatment of murine BMMs with LFn-Rod and LFn-Needle led to robust IL-1ß release at 4 and 20 hrs following stimulation (**Figure 30**). Treatment with 100 ng/mL of RANKL for five days significantly dampened IL-1ß release (**Figure 30**). Additional experiments revealed that reduced duration and amount of RANKL treatment still prevents IL-1ß signaling, as two days of 10 ng/mL was able to significantly decrease NLRC4-mediated IL-1ß release (**Figure 31**). To determine if RANKL-mediated dampening of the inflammasome during STm infection was dependent on host innate immune receptors, we measured IL-1ß release following infection of RANKL treated WT, *TLR4*$^{-/-}$, and *MyD88*$^{-/-}$ cells. Infection with WT IR715 STm led to IL-1ß release in WT, *TLR4*$^{-/-}$, and *MyD88*$^{-/-}$ cells, which was reduced in the presence of RANKL (**Figure 32**). NLRP3 induction with LPS and ATP led to IL-1ß release in WT and *MyD88*$^{-/-}$ but not *TLR4*$^{-/-}$ cells (**Figure 32**). IL-1ß release in both RANKL and non-RANKL treated BMMs was lower in *TLR4*$^{-/-}$, and *MyD88*$^{-/-}$ cells compared to WT cells. Collectively, these data indicate that RANKL dampens murine and human monocyte IL-1ß release in response to STm infection. Furthermore, these data suggest that RANKL blocks IL-1ß response from specific STm NLRP3 and NLRC4 inflammasome inducers.

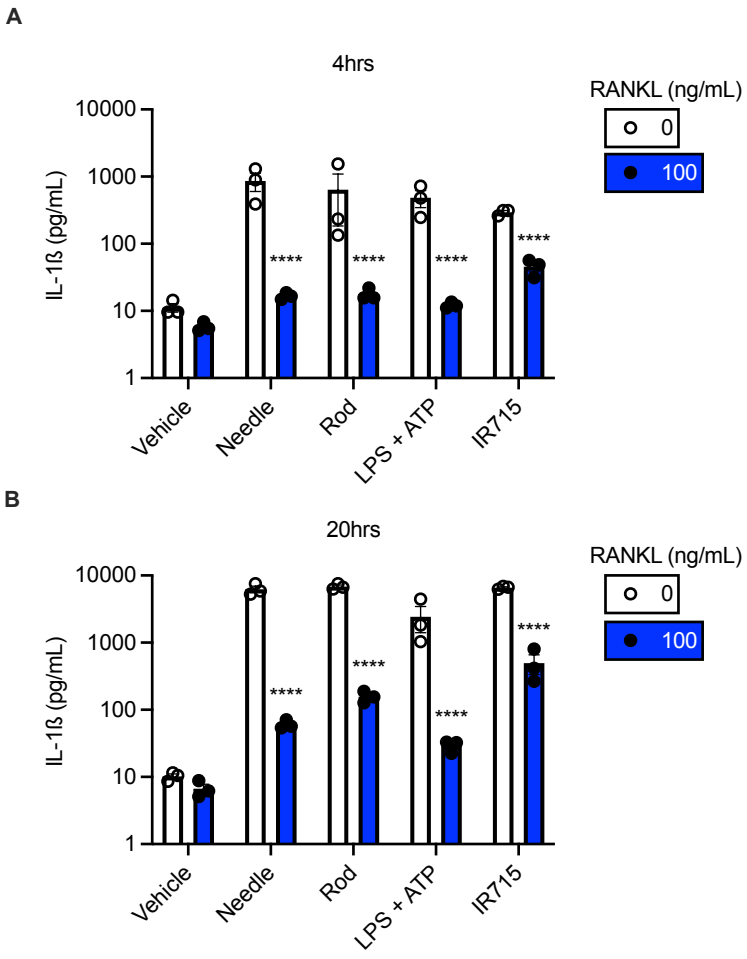

Figure 30. RANKL blunts IL-1ß release following NLRC4 activation.

Murine BMMs derived from C57BL/6J mice were cultured for five days in the presence of M-CSF (CMG14-12 supernatant 5% v/v) with either 0 or 100 ng/mL RANKL. Cells were either treated with LPS and *B. anthracis* protective antigen (PA) (vehicle), infected with IR715 (MOI = 1), or treated with LPS for 3.5hr followed by 30 minutes of 5 mM ATP. For NLRC4 activation, cells were treated with PA and T3SS Rod or Needle proteins conjugated to the *B. anthracis* Lethal Factor N-terminal domain after 24 hr of priming with LPS. Cell supernatants were collected at 4 hr (A) or 20 hr (B) post-infection and assessed for IL-1ß content via ELISA. Error bars represent mean ± S.E.M. Data analyzed via 2-way ANOVA with Šidák multiple comparisons test. **** $p<0.0001$ compared to 0 ng/mL RANKL for a given time condition.

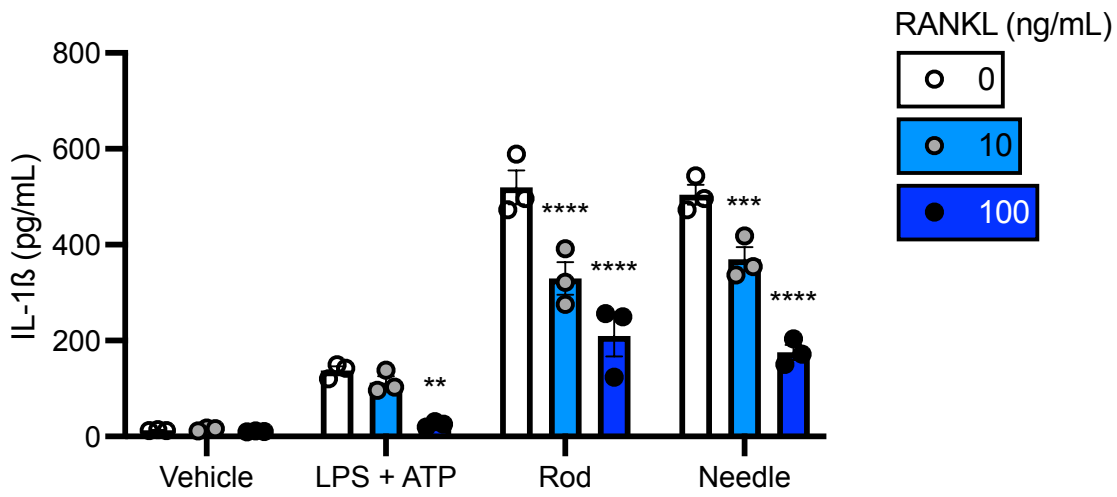

Figure 31. Two days of RANKL reduces NLRC4-mediated IL-1ß release.

Murine BMMs derived from C57BL/6J mice were cultured for five days in the presence of M-CSF (CMG14-12 supernatant 5% v/v) with either 0, 10, or 100 ng/mL RANKL for two days. Cells were either treated with LPS and *B. anthracis* protective antigen (PA) (vehicle), infected with IR715 (MOI = 1), or treated with LPS for 3.5hr followed by 30 minutes of 5 mM ATP. For NLRC4 activation, cells were treated with *B. anthracis* protective antigen (PA) and T3SS Rod or Needle proteins conjugated to the *B. anthracis* Lethal Factor N-terminal domain after 24 hr of priming with LPS. Cell supernatants were collected 4 hr post-infection and assessed for IL-1ß content via ELISA. Error bars represent mean ± S.E.M. Data analyzed via 2-way ANOVA with Dunnet post-hoc test. ** $p<0.01$, *** $p<0.001$, **** $p<0.0001$ compared to 0 ng/mL RANKL for a given time condition.

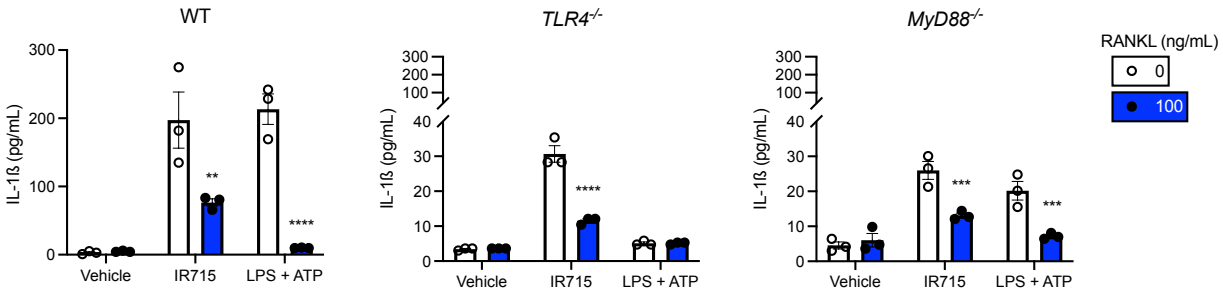

Figure 32. RANKL reduces IL-1ß release during STm infection in *TLR4*$^{-/-}$ and *MyD88*$^{-/-}$ cells.

Murine BMMs derived from C57BL/6J mice were cultured for five days in the presence of M-CSF (CMG14-12 supernatant 5% v/v) with either 0 or 100 ng/mL RANKL for five days. Cells were either treated with LPS (vehicle), infected with IR715 (MOI = 1), or treated with LPS for 3.5hr followed by 30 minutes of 5 mM ATP. Cell supernatants were collected 4 hr post-infection and assessed for IL-1ß content via ELISA. Error bars represent mean ± S.E.M. Data analyzed via 2-way ANOVA with Šidák post-hoc test. ** $p<0.01$, *** $p<0.001$, **** $p<0.0001$ compared to 0 ng/mL RANKL for a given time condition.

RANKL prevents induction of *IRF8* during STm infection

To explore the mechanisms of enhanced bacterial burdens and dampened IL-1ß response in RANKL-treated monocytes, we measured the gene expression of *IRF8*, which has been shown to be necessary for controlling STm infection by activating expression of components of the NLRC4 inflammasome. IRF8 has also been demonstrated to become epigenetically silenced during RANKL exposure (183, 189, 191). Infection with STm induces *IRF8* expression (**Figure 33**). However, treatment with 5 days of RANKL prevents *IRF8* expression during STm infection (**Figure 33**). Because RANKL has been previously demonstrated to repress *IRF8* expression through DNMT3a DNA methylation and EZH2 histone H3K27me3 methylation, we tested whether increased STm burdens and reduced IL-1ß release persisted following RANKL withdrawal (189, 191). Continuous 100 ng/mL RANKL treatment (no withdrawal) for two and five days led to a 1-2 log increase in bacterial burdens (**Figure 34**). RANKL withdrawal for two days reversed the increased bacterial burdens observed in BMMs treated with two but not five days of RANKL treatment (**Figure 34**). RANKL withdrawal for nine days completely reversed the increased bacterial burdens during continuous RANKL treatment (**Figure 34**). qRT-PCR for *IRF8* revealed that *IRF8* was repressed 48 hr following five days of 100 ng/mL RANKL treatment (**Figure 35**). We next measured IL-1ß levels following RANKL withdrawal. RANKL withdrawal for 24 hrs from BMMs treated with 100 ng/mL of RANKL for 5 days did not affect the RANKL-mediated reduction in IL-1ß (**Figure 36**). Collectively, these data demonstrate the RANKL silences *IRF8* expression during STm infection and that RANKL-mediated dampening of IL-1ß release in response to STm is maintained after RANKL withdrawal.

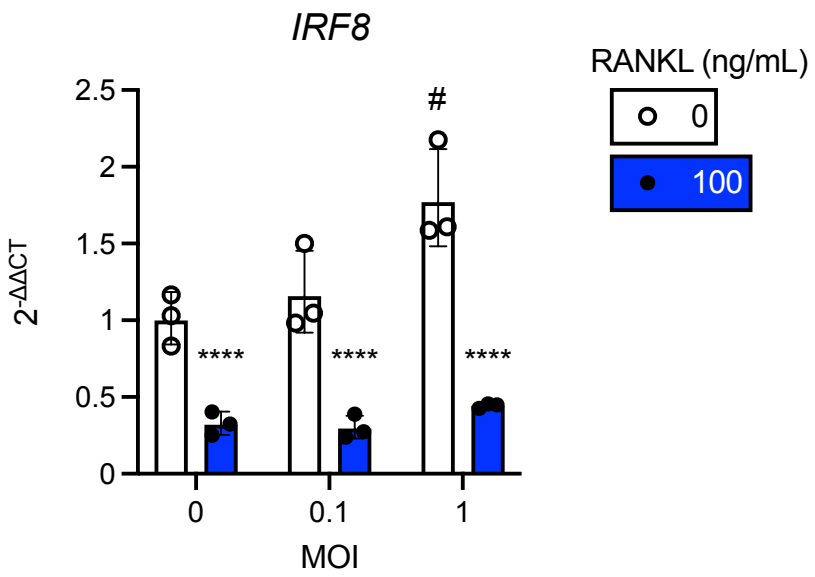

Figure 33. RANKL prevents STm induction of *IRF8* expression.

Murine BMMs derived from C57BL/6J mice were cultured for 5 days in the presence of M-CSF (CMG14-12 supernatant 5% v/v) with 0 or 100 ng/mL RANKL for five days. Cells were mock infected (MOI = 0) or infected with WT IR715 (MOI = 0.1 or 1) for 6 hrs, after which time RNA was isolated and *IRF8* levels were measured via qRT-PCR with the $\Delta\Delta C_T$ method, normalized to *ACTB* expression. Error bars represent mean ± S.E.M. Data analyzed via 2-way ANOVA with Tukey post-hoc test. **** $p<0.0001$ compared to 0 ng/mL RANKL for a given MOI. # $p<0.05$ compared to uninfected MOI = 0) 0 RANKL condition.

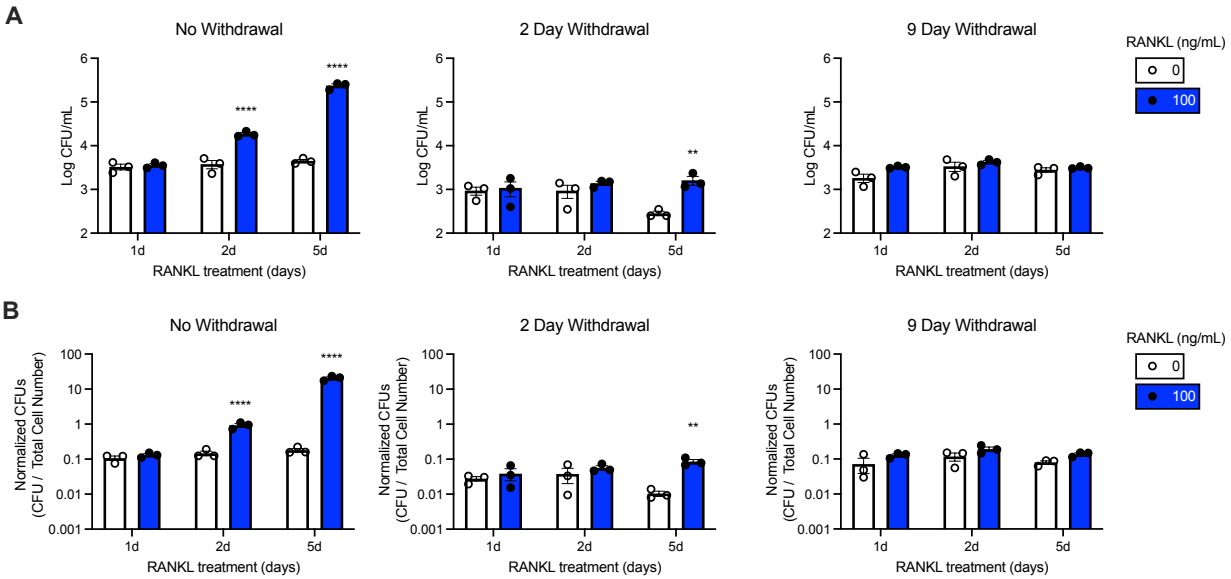

Figure 34. RANKL withdrawal partially reverses enhanced intracellular STm burdens.

Bone marrow macrophages (BMMs) were derived from C57BL/6J mice and cultured in the presence of M-CSF (CMG14-12 supernatant 5% v/v) with either 0 or 100 ng/mL RANKL for 1, 2, or 5 days. Cells were either infected without RANKL withdrawal (no withdrawal) or following RANKL withdrawal for 2 or 9 days. BMMs were infected (MOI = 1) with WT IR715 in a gentamicin protection assay for 24 hours. Cell lysates were serially diluted and plated for bacterial CFUs (A). Prior to lysis, cells were imaged on a Cytation 5 imaging system and counted using Gen 5 software to normalize bacterial burdens to cell number (B). Error bars represent mean ± S.E.M. Data analyzed via 2-way ANOVA with Tukey post-hoc test. ** $p<0.01$, **** $p<0.0001$ compared to 0 ng/mL RANKL for a given time duration of RANKL treatment.

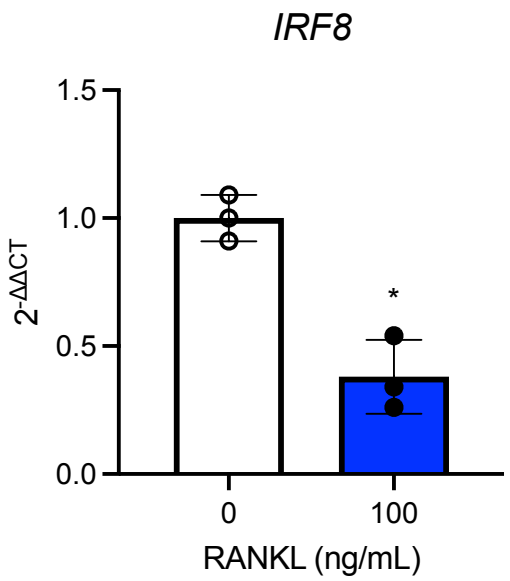

Figure 35. RANKL represses *IRF8* expression following two days of withdrawal.

Bone marrow macrophages (BMMs) were derived from C57BL/6J mice and cultured in the presence of M-CSF (CMG14-12 supernatant 5% v/v) with either 0 or 100 ng/mL RANKL for 5 days. RANKL was then withdrawn for 2 days, after which RNA was isolated and *IRF8* levels were measured via qRT-PCR with the $\Delta\Delta C_T$ method. Error bars represent mean ± S.E.M. Data analyzed via Student's t-test. * $p<0.05$.

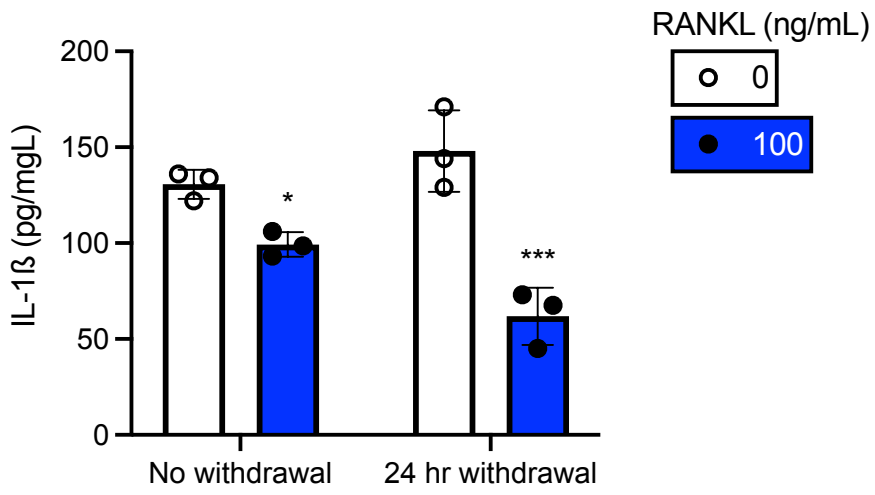

Figure 36. RANKL withdrawal does not reverse reduced IL-1ß production during STm infection.

Murine BMMs derived from C57BL/6J mice were cultured for five days in the presence of M-CSF (CMG14-12 supernatant 5% v/v) with 0 or 100 ng/mL RANKL for five days. RANKL was subsequently withdrawn for 0 hrs (no withdrawal) or 24 hrs prior to infection with WT STm IR715 (MOI = 1). Cell supernatants were collected 4 hr post-infection and assessed for IL-1ß content via ELISA. Error bars represent mean ± S.E.M. Data analyzed via 2-way ANOVA with Dunnet post-hoc test. **** $p<0.0001$ compared to 0 ng/mL RANKL for a given condition.

To determine if STm modulates RANKL signaling *in vivo*, we utilized a reporter mouse, whereby TdTomato expression is driven by the promoter of a RANKL-regulated gene, *Acp5* (encoding TRAP). Intestinal infection with STm increased TdTomato expression among mononuclear cells, and the majority of TdTomato^{+} cells were detected in the Cd11b$^{-/lo}$Ly6C^{hi} fraction (**Figure 37**). To investigate the contribution of RANKL to antibacterial and inflammatory responses to STm *in vivo*, we treated mice with either IgG isotype or anti-RANKL monoclonal antibody 48 or 24 hr prior to gastrointestinal infection with STm. To determine if RANKL blockade impacted RANKL signaling within the skeleton, we performed micro CT analysis, which demonstrated a significant increase in trabecular BV/TV in mice receiving anti-RANKL antibody treatment (**Figure 38**). We did not detect differences in weight loss or bacterial burdens in the bone, spleen, liver, mesenteric lymph nodes (MLNs), or Peyer's patches during infection between IgG isotype or anti-RANKL treated groups (Figure **39**). Anti-RANKL treatment led to a significant increase in STm burdens within the stool (**Figure 39**).

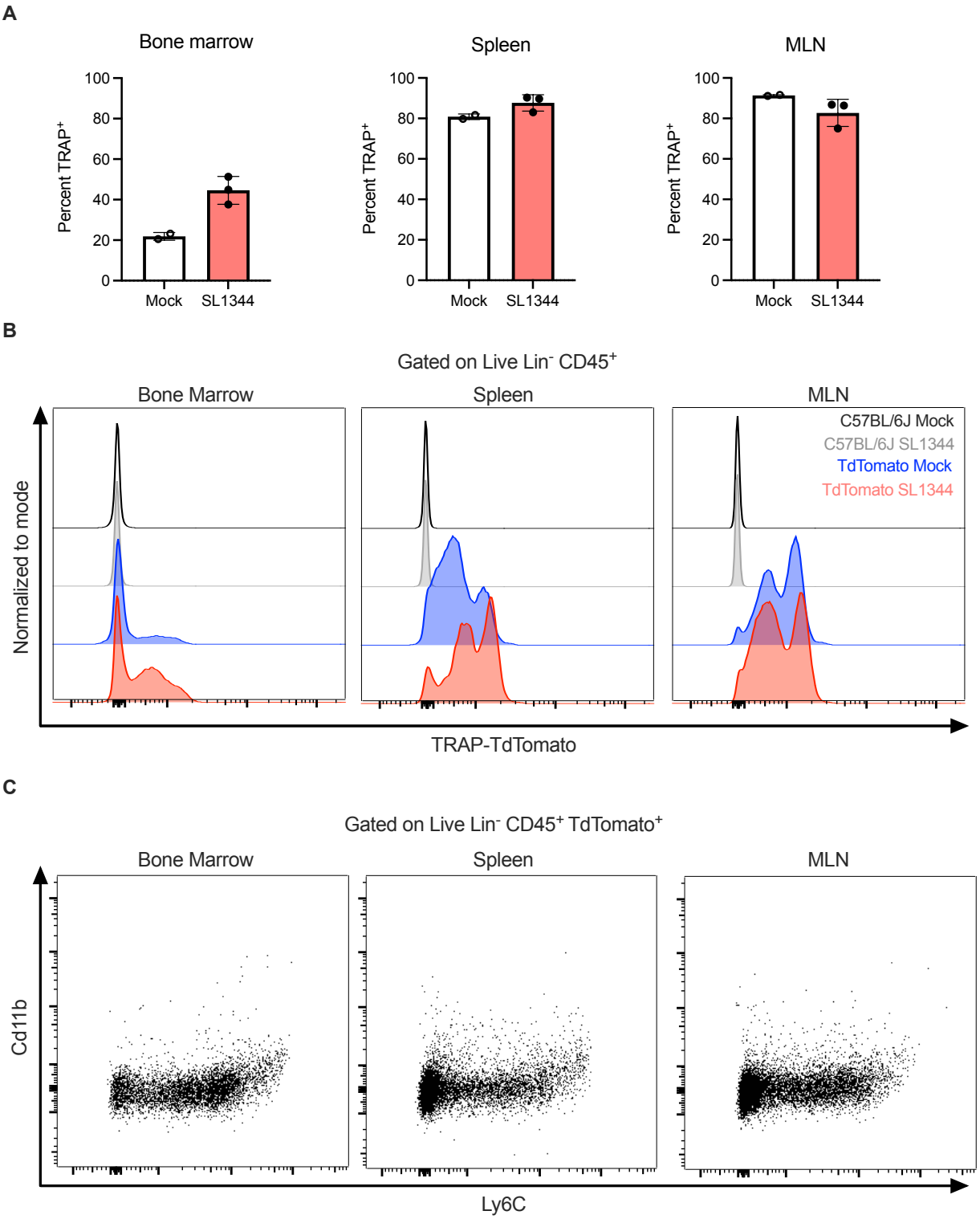

Figure 37. STm may promote RANKL signaling *in vivo*.

C57BL/6J or TdTomato-TRAP reporter mice (TdTomato) mice were orally administered 20 mg streptomycin 24 hr prior to infection. Mice were infected with 10^9 CFU SL1344 STm via orogastric gavage, and after four days organs were harvested and processed as single cell suspensions and stained with a cocktail of surface antibodies to identify mononuclear cells as live, $CD45^+$Lin (CD3, B220, Terr119, Ly6G) and quantify percent $TdTomato^+$ cells from TdTomato-TRAP reporter mock or infected mice (A). Representative histograms of mononuclear cell TdTomato expression (B). Gated $TdTomato^+$ mononuclear cells assessed for Cd11b and Ly6C expression from SL1344 infected TdTomato-TRAP reporter mice (C).

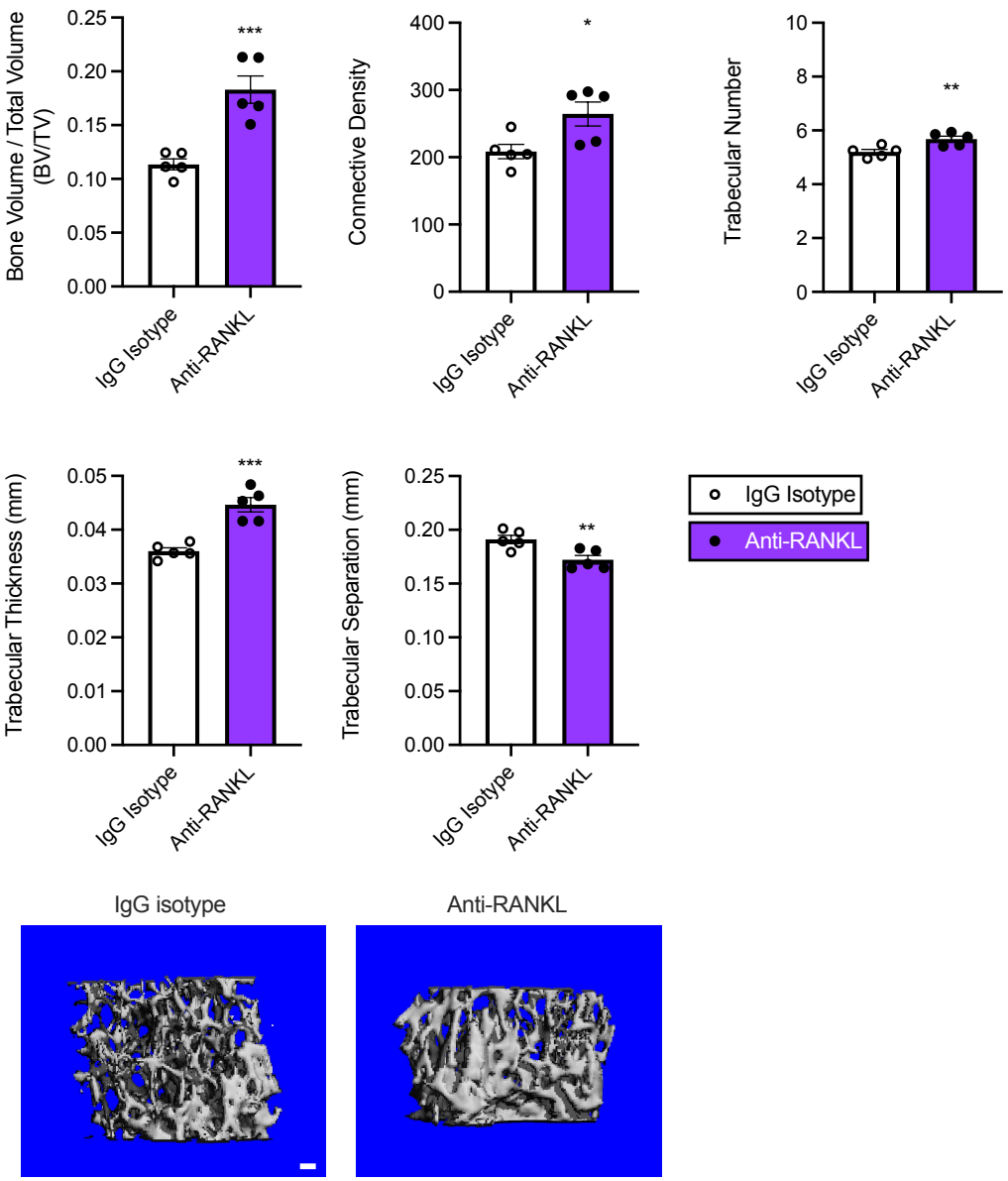

Figure 38. Anti-RANKL treatment increases trabecular bone volume in STm infection.

C57BL/6J mice were treated with 200 µg IgG isotype or anti-RANKL monoclonal antibody 48 hrs prior to infection with STm. Mice were orally administered 20 mg streptomycin 24 hr prior to infection. Mice were then gavaged with 10^9 CFU WT SL1344 STm. Four days post-infection, femurs were collected and assessed for trabecular bone parameters via micro CT. Scale bar = 100 µm Error bars represent geometric mean ± S.E.M. Data analyzed via Student's t-test. * $p<0.05$, ** $p<0.01$, *** $p<0.001$.

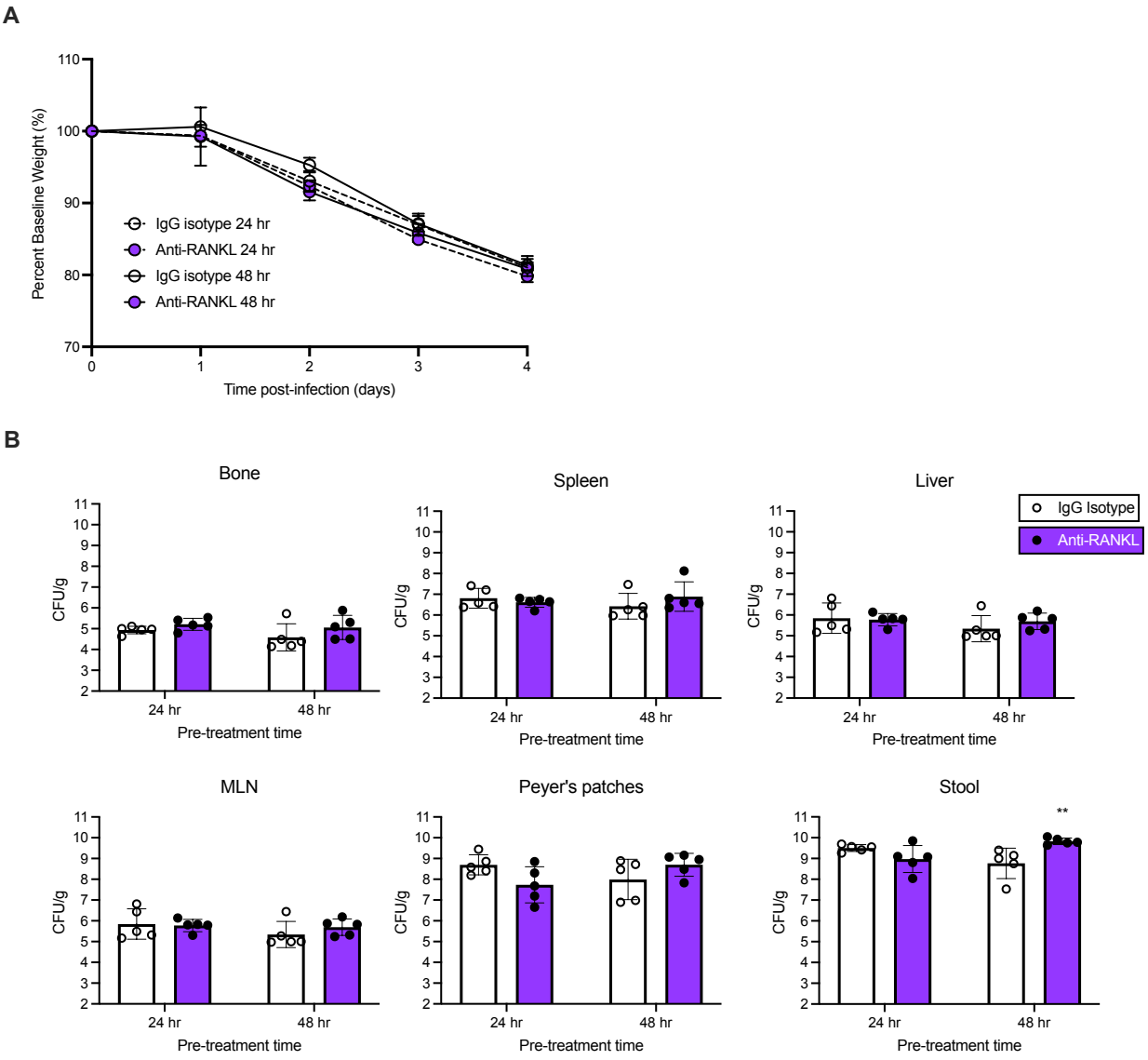

Figure 39. *In vivo* RANKL blockade during STm infection may enhance bacterial burdens within the stool.

C57BL/6J mice were treated with 200 µg IgG isotype or anti-RANKL monoclonal antibody at 24 or 48 hrs prior to infection. Mice were orally administered 20 mg streptomycin 24 hr prior to infection. Mice were infected with 10^9 CFU WT SL1344 STm via orogastric gavage and weighed daily to monitor for disease progression for four days post-infection. (A) Percent baseline weight changes over the course of infection. (B) Four days post-infection, tissues were

harvested, homogenized, serially diluted, and plated on MacConkey agar for CFU enumeration normalized to tissue weight (g). Error bars represent geometric mean ± S.D. Data analyzed via 2-way ANOVA with Tukey post-hoc test. ** $p<0.01$ compared to 48 hr IgG isotype.

STm promotes osteoclastogenesis in RANKL-treated monocytes

To determine if STm infection promotes OC formation, we performed a modified gentamicin protection assay whereby BMMs were treated with two days of 35 ng/mL RANKL and then infected with STm for 72 hours in the absence (precommitment) or continuation of RANKL treatment. Cultures were maintained in gentamicin to kill extracellular bacteria. Infection with *invA spiB* and WT IR715 significantly increased OC formation in cells both pre-committed and continuously treated with RANKL compared to uninfected cells (**Figure 40**). Infection with WT IR715 led to a significant increase in osteoclastogenesis compared to cells infected with *invA spiB* (**Figure 40**). To assess the contribution of the host restriction factor NRAMP1, we performed similar experiments in BMMs derived from NRAMP$^{+/+}$ CBA/J mice. Infection with WT IR715 led to a significant increase in OC formation compared to uninfected controls (**Figure 41**). We next sought to determine the impact of STm induced signaling of TLR4 and MyD88 on osteoclastogenesis by infecting BMMs derived from C57BL/6J WT, *TLR4*$^{-/-}$, or *MyD88*$^{-/-}$ mice with WT STm. Infection in WT, *TLR4*$^{-/-}$, and *MyD88*$^{-/-}$ cells resulted in significantly increased osteoclastogenesis when cells were continuously treated with RANKL (**Figure 42**). For cells pre-committed with RANKL, WT, but not *TLR4*$^{-/-}$ or *MyD88*$^{-/-}$, demonstrated enhanced OC formation upon infection with WT IR715 (**Figure 42**).

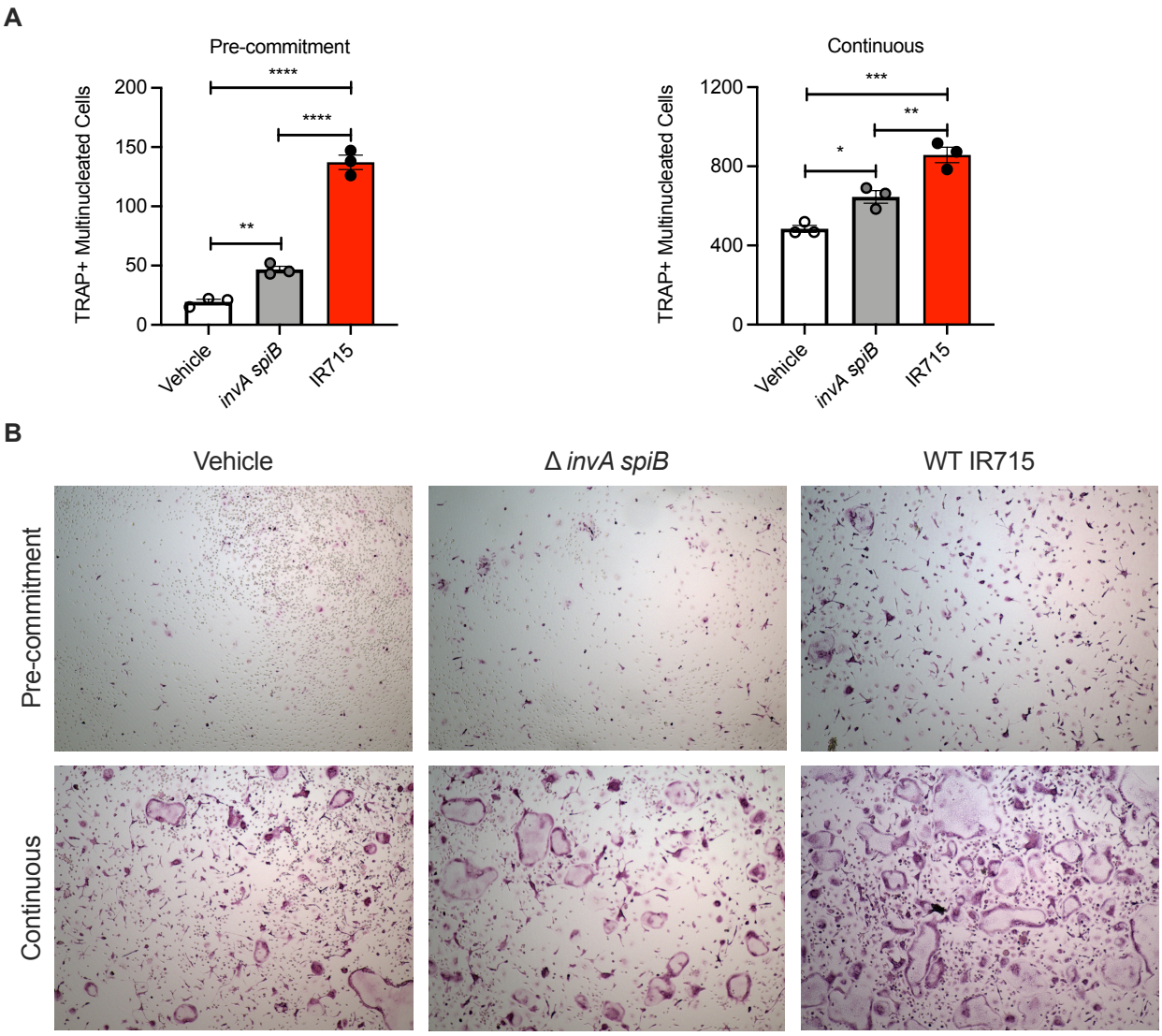

Figure 40. STm enhances OC formation *in vitro*.

Murine BMMs derived from C57BL/6J mice were cultured for two days with M-CSF (CMG14-12 supernatant 5% v/v) and 35 ng/mL RANKL. Cells were then mock-infected (vehicle) or infected with the indicated strain of STm (MOI = 1) in a gentamicin protection assay. Following 1 hr treatment with 100 µg/mL gentamicin, cells were switched to culture media containing 10% FBS and 10 µg/mL gentamicin with (continuous) or without (pre-commitment) 35 ng/mL RANKL and cultured for additional 72 hrs. Cells were then fixed and stained for tartrate resistant acid phosphatase (TRAP), imaged with a Cytation 5 imaging system (color brightfield, 4x) and

manually enumerated for $TRAP^+$ multi-nucleated cells (A). Representative images of TRAP-stained cells (B). Error bars represent mean ± S.E.M. Data analyzed via One-way ANOVA with Tukey multiple comparisons test. * $p<0.05$, ** $p<0.01$, *** $p<0.001$, **** $p<0.0001$.

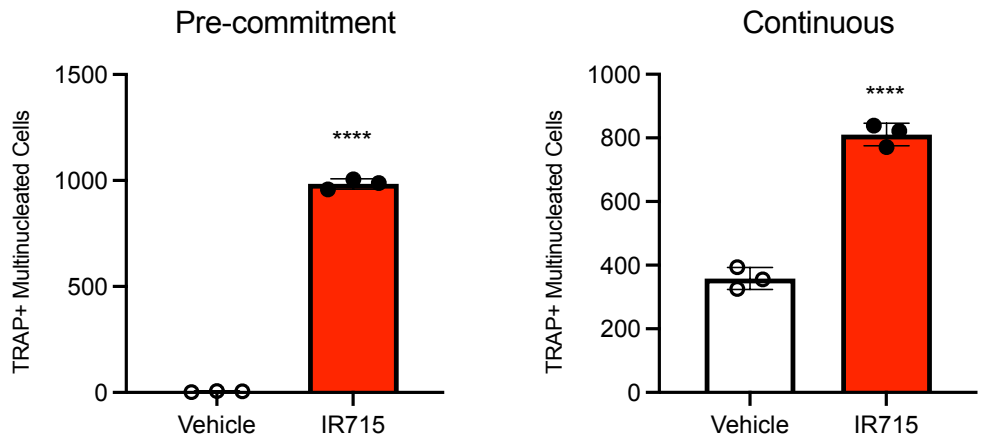

Figure 41. STm enhances osteoclastogenesis in NRAMP$^{+/+}$ cells.

Murine BMMs derived from CBA/J mice were cultured for two days with M-CSF (CMG14-12 supernatant 5% v/v) and 35 ng/mL RANKL. Cells were then mock-infected (vehicle) or infected with WT IR715 (MOI = 1) in a gentamicin protection assay. Following 1 hr treatment with 100 µg/mL gentamicin, cells were switched to culture media containing 10% FBS and 10 µg/mL gentamicin with (continuous) or without (pre-commitment) 35 ng/mL RANKL and cultured for additional 72 hrs. Cells were then fixed and stained for tartrate resistant acid phosphatase (TRAP), imaged with a Cytation 5 imaging system (color brightfield, 4x) and manually enumerated for TRAP^{+} multi-nucleated cells. Error bars represent mean ± S.E.M. Data analyzed via one-way ANOVA with Tukey multiple comparisons test. **** p<0.0001.

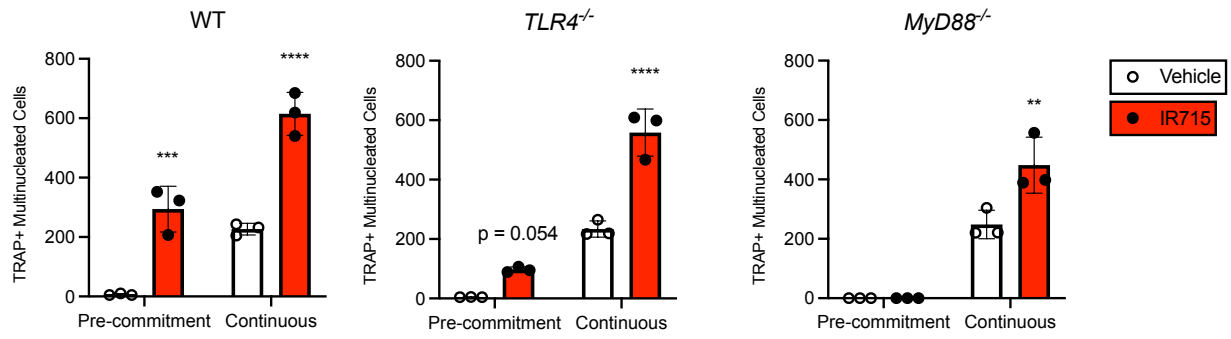

Figure 42. Increased osteoclastogenesis following STm infection is partially dependent upon TLR4 and MyD88.

Murine BMMs derived from WT C57BL/6J (WT), *TLR4*$^{-/-}$, and *MyD88*$^{-/-}$ mice were cultured for two days with M-CSF (CMG14-12 supernatant 5% v/v) and 35 ng/mL RANKL. Cells were then mock-infected (vehicle) or infected with WT IR715 (MOI = 1) in a gentamicin protection assay. Following 1 hr treatment with 100 µg/mL gentamicin, cells were switched to culture media containing 10% FBS and 10 µg/mL gentamicin with (continuous) or without (pre-commitment) 35 ng/mL RANKL and cultured for additional 72 hrs. Cells were then fixed and stained for tartrate resistant acid phosphatase (TRAP), imaged with a Cytation 5 imaging system (color brightfield, 4x) and manually enumerated for TRAP^{+} multi-nucleated cells. Error bars represent mean ± S.E.M. Data analyzed via 2-way ANOVA with Šidák multiple comparisons test. ** p<0.01, *** p<0.001, **** p<0.0001.

Discussion

These data demonstrate that RANKL promotes intracellular survival within mouse and human monocytes. RANKL led to enhanced STm bacterial burdens as early as 24 hours post-treatment and occurred at RANKL doses insufficient to induce osteoclast formation *in vitro* (10 ng/mL). Dynamic imaging revealed that STm replicated to higher titers on a per cell basis. RANKL-mediated enhanced bacterial burdens were not dependent on host-restriction factors such as NRAMP1, TLR4, or MyD88. These data suggest that RANKL promotes STm survival, which may be mediated by reduced host cell anti-bacterial immunity and/or enhanced bacterial replication. Despite a 50-100 fold increase in intracellular bacteria in RANKL treated monocytes, RANKL treatment significantly dampened IL-1ß release during infection with STm as well as during NLRP3 and NLRC4 activation. Reduced IL-1ß release was associated with a reduction in *IRF8* expression. RANKL continued to reduce IL-1ß release in *TLR4*$^{-/-}$ and *MyD88*$^{-/-}$ cells, although both *TLR4*$^{-/-}$ and *MyD88*$^{-/-}$ demonstrated a reduced capacity to release IL-1ß in response to STm compared to WT cells. These results indicate that RANKL dampens the inflammasome response to STm PAMPs. Additional studies revealed that STm promotes osteoclastogenesis *in vitro*. Increased osteoclast formation during STm infection was not dependent on host restriction factors such as NRAMP1, TLR4, or MyD88 during continuous RANKL treatment, while pre-commitment alone with RANKL was insufficient to increase osteoclastogenesis in *TLR4*$^{-/-}$ and *MyD88*$^{-/-}$ cells. Taken together, these findings suggest that RANKL strongly patterns monocytes to differentially respond to STm and that STm alters RANKL-experienced monocyte cell fate.

STm is able to colonize host niches during gastrointestinal infection by i) epithelial phagocytosis, ii) infecting and persisting within in CD18^{+} and recently identified CD9^{+}

monocytes, and iii) usurping M cells to bypass the epithelial barrier and gain access to the underlying lamina propria and lymphoid tissue (175, 176, 178, 224, 225). RANKL is essential for M cell development, and the Peyer's patch microenvironment is rich in RANKL signaling, with multiple cells expressing RANK and RANKL (188, 221). Recent work has demonstrated that RANKL is important *in vivo* for STm pathogenesis, as mice lacking the soluble decoy receptor for RANKL, OPG, demonstrated higher bacterial burdens and increased mortality during gastrointestinal STm infection (188). However, studies to date have yet to examine the contribution of RANKL on monocyte antibacterial and inflammatory response to STm infection. Mononuclear phagocytes, including monocytes, are found within Peyer's patches and the surrounding lamina propria. We observed a marked increase in STm survival within monocytes treated with RANKL. We also observed increased intracellular STm on a per cell basis utilizing kinetic imaging of chromosomally integrated STm reporter strains. While preliminary studies indicate that STm infection increases RANKL signaling *in vivo*, future studies should confirm these findings and precisely measure RANKL and OPG abundance in STm infected tissues.

One might expect that an increase in intracellular bacterial burdens would lead to a corresponding increase in inflammasome activation and resultant IL-1ß release. Contrary to this expectation, we found that despite equivalent bacterial burdens 4 hours post infection and significantly enhanced bacterial burdens 16-24 hours post infection, RANKL treated monocytes produced significantly less IL-1ß during STm infection compared to non-RANKL controls. *In vivo*, the cellular source of IL-1ß during intestinal STm infection are dependent upon the location and timing of infection, with evidence supporting both epithelial cells and leukocytes as important producers of IL-1ß in response to STm (176, 177, 231, 232).

Previous work has demonstrated that the NLRP3 and NLRC4 inflammasomes are crucial for restraining STm infection (183–186). Consistent with these data, RANKL dampens IL-1ß release during NLRC4 and NLRP3 activation by purified danger signals and PAMPs. Because the majority of IL-1ß release is thought to occur through NLRC4 signaling, we investigated *IRF8*, which was previously demonstrated to transcriptionally regulate components of the NLRC4 inflammasome (183). Intriguingly, RANKL has been shown to repress *IRF8* expression in the context of osteoclast formation through epigenetic silencing of anti-osteoclastogenic factors (189–191). Consistent with this prior work, we demonstrated that STm infection of BMMs induces *IRF8* expression in the absence of RANKL and that RANKL treatment silences *IRF8* expression during STm infection.

Given that RANKL leads to changes in the epigenetic landscape, we questioned whether the increased bacterial burdens and dampened IL-1ß response would persist following the removal of RANKL. We found that RANKL withdrawal partially reversed the increase in bacterial burdens but not the dampened reduced inflammasome response. Importantly, *IRF8* expression was still repressed following RANKL withdrawal. These data indicate a dissociation in the RANKL-mediated increase in STm replication and the reduction in inflammasome response to STm infection. The increase in bacterial burdens during RANKL treatment may reflect a combination of diverse functions RANKL imparts on monocytes, such as driving cytoskeletal rearrangements, enhancing pro-survival pathways, and inhibiting anti-apoptotic signaling. Conversely, persistently lower IL-1ß release after RANKL may support an epigenetic regulatory role of STm-responsive inflammasomes during infection.

This work also examined the role of specific host restriction factors and PRR signaling components. Infection of *MyD88*$^{-/-}$ cells did not lead to an enhancement in STm burdens at

baseline, likely reflecting compensatory functions that alternative PRR adaptors (*e.g.*, TRIF) contribute to anti-STm immunity, as has been previously reported (233). Similarly, TLR4 was dispensable for restricting STm growth in non-RANKL treated cells, perhaps indicating compensatory roles for alternative TLRs in responding to STm infection as others have demonstrated (181). Both *TLR4*$^{-/-}$ and *MyD88*$^{-/-}$ cells demonstrated increased STm replication during STm infection, indicating that RANKL regulation of these immune pathways is not required for enhanced intracellular STm burdens. IL-1ß release was similarly blunted in both *TLR4*$^{-/-}$ and *MyD88*$^{-/-}$ cells, indicating that TLR4 and MyD88 are dispensable for RANKL-mediated dampening of IL-1ß production during STm infection. Notably, IL-1ß production in *TLR4*$^{-/-}$ and *MyD88*$^{-/-}$ cells was reduced compared to that of WT cells in both RANKL and non-RANKL treatment conditions. LPS and ATP stimulation was unable to induce IL-1ß release in *TLR4*$^{-/-}$ cells, consistent with the role of TLR4 recognizing extracellular LPS. Detectable IL-1ß release during STm infection in *TLR4*$^{-/-}$ and *MyD88*$^{-/-}$ cells likely reflects a combination of TRIF-dependent pathways or non-canonical inflammasome activation. Importantly, utilizing either murine NRAMP$^{+/+}$ cells or purified human CD14^{+} monocytes revealed that both increased intracellular STm burdens as well as reduced IL-1ß response in RANKL-treated monocytes was not dependent on NRAMP. These results point towards NRAMP independent mechanisms of increased bacterial survival within both human and murine monocytes.

Preliminary *in vivo* data suggests that RANKL signaling is rich in lymphoid tissues, as evidenced by high baseline TRAP expression observed in mononuclear phagocytes within the spleen and MLN. Furthermore, STm infection appears to possibly increase RANKL signaling in the bone marrow and spleen. These data indicate that mononuclear cells that encounter STm are located in niches with robust RANKL signaling and that STm infection might further enhance

RANKL signaling *in vivo*. Pre-treatment with anti-RANKL for 24 or 48 hrs did not significantly alter weight loss during infection or bacterial burdens within the bone, spleen, Peyer's patches, or MLN. However, we did observe an increase in luminal STm detected within the stool of mice treated with anti-RANKL 48 hrs prior to infection. These data may reflect the important role that secretory IgA producing B cells play in limiting luminal STm growth that has been previously shown to be modulated by RANKL signaling (188).

Studies described in this chapter also investigated the potential of STm to alter osteoclastogenesis. WT STm infection increased OC formation in BMMs compared to vehicle or infection with an *invA spiB* mutant. Increased osteoclastogenesis occurred during both continuous treatment with RANKL and in cells that were only pre-committed with RANKL. Given that RANKL enhances bacterial burdens, increased OC formation may reflect an increased abundance of pro-osteoclastogenic PAMPs, such as LPS. Additionally, although RANKL dampens IL-1ß production during STm infection, RANKL-experienced cells are still able to produce this inflammatory cytokine. IL-1ß, originally denoted as "osteoclast activating factor" for its potent osteoclastogenic effects, likely also contributes to increased osteoclast formation during STm infection. However, studies demonstrating that STm enhances OC formation even in *MyD88*$^{-/-}$ and *TLR4*$^{-/-}$ cells indicate that autocrine IL-1ß and MyD88-depedent sensing of STm PAMPs do not fully explain the increase in OC formation during STm infection.

There are limitations of this work that will drive future studies. The precise mechanisms of RANKL-mediated enhanced STm intracellular burdens are currently unknown. Determining both the bacterial factors as well as host determinants (*e.g.*, altered nutrient availability) that allow for STm to persist within RANKL-treated monocytes will be an important future direction of this work. Experiments in Chapter IV indicate that enhanced STm survival may not depend

upon RANKL-mediated epigenetic changes, as increased STm burdens did not persist following RANKL withdrawal. Attractive alternative explanations for RANKL include the pro-survival and anti-apoptotic actions that RANKL imparts on monocytes. Specific bacterial effectors that are dependent on T3SS1 or T3SS2 should also be investigated to determine if these effectors can alter RANKL-treated monocytes in such way to promote their survival. While data from these studies strongly indicate that RANKL dampens the NLRP3 and NLRC4 inflammasomes during either activation by purified PAMPs or by live infection, the precise mechanisms of reduced IL-1ß signaling are unknown. Future studies should continue to test the hypothesis that RANKL epigenetic silencing of *IRF8* plays a role in mediating reduced IL-1ß production utilizing *IRF8*$^{-/-}$ cells, *IRF8* overexpression, conditional genetic ablation of monocyte RANK, and additional pharmacologic blockade *in vitro* and *in vivo*. Complementary hypotheses, such as altered subcellular replication of STm in RANKL treated monocytes as well as the impact of TLRs and alternative RANKL regulated genes involved in antibacterial immunity (*e.g.*, BLIMP-1) should also be tested in future works. Data described in this chapter also implicate that STm influences OC formation. Future studies should examine the STm specific effectors that may drive this process and delineate the relative contributions of specific host factors, such as IL-1ß signaling. In total, this work demonstrates that RANKL renders monocytes more susceptible to STm intracellular survival during infection while simultaneously dampening the monocyte IL-1ß inflammasome response to STm specific PAMPs. These data also demonstrate that STm can alter monocyte cell fate by promoting osteoclast differentiation in RANKL-experienced monocytes.

CHAPTER V: CONCLUSIONS AND FUTURE DIRECTIONS

Summary of experimental findings: Intestinal inflammation and osteoclastogenesis

Crosstalk between the gastrointestinal tract and the bone environment is increasingly becoming recognized as an important bi-directional axis to maintain both intestinal and skeletal homeostasis. However, the mechanisms that govern interactions between these two spatially distinct organs, especially during pathologic conditions, are not fully described. A major goal of this work (Chapter III) was to uncover mechanisms of bone loss in the setting of gastrointestinal inflammation, as is often observed clinically during IBD.

There are many established animal models of IBD, each with a unique combination of advantages that closely mimic human pathology and disadvantages that can overlook or overemphasize specific facets of this disease. Therefore, it is critical to employ multiple experimental murine models of IBD to more fully model the constellation of genetic, microbial, immune factors that contribute to IBD pathogenesis. I utilized chemical, T cell, and infectious driven models of IBD to better understand how bone loss occurs during intestinal inflammation. These distinct models of intestinal inflammation revealed the pathologic expansion of a specific osteoclast precursor population characterized by a unique pattern of surface receptors associated with osteoclast formation. Increased MDL-1 was chief among the pro-osteoclastogenic coreceptors increased during DSS colitis and anti-MDL-1 treatment inhibited increased osteoclastogenesis in OCPs derived from mice with colitis. Anti-MDL-1 treatment protected against bone loss during IBD. Surprisingly, this protection against bone loss during IBD was not associated with protection against intestinal inflammation, suggesting that MDL-1 blockade may uncouple intestinal inflammation from bone loss during chemically induced colitis.

Future Directions: Intestinal inflammation and osteoclastogenesis

While this work strongly implicates MDL-1$^+$ OCPs in the pathogenesis of bone loss during IBD, several important future directions remain to more firmly confirm and mechanistically extend this discovery. The following sections are organized by experimental priority.

Explore the mechanism of action of anti-MDL-1 blockade

While the data presented in Chapter III strongly suggest that MDL-1 is an important mediator of bone loss during IBD, the precise mechanism by which anti-MDL-1 antibody protects against bone loss during colitis remains unanswered. Prior research implicates several possibilities that are currently being explored. Anti-MDL-1 antibody most likely protects against bone loss during IBD by 1) inhibiting the release of MDL-1 associated cytokines or signaling byproducts (*e.g.*, nitric oxide species), 2) antibody-mediated depleting of MDL-1$^+$ cells, 3) indirect impact on skeletal architecture on non-skeletal cells (*e.g.*, granulocytes), or 4) treatment of the underlying intestinal inflammation. It is unlikely that MDL-1 directly impacts osteoblast function given that these cells do not express MDL-1 (139). However, measuring markers of bone turnover, such as osteoblast-specific alkaline phosphatase in conjunction with markers for resorptive bone turnover (such as C-terminal telopeptide [CTX]) will more firmly determine if MDL-1 mediated protection against bone loss during IBD is governed by OCs, OBs, or both.

Given that we did not detect differences in weight or histopathology score between isotype treated and anti-MDL-1 treated mice during DSS colitis, it is unlikely that anti-MDL-1 treatment is treating the underlying intestinal inflammation as a mechanism of protection against bone loss during chemical colitis. However, MDL-1 is highly expressed on granulocytes, which are mobilized during DSS colitis (234). It is therefore possible that anti-MDL-1 treatment is

modulating granulopoiesis to augment neutrophil development within the bone marrow or neutrophil chemotaxis to the inflamed colon. This outcome is not likely given that we did not observe differences in colon histologic injury scores and that prior research has highlighted the importance of neutrophils in mediating histologic pathology during DSS colitis (234).

Flow cytometry on the bone marrow, blood, and lamina propria from mice with DSS colitis and treated with either isotype or anti-MDL-1 antibody will test the hypothesis that anti-MDL-1 treatment results in cell depletion. These studies should be performed at time points where we observed an increase in OCPs during DSS colitis (*e.g.*, day 7). These experiments should evaluate the abundance of pre-osteoclast populations (*e.g.*, LSKs, OCPs, and monocytes), as well as granulocytes and lymphocytes in these tissues and determine the surface expression of MDL-1 on these populations. Additional studies should determine if anti-MDL-1 treatment alters cell death (*e.g.*, by examining propidium iodide and annexin V staining) or cellular proliferation (*e.g.*, by examining Ki67 staining). Staining histologic sections (femurs and colons) for granulocytes and monocytes would also help clarify these results.

Femurs from the completed studies investigating the efficacy of anti-MDL-1 treatment will be processed for histologic staining of OCs for histomorphometric analysis. Evaluating the cytokines within the bone marrow microenvironment from frozen femur homogenates obtained from isotype or anti-MDL-1 treated will be tested via targeted ELISA for the abundance of MDL-1-associated cytokines (*e.g.*, TNF-α). Prior research has also demonstrated a role for NO regulation of TNF-α converting enzyme (TACE) as one mechanism of pathologic MDL-1^{+} immature myeloid during a liver injury model of sepsis (148). Accordingly, measuring TACE activity, NO species, as well as the machinery regulating NO production (eNOS and iNOS) represent important areas of future investigation. Mechanistically, nitric oxide is hypothesized as

an important mediator of inflammatory bone loss and linked to OCP function and osteoclastogenesis (82, 235, 236). Collectively, these studies will help pin down a potential mechanism or mechanisms of how anti-MDL-1 treatment protects against bone loss during intestinal inflammation.

Determine if anti-MDL-1 treatment is specific to bone loss during DSS colitis

Additional studies should determine whether anti-MDL-1 protects against bone loss in alternative models of colitis. To accomplish this goal, ongoing studies will evaluate if anti-MDL-1 treatment prevents bone loss during ACT colitis. Mice will be treated weekly with 2.5 mg/kg anti-MDL-1 antibody starting at four weeks post-transfer. Femurs will be collected and processed for micro CT, histology, and cytokine analysis. Colons will also be processed for histologic injury scoring. Future studies should also extend these experiments to infectious models of colitis and explore links between MDL-1 and anti-bacterial immunity during infectious colitis.

Examine the specific cytokine(s) that induce expression of MDL-1 in OCPs during intestinal inflammation

Although prior work has demonstrated that several cytokines can induce MDL-1 on immature myeloid cells, including G-CSF and TNF-α, future studies should determine specific colitis-associated cytokines that induce MDL-1 on purified OCPs (139, 148, 195, 197, 237). To accomplish this, future experiments should sort OCPs from WT mice and stimulate with a range and combination of cytokines that we found to be associated with experimental colitis, including TNF-α, G-CSF, CCL-2, and IL-23. Following stimulation, cells should be assessed for either *CLEC5A* expression (via qRT-PCR), or surface MDL-1 expression via flow cytometry or Western blot to capture both transcriptional and protein-level changes to MDL-1. An alternative

approach to these studies would be to stimulate WT purified OCPs with serum from mice with or without colitis to more broadly assess how complex, physiologically relevant cytokine mixtures impact MDL-1 expression on OCPs. Serum needed for these studies is already collected and a range of cytokine concentrations have already been tested in murine BMM monocultures and OC-OB co-cultures. A complementary, unbiased approach to these studies should utilize bulk RNA-Seq to define the transcriptional changes to OCPs that occur over the course of DSS colitis. These studies should evaluate early time points during colitis (*e.g.*, days 1, 3, and 7) and sort OCPs from mice with or without colitis. Alternatively, additional studies should sort MDL-1^+ and MDL-1^- OCPs for bulk RNA-seq, or move towards single-cell sequencing technologies to resolve the heterogeneity within OCPs.

Evaluate the suppressive capacity of MDL-1^+ OCPS

OCPs were first identified in the context of an inflammatory murine model of arthritis and were shown to demonstrate T cell suppressive activity similar to MDSCs (82). However, the suppressive activity of OCPs during colitis has not been tested. It is possible that OCPs traffic to the intestine to suppress T cell driven inflammation. To test this hypothesis in future studies, OCPs will be isolated from mice with or without DSS-colitis via FACS. Concurrently, splenocytes from Thy1.1 mice and $CD4^+CD25^+$ T-regs from WT mice will be purified via FACS. Thy1.1 splenocytes will be labeled with cell trace violet. Purified OCPs will be co-cultured with labeled Thy1.1 splenocytes at decreasing ratios (1:2, 1:4, 1:8, 1:16, 1:32, and 1:64) and activated with anti-CD3/28. As a positive control, labeled Thy1.1 splenocytes will be co-cultured with FACS-purified WT T-regs. After 3 days of culture, Thy1.1^+ T cells will be assessed for cell trace violet staining to determine the suppressive capacity of OCPs derived from mice with or without colitis. Follow-up studies should also evaluate the suppressive capacity of OCPs isolated from

mice with alternative models of colitis, such as ACT. It is possible that OCPs derived from mice with colitis exhibit enhanced suppressive activity compared to controls. Should this occur, follow-up studies should evaluate if intraperitoneal injection of OCPs from mice with colitis improves intestinal inflammation compared to controls.

Extend murine findings to human correlates of bone loss during IBD

Work described in Chapter III implicates MDL-1 in the pathogenesis of bone loss during murine experimental colitis. Future studies should extend these findings to humans using a combination of human samples and mining publicly available data sets. Because OCPs are found within the bone marrow, and the markers of these cells are poorly described in circulation, their precise peripheral correlate has not yet been defined. However, it is evident that circulating human monocyte populations, particularly $CD14^{+}CD16^{-}$ populations are capable of osteoclastogenesis when exposed to M-CSF and RANKL (238). Therefore, future studies should evaluate MDL-1 expression in human monocyte populations from healthy controls compared to patients with IBD. Importantly, where possible, factors such as disease activity and medication use should be documented to evaluate how active inflammation or various therapeutics impact monocyte MDL-1 expression. This should be done via flow cytometry to delineate which specific cell populations express MDL-1 in PBMCs. To this end, preliminary studies have begun to test the expression of MDL-1 on human PBMCs from healthy controls or patients with IBD (**Figure 43**).

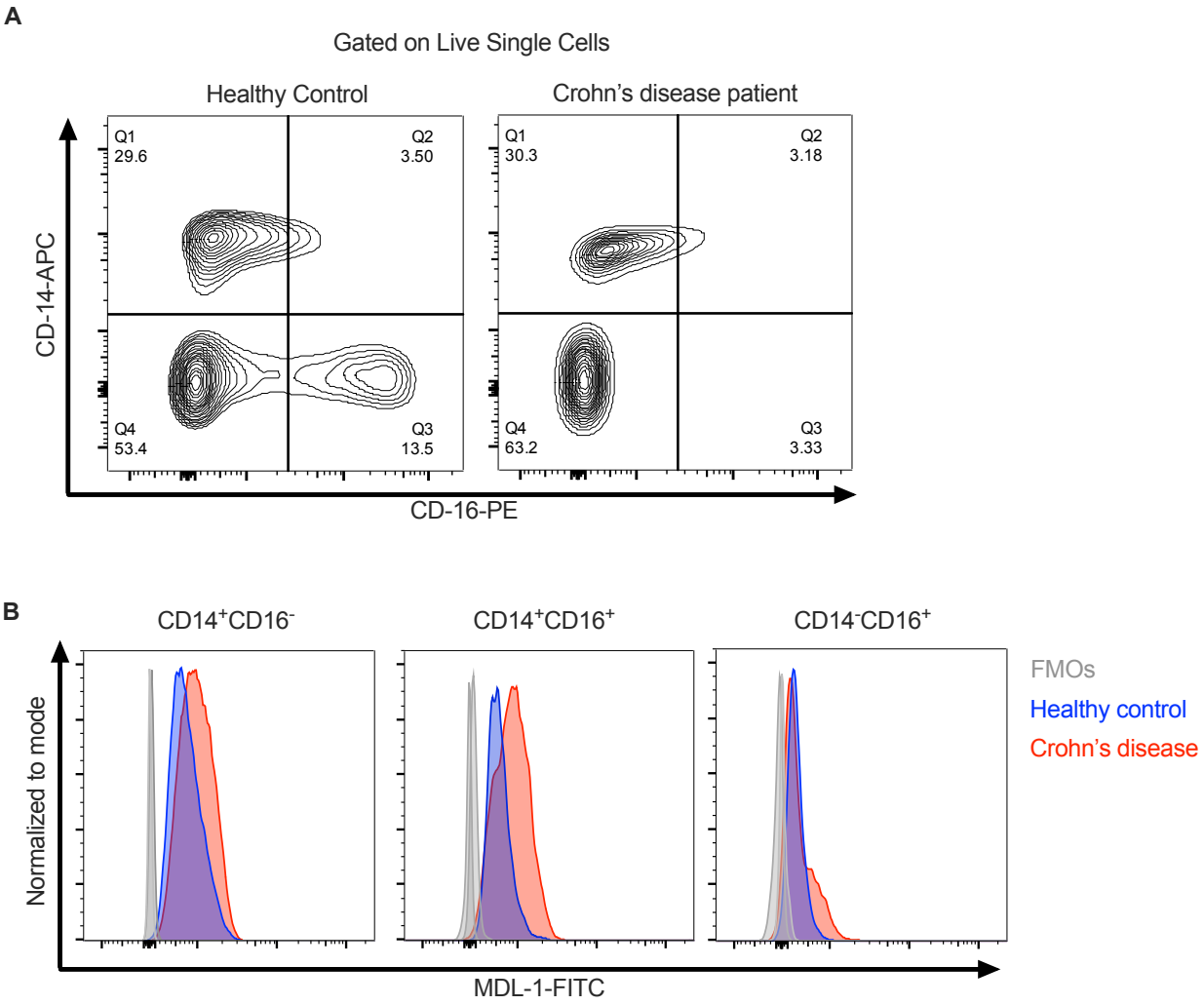

Figure 43. MDL-1 expression on human PBMCs.

Human PBMCs from pooled healthy controls (Zenbio), or freshly isolated PBMCs from a patient with Crohn's disease were stained with a cocktail of surface antibodies to identify live CD14 and CD16 monocytes and evaluate MDL-1 surface expression (human anti-MDL-1-FITC clone # REA912, Miltenyi). FMO = fluorescence minus one control. Samples collected with informed consent through IRB# 200422 in collaboration with Dr. Lori Coburn, Dr. Jeremy Goettel, and Justin Jacobse.

To evaluate MDL-1 expression in patients with IBD using publicly available data sets, several approaches should be taken. There are no data sets investigating samples from bone marrow of patients with IBD. Many data sets evaluating gene expression from inflamed and uninflamed intestinal tissue exist, several of which demonstrate enriched gene expression of *CLEC5A* (239). However, the contribution of intestinal mononuclear cells to OC formation *in vivo* remains unclear. Therefore, one should evaluate gene expression in either single-cell or bulk RNA-seq data sets from patient PBMCs. For bulk RNA-sequencing, because monocytes (and by extension, OCPs) likely represent a small fraction of the circulating cells, data sets that utilize deep sequencing methodologies (*e.g.*, those investigating rare sequences such as long-non-coding RNAs) should be used for analysis. Preliminary investigations evaluating *CLEC5A* expression in IBD patient PBMCs in one such study demonstrate increased expression of *CLEC5A* in patients with IBD compared to age and sex matched healthy controls and compared to patients with irritable bowel syndrome and Celiac disease (**Figure 44**).

Additional studies in murine models of colitis could help translate these results to human patients. Although we observed an increase in BV/TV when mice were treated with anti-MDL-1 antibody during DSS colitis, we did not directly measure how this increase in BV/TV correlated with fracture risk. Future studies should investigate bone fragility and fracture risk through moment of inertia and three-point bend tests to more rigorously assess improvements in bone quality. Collectively, these future studies will enhance the translatability of these findings to human patients.

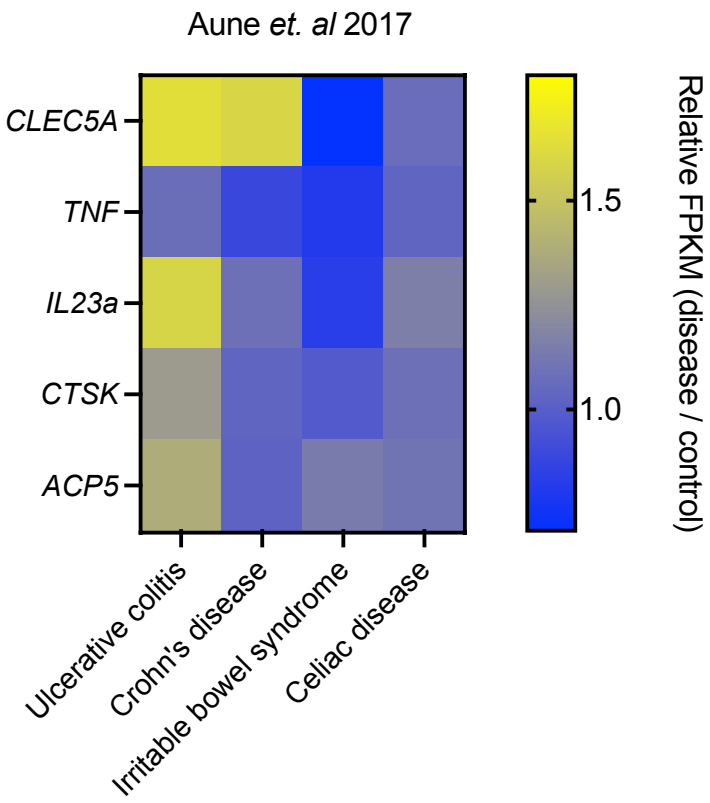

Figure 44. Expression of MDL-1 and osteoclast related genes using publicly available RNA-seq from human PBMCs.

Data derived from Aune, *et al*., (240) in which blood samples were obtained from age and gender matched healthy controls (N = 8) and patients with either ulcerative colitis (N = 6), Crohn's disease (N = 6), irritable bowel syndrome (N = 6), and Celiac disease (N = 6). RNA was extracted and submitted for RNA sequencing with an average sequencing depth of 3.5×10^7 reads ($\pm 9 \times 10^6$) through the Vanderbilt Technologies for Advanced Genomics (VANTAGE) as outlined in Aune, *et al*., (240). Only differentially expressed genes with a cutoff of 0.5 fragments per kilobase per million reads (FPKM) were reported. For each gene reported above, average FPKM for a given disease condition were normalized to the average FPKM from healthy controls and reported as fold change.

Determine the relative contributions of inflammatory cytokine environment and the presence of MDL-1$^+$ OCPs

An important remaining question is whether MDL-1$^+$ OCPs can enhance osteoclastogenesis outside of the inflammatory skeletal environment within mice with colitis. To test this, future studies are planned to FACS purify OCPs from TdTomato-TRAP reporter mice with or without DSS colitis. These OCPs will be transferred into WT mice via intra-femoral injection. PBS will be injected within the contralateral femurs of the same mice. Femurs will be harvested 14 days following injection and evaluated for changes in trabecular bone volume. These data will help determine cell-intrinsic contributions to reduced trabecular bone from OCPs. Flow cytometry of bone marrow will confirm engraftment of TdTomato$^+$ OCPs and immunofluorescence of femurs will confirm if osteoclasts in recipient mice are TdTomato$^+$. Engraftment of OCPs without a reduction in trabecular BV/TV would indicate the surrounding cytokine milieu or local interactions with surrounding cells are crucial for driving enhanced osteoclastogenesis.

Evaluate if expansion of MDL-1$^+$ OCPs is specific to intestinal inflammation

The studies described in Chapter III were focused upon models of intestinal inflammation. Therefore, we did not test additional models of local or systemic inflammation. Given that OCPs expressing MDL-1 have been previously described in murine models of inflammatory arthritis models, it is worth testing how specific the proliferation of OCPs is to gastrointestinal inflammation (82). Previous studies have also implicated MDL-1$^+$ in the pathogenesis of a murine liver injury model of sepsis (148). Future studies should evaluate whether systemic bacterial infection or LPS injection similarly induce MDL-1 expression on

OCPs. These studies may reveal unexpected roles of MDL-1 signaling in anti-bacterial immunity.

Determine the ligand(s) of MDL-1 during intestinal inflammation

To date, the only identified ligand for MDL-1 is dengue virus (196). However, signaling through MDL-1 is clearly important *in vivo* and *in vitro* for osteoclastogenesis (215). Ligands for activating osteoclast co-receptors are poorly described and likely promiscuous. Such ligands may also be tissue specific. Some evidence implicates galectin-9 as a potential ligand for MDL-1 (241). Galectin-9 has been previously reported to bind T cell immunoglobulin and mucin domain-containing protein 3 (TIM-3) as a mechanism to repress activated Th1 T cells (242–244). Future studies should test if galectin-9 promotes MDL-1 signaling in OCPs. This can be accomplished by FACS purifying OCPs from mice with or without colitis and treating with a range of recombinant galectin-9 in the presence of M-CSF and RANKL and assess for osteoclastogenesis. To determine if MDL-1 binds galectin-9, surface plasmon resonance studies can be performed to assess galectin-9 and MDL-1 interactions. Additional studies with recombinantly expressed MDL-1 and site-directed mutagenesis would help determine the specific MDL-1 residues driving interactions with potential ligands.

Summary of experimental findings: RANK/RANKL and STm pathogenesis

Experiments in Chapter IV set out to uncover how RANK/RANKL signaling impacts bacterial replication, antibacterial immunity, and cell fate during monocyte infection with STm. Monocytes are an important cell type that contributes to STm restriction in the host during intestinal infection, and prior work has demonstrated that some monocyte populations serve as a reservoir of STm infection. Furthermore, RANKL signaling is relevant for monocyte responses *in vivo*, as monocytes encounter STm in areas replete with RANKL. Data described in Chapter IV demonstrate that RANKL enhances STm survival within murine and human monocytes. Despite enhanced bacterial burdens, RANKL treated monocytes infected with STm or stimulated with purified NLRP3 or NLRC4 agonists exhibited significant impairments in IL-ß release compared to non-RANKL treated controls. Reductions in IL-1ß in response to STm or purified STm inflammasome activators were associated with reductions in *IRF8* expression. Furthermore, reduced IL-1ß persisted with RANKL withdrawal. On the host side, RANKL-mediated enhanced STm survival and dampened IL-1ß production were not dependent upon TLR4 or MyD88. In addition to these studies, experiments in Chapter IV demonstrated that STm promotes OC formation. Increased osteoclastogenesis during STm infection was partially dependent upon TLR4 and MyD88.

Future directions:

These data strongly argue that 1) STm survives within RANKL-treated monocytes, 2) RANKL dampens monocytic NLRP3 and NLRC4 inflammasome responses to STm infection and STm PAMPs, and 3) that STm promotes osteoclastogenesis. However, future work is needed to expand upon the mechanism by which STm interacts with RANKL-experienced monocytes to alter bacterial survival, anti-bacterial immunity, and osteoclastogenesis.

Evaluate the mechanisms for enhanced STm survival within RANKL-treated monocytes

RANKL increases STm survival within monocytes, and this increase in bacterial burdens did not persist following RANKL withdrawal. Future studies should test whether the following downstream functions of RANKL contribute to enhanced STm burdens, including 1) induction of pro-survival pathways 2) induction of anti-apoptotic pathways 3) increased host glycolytic metabolism, and 4) altered cytoskeletal rearrangements.

RANKL and M-CSF enhance pro-survival pathways through Src (106, 107). M-CSF additionally promotes survival in monocytes through the induction of anti-apoptotic factors such as Bcl-2 (106, 107). However, few studies have examined how intracellular infection of RANKL-experienced monocytes or mature osteoclasts alters cell survival. Given that prior studies have demonstrated cell death of mature OCs following RANKL withdrawal, it is possible that monocytes experiencing RANKL withdrawal are more prone to apoptosis, which is exacerbated during STm infection (106). Additional studies should investigate shorter RANKL withdrawal time courses to evaluate if enhanced STm burdens are dependent upon concurrent RANKL signaling. Protein lysates from these studies should be collected in parallel to probe for Src and Bcl-2 by Western blot. RANKL also promotes signaling through several tyrosine kinases that promote cell survival and the calcium signals needed for osteoclastogenesis, such as Bruton's tyrosine kinase (BTK) and tyrosine-protein kinase (TEC) (245, 246). BTK/Tec have been previously shown to regulate OC differentiation in conjunction with ITAM co-receptor signaling (245). Accordingly, it is possible that STm infection strengthens BTK/Tec signaling in RANKL-primed monocytes. This hypothesis should be evaluated by staining for these proteins via Western blot in RANKL naïve or experienced monocytes infected with STm. Additionally, pharmacologic modulation of BTK/Tec with FDA-approved tyrosine kinase inhibitors (*e.g.*,

Tofacitinib) should be evaluated to test if these treatments are able to reverse RANKL-mediated enhanced bacterial burdens. Studying BTK/Tec signaling in the context of STm biology also represents one thread to intertwine ITAM osteoclast co-receptor biology discussed in Chapter III with anti-bacterial and inflammatory responses described in Chapter IV.

In addition to testing the role of cell survival and anti-apoptotic factors induced by RANKL, future studies should also examine if RANKL mediated changes to monocyte metabolism contribute to enhanced intracellular STm burdens. Metabolic reprogramming of monocytes is an integral part of RANKL-driven osteoclatogenesis (191, 247–250). Mature OCs have increased mitochondria and successful osteoclastogenesis requires both mitochondrial respiration and glycolytic metabolism (247, 248, 250, 251). STm has also been demonstrated to reprogram macrophage metabolism towards increased glycolysis (252). Accordingly, RANKL and STm may synergistically create a host niche favorable for STm replication and osteoclastogenesis due to shifts in nutrient availability and metabolic changes. Several future studies should test this hypothesis. Oxygen consumption rate and extracellular acidification rate during STm infection in RANKL-experienced or naïve monocytes during STm infection can be measured via Seahorse metabolic flux assays and compared to macrophages stimulated with either LPS or heat-killed STm. These studies should be performed at time points where we observe RANKL-mediated enhanced intracellular STm burdens (*e.g.*, 24 hrs post-infection). In addition to metabolic flux assays, pharmacologic modulation of host cell metabolism with drugs such as rapamycin should be performed to modulate glycolysis and determine the impact on intracellular STm infection.

Yet another impact that RANKL imparts upon monocytes is dramatic cytoskeletal rearrangements. Because STm T3SS1 effectors also lead to dramatic alterations of host

cytoskeletal architecture, it is unclear how the competing actions of RANKL and STm T3SS1 effectors will play out within the infected RANKL-experienced monocyte. Future work examining OC function by bone resorption during STm infection will help clarify if infected OCs have an altered capacity to resorb bone, a process that is dependent on cytoskeletal rearrangements. While STm predominately replicates in the SCV, some cytoplasmic replication occurs in mononuclear cells. It is possible that cytoskeletal rearrangements lead to enhanced SCV replication in RANKL-treated monocytes. Alternatively, STm could shift towards a predominantly non-SCV / cytoplasmic replication in RANKL experienced monocytes. Future studies should utilize imaging approaches and fluorescent STm reporters to visualize intracellular STm and SCV-associated proteins. Future work should also employ novel two-color fluorescent STm reporters that allow one to discriminate between SCV and cytoplasmic replication (253).

Determine the role of *IRF8* in reduced IL-1ß production during STm infection

While work described in Chapter IV demonstrates that reduced IL-1ß signaling is associated with reductions in *IRF8*, future studies are required to test the hypothesis that RANKL-mediated silencing of *IRF8* results in reduced inflammasome activation in response to STm. Future experiments should evaluate additional readouts of inflammasome activation, including gasdermin D cleavage as well as perform studies in cells derived from *Caspase1/11*$^{-/-}$ mice. Additional studies should also overexpress *IRF8* in RANKL treated monocytes to determine if IL-1ß signaling is restored in this scenario. Overexpression experiments of downstream NAIPs should be performed to determine the relative contributions of *IRF8* downstream inflammasome components in mediating IL-1ß release in response to STm infection.

It is possible that *IRF8* silencing is not solely responsible for reductions in IL-1ß release. Should this appear to be the case, additional studies investigating the role of BLMIP-1, TLRs, as well as STm subcellular localization should be investigated. It is possible that RANKL promotes STm SCV replication or alters the SCV in such a way that prevents detection of STm PAMPs even when *IRF8* is restored by overexpression. The studies described in the previous section will help test this possibility. Because *in vivo* inflammasome responses to STm infection are likely derived from multiple cellular sources, future studies are needed to clarify the *in vivo* relevance of monocyte RANKL signaling in STm response. Experiments utilizing conditional knockout of the RANK receptor using a tamoxifen inducible CSF1R-cre mice will be critical for accomplishing this goal. Complementary approaches using organoids should also be examined to investigate the relative role of epithelial inflammasome responses to STm in the presence of RANKL. Should these studies indicate that *IRF8* is not responsible for reduced IL-1ß signaling in response to STm infection, future studies could employ clustered regularly interspaced short palindromic repeats (CRISPR)-based screening approaches to identify alternative host factors that contribute to preventing inflammasome responses during STm infection within monocytes.

Explore the STm effectors and host factors needed for enhanced osteoclastogenesis

Data described in Chapter IV establish that STm enhances osteoclastogenesis. However, the mechanisms by which this occurs remain unclear. Data from *invA spiB* mutants, as well as *TLR4*$^{-/-}$ and *MyD88*$^{-/-}$ cells suggest that enhanced osteoclastogenesis is not solely dependent upon sensing MyD88-dependent PAMPs or autocrine IL-1ß signaling. Additional autocrine host signaling may promote osteoclastogenesis during STm infection, such as TNF-α, and should be measured in cell culture supernatants. Follow-up studies should utilize anti-TNF-α treatment to test the role of this cytokine in driving enhanced osteoclastogenesis during STm infection.

Future experiments should explore which STm effectors promote osteoclastogenesis. These studies should utilize T3SS2 mutants (*e.g.*, *sseD*) to evaluate if T3SS1 effectors or intracellular STm PAMPs are sufficient to enhance osteoclastogenesis. Additional studies should generate additional bacterial mutants that test this hypothesis. Prior work indicates that the T3SS1 effector, SopB, is critical in reprogramming epithelial cells during STm infection by modulating host RANK/RANKL signaling (223). Accordingly, future studies should test the specific hypothesis that SopB enhances osteoclastogenesis through both generation of a *sopB* mutant, as well as treatment of RANKL-treated monocytes with purified SopB.

Establish a model of STm osteomyelitis

While studies presented in this dissertation did not evaluate STm osteomyelitis, future work utilizing fluorescent STm strains, TdTomato-TRAP reporter mice, as well as mice deficient in key innate signaling pathways will 1) help establish a murine model of STm osteomyelitis that impacts many immunocompromised patients and 2) aid in determining how the location of RANKL signaling dictates anti-bacterial and inflammatory responses to STm infection. *In vitro* work highlighting direct interactions between STm and mature OCs is directly relevant to modeling the host-microbial interactions that occur during STm-driven osteomyelitis. Understanding how the location of RANKL signaling modulates host immune response to STm is important given emergent work highlighting diverging functions of the soluble decoy receptor for RANKL, OPG, depending on the location of OPG production (222). Osteomyelitis should be achieved using our lab's published protocols in mice naturally resistant to STm, such as CBA/J mice (254–258). Fluorescent reporter mice, as well as TdTomato-TRAP reporter mice backcrossed to a CBA/J background will help test the hypothesis that RANKL experienced monocytes, or mature osteoclasts, serve as a bona fide *in vivo* reservoir of STm replication

during osteomyelitis. These studies will also serve as a comparison to either orogastric or intraperitoneal infection with STm, in which STm will encounter monocytes that will have experienced different levels of RANKL *in vivo*. Additional experiments should measure RANKL and OPG abundance at various tissue sites during these multiple routes of infection (*e.g.*, orogastric, intraperitoneal, intrafemoral, and intravenous).

APPENDICES

Two appendices are outlined below that describe studies that are tangentially related to the results presented in the main dissertation. The appendices are titled:

A: Role of IL-12/23 signaling and adaptive immunity in IBD-associated bone loss

B: Impact of microbiota on bone loss during intestinal inflammation

A: Role of IL-12/23 signaling and adaptive immunity in IBD-associated bone loss

Introduction

One original goal of this work was to determine the impact of IBD-associated cytokines and the adaptive immune system on bone loss during intestinal inflammation. We discovered that several cytokines linked to altered bone homeostasis are increased in the femurs of mice subjected to DSS and ACT colitis when compared to controls (**Figure 9**). Of particular interest, IL-12/23p40 (p40), the common subunit of IL-12 and IL-23 heterodimers, demonstrated one of the greatest relative increases in both colitis models (**Figure 9**). IL-12 and IL-23 are canonically thought to promote Th1 and Th17 cell differentiation, respectively. Intriguingly, these cytokines coordinate opposing effects in skeletal biology, although the precise mechanisms are unclear: IL-12 decreases bone resorption, whereas IL-23 promotes bone resorption (259–261). Although blockade of both IL-12 and IL-23 through anti-p40 antibody treatment improves IBD symptoms in some patients, systemic p40 blockade has unknown consequences on bone remodeling. New medications that selectively target IL-23 have shown promise in treating IBD, and we set out to evaluate how selective IL-23 blockade may impact bone remodeling during colitis. The goal of these studies was to examine how IL-12/23 signaling impacts bone health during colitis through investigation of 1) direct effects on bone cells and 2) indirect actions on T cells.

Results

To test if IL-23 induces OC formation, I treated murine BMMs with a range of IL-23 doses, as well as IL-12/23p40, and IL-12. TNF-α was used as a positive control to induce osteoclast formation and OPG was used as a negative control to inhibit RANKL-mediated OC formation. IL-23, IL-12/23p40, and IL-12 did not enhance osteoclastogenesis in monoculture in either continuous RANKL, or with BMMs pre-committed to the OC lineage with two days of

RANKL treatment (**Figure 45**). Similarly, co-culture of OCs and OBs in the presence of IL-23 did not impact osteoclastogenesis (**Figure 45**). Because pre-osteoclast populations within the skeletal environment during intestinal inflammation are surrounded by a complex cytokine milieu, we tested if multi-cytokine interactions influenced osteoclastogenesis. Given that we previously detected increased IL-23 and TNF-α within the femurs of mice with colitis, we tested whether pre-treatment of RANKL-primed BMMs with IL-23 would enhance osteoclastogenesis in the presence a low dose of TNF-α that does not induce robust osteoclastogenesis. We found that IL-23 pretreatment increased osteoclastogenesis following addition of low dose TNF-α (**Figure 46**).

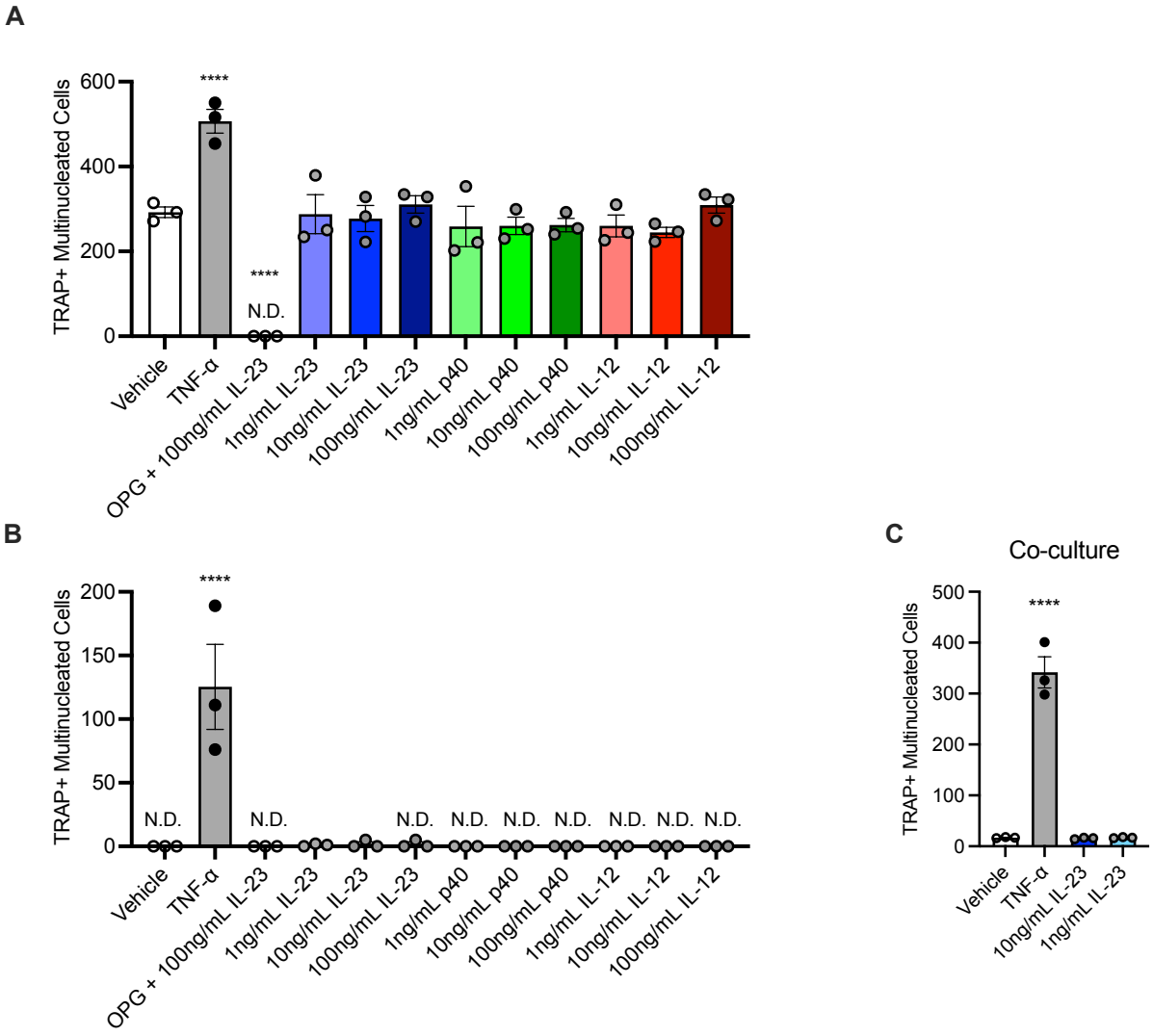

Figure 45. IL-23 does not directly promote osteoclastogenesis.

(A) Murine BMMs derived from C57BL/6J mice were cultured for seven days with M-CSF (CMG14-12 supernatant 5% v/v) and RANL (35 ng/mL) in the presence of the indicated concentration of IL-23, IL-12/23 p40 (p40), or IL-12. TNF-α was used at 20 ng/mL and OPG was used at 100 ng/mL. Low endotoxin bovine serum albumin (BSA) was used as a vehicle control. (B) Murine BMMs were cultured with M-CSF (CMG14-12 supernatant 5% v/v) and RANL (35 ng/mL) for two days, followed, after which RANKL was withdrawn and the indicated

concentration of IL-23, IL-12/23 p40 (p40), or IL-12 were added to the culture media. TNF-α was used at 20 ng/mL and OPG was used at 100 ng/mL. Low endotoxin bovine serum albumin (BSA) was used as a vehicle control. (C) BMMs and osteoblasts were co-cultured in a 1:1 ratio without the addition of exogeneous M-CSF or RANKL for fourteen days in the presence of the indicated cytokine. TNF-α was used at 20 ng/mL and low endotoxin BSA was used as a vehicle control. Cells were then fixed and stained for tartrate resistant acid phosphatase (TRAP) and manually enumerated for $TRAP^+$ multi-nucleated cells. N.D. = not detected. Error bars represent mean ± S.E.M. Data analyzed via One-way ANOVA with Dunnett multiple comparisons test. **** $p<0.0001$ compared to vehicle control.

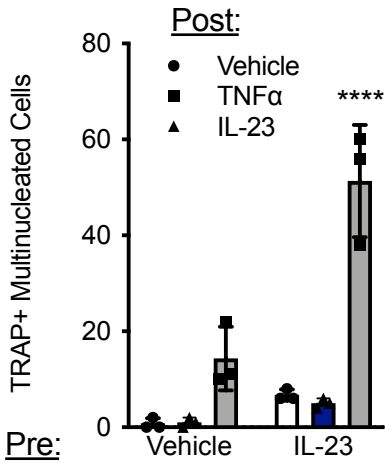

Figure 46. IL-23 pre-treatment augments TNF-α mediated osteoclastogenesis.

BMMs were cultured for two days with M-CSF (CMG14-12 supernatant 5% v/v), RANKL (35 ng/mL), and either vehicle or 100 ng/mL IL-23. RANKL was withdrawn from the culture media and BMMs were subsequently cultured in media containing M-CSF (CMG14-12 supernatant 5% v/v), IL-23 (100 ng/mL), and TNF-α (5 ng/mL) for an additional three days. Error bars represent mean ± S.E.M. Data analyzed via Two-way ANOVA with Šidák multiple comparisons test. **** $p<0.0001$ compared to vehicle control for a given post-RANKL condition.

We next set out to examine the relative role of the adaptive immune system in contributing to bone loss during intestinal inflammation. Co-culturing activated splenocytes from mice treated with 3% DSS for 7 days, but not controls, enhanced osteoclastogenesis (**Figure 47**). To determine if lymphocytes demonstrated increased surface RANKL expression *in vivo* during DSS colitis, we measured RANKL expression on lymphocyte populations during DSS colitis. $CD4^+$ T cells and B cells demonstrated increased surface RANKL expression during DSS colitis (**Figure 48**). We next examined the effector function of T cells within the skeletal environment during ACT colitis. ACT colitis did not impact surface CD4 T cell abundance or RANKL expression of $CD4^+$ T cells within the bone marrow (**Figure 49**). ACT resulted in a significant increase in $IFN\gamma^+$ and $Tbet^+$ T cells and a significant reduction in $IL\text{-}17^+$ and $ROR\gamma t^+$ T cells compared to non-colitis controls (**Figure 49**).

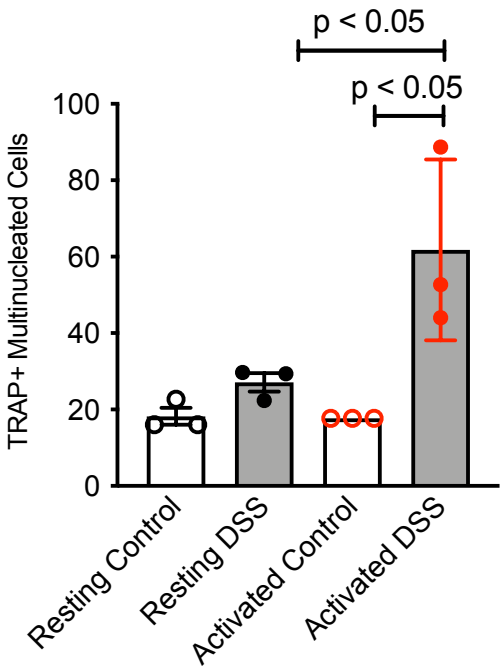

Figure 47. Activated splenocytes from mice with colitis enhance osteoclastogenesis.

Mice were administered 3% DSS to induce colitis or maintained on normal drinking water (control) for 7 days. Splenocytes were isolated and co-cultured with BMMs that had been cultured for two days with M-CSF (CMG14-12 supernatant 5% v/v) and RANKL (35 ng/mL). Co-cultures were maintained with supplementation of M-CSF (CMG14-12 supernatant 5% v/v) but not RANKL in either activating (anti-CD-3/28 and IL-2) or resting (IL-7) conditions. Cells were then fixed and stained for tartrate resistant acid phosphatase (TRAP) and manually enumerated for $TRAP^{+}$ multi-nucleated cells. Error bars represent mean ± S.D. Data analyzed via One-way ANOVA with Tukey multiple comparisons test.

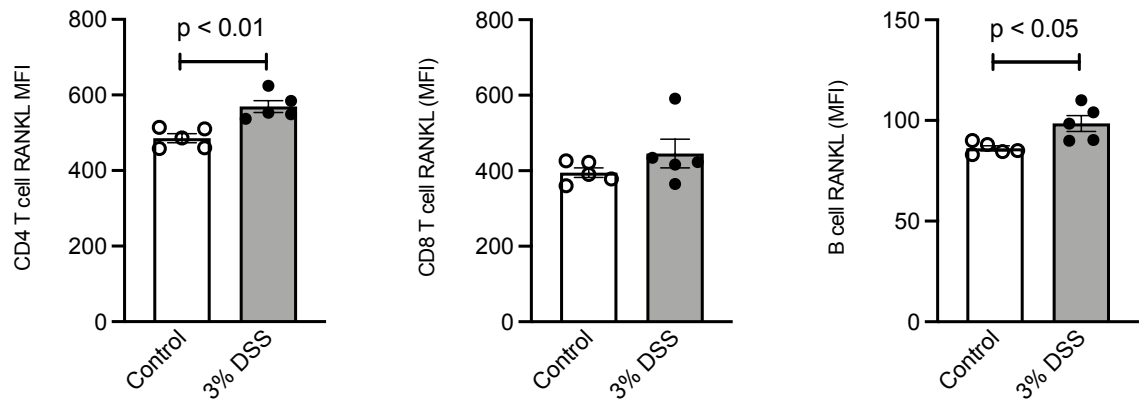

Figure 48. DSS-colitis alters lymphocyte surface RANKL expression.

Mice were administered 3% DSS to induce colitis or maintained on normal drinking water (control) for 7 days, after which single cell bone suspensions for bone marrow were analyzed for surface expression of RANKL by staining with a cocktail of surface antibodies to identify CD4 T cells (Live $CD45^{+}B220^{-}TCR\beta^{+}CD4^{+}CD8^{-}$), CD8 T cells (Live $CD45^{+}B220^{-}TCR\beta^{+}CD4^{-}CD8^{+}$), and B cells (Live $CD45^{+}B220^{+}TCR\beta^{-}$). Error bars represent mean ± S.E.M. Data analyzed via Student's t-test.

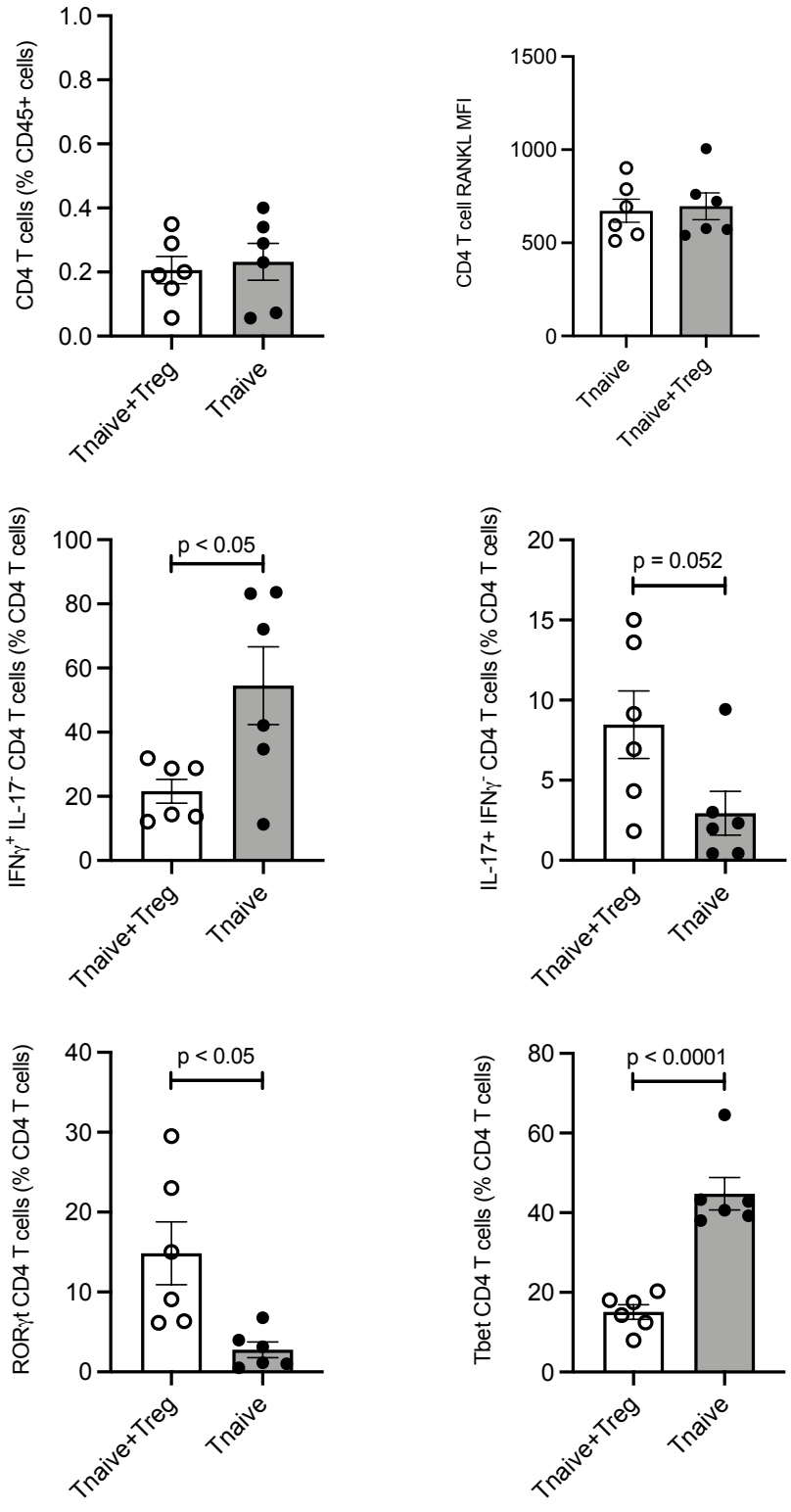

Figure 49. Adoptive T cell transfer colitis alters T cell effectors within the bone marrow.

Rag1$^{-/-}$ mice were subjected to ACT colitis by intraperitoneal injection of either 5.0 x 10^5 naïve T cells or a non-colitis control co-injection of a 5:1 ratio of naïve T cells to T-regulatory cells (T-regs). Following 5 weeks of colitis, single cell suspensions of bone marrow were stained with a cocktail of surface antibodies to identify $CD4^+$ T cells (Live $CD45^+TCR\beta^+CD4^+$) as well as surface RANKL. For intracellular cytokine stimulation and staining, bone marrow was plated and stimulated for 6 hrs with PMA/ionomycin with Golgi-stop and subsequently stained for surface markers to identify T cells. Cells were then fixed, permeabilized, and stained for the intracellular effector cytokines interferon gamma (IFNγ) and IL-17. For transcription factor staining, single cell bone marrow suspensions were stained with a cocktail of surface antibodies to identify $CD4^+$ T cells and subsequently fixed, permeabilized, and stained for intracellular transcription factors RORγT and Tbet. Error bars represent mean ± S.E.M. Data analyzed via Student's t-test.

Discussion

These data suggest that IL-23 does not directly impact osteoclastogenesis, as has been previously published (259, 262, 263). One important difference between these results and previously published findings is that IL-23 has been shown to enhance osteoclastogenesis in human PBMCs. Importantly, PBMCs contain T cells capable of producing the osteoclastogenic cytokine IL-17 after IL-23 treatment. We found that IL-23 enhanced TNF-α mediated osteoclastogenesis. However, the mechanism or physiological relevance of this finding remains unclear.

Data described in this section also suggest that intestinal inflammation impacts lymphocyte effector function within the bone marrow. DSS colitis led to a significant increase in surface RANKL expression on CD4 T cells and B cells. However, this increase in RANKL on these specific populations is dispersible for bone loss during DSS colitis, as *Rag1*$^{-/-}$, which lack mature CD4 T cells and B cells, still incur bone loss. Activated splenocytes also enhanced osteoclastogenesis in co-culture with RANKL-primed BMMs. During ACT colitis, we observed a significant increase in Th1 associated CD4 T cells, as detected by transcription factors and effector cytokine secretion. These data may represent one potential mechanism by which OCPs are induced in this model of colitis, as prior work has shown that OCPs expand in a murine model of inflammatory arthritis and suppress Th1 cells (82). IFNγ has been shown to inhibit osteoclastogenesis *in vitro* utilizing monocyte monocultures (130). However, the role of IFNγ *in vivo* is complex, and studies have demonstrated that IFNγ associated with a Th1 response ultimately promotes osteoclastogenesis (124). Collectively, these studies complement innate-focused studies in Chapter III to demonstrate that changes within the adaptive immune system also occur during intestinal inflammation and have the potential to modulate OC biology. Studies

in this appendix also indicate that IL-23 does not have a direct impact on murine osteoclast precursors.

Several limitations of this work should drive future studies. Studies are needed to specifically investigate the role of IL-23 in cultures of purified human monocytes. Future studies should evaluate how IL-23 treatment impacts *TNRFSF11A* (encoding RANK) and *NFATC1* expression in RANKL treated monocytes. Additional work should evaluate the impact of anti-IL-23p19 treatment on bone loss during colitis. Future work should perform more refined co-culture experiments with lymphocytes and BMMs to exclude the potential confounder of increase monocytic osteoclast progenitors residing within the spleen of mice with colitis. Co-culture experiments should also isolate monocyte populations from mice with and without colitis to rigorously assess the relative contribution of innate and adaptive cells in modulating osteoclastogenesis during intestinal inflammation. Futures studies should also examine how the relative abundance of Th1 and Th17 cells within the bone marrow change over time during ACT colitis. Finally, to complement studies with MDL-1, future work should evaluate how if MDL-1 alters lymphocyte effectors during ACT colitis.

B: Impact of microbiota on bone loss during intestinal inflammation

An original goal of this thesis work was to examine the contribution of dysbiosis during intestinal inflammation in driving bone loss. We first performed cage-transfer experiments to assess if bone loss was a microbiota transmissible trait, or if control stool was protective against bone loss during intestinal inflammation. Cage manipulation did not alter weight loss or histologic evidence of colitis (**Figure 50**). Transferring control mice to cages that had previously housed mice with DSS colitis did not alter trabecular BV/TV (**Figure 50**). Similarly, transferring mice with DSS-colitis into cages that had previously housed control mice did not improve trabecular BV/TV compared with mice that were maintained in colitis-caging conditions (**Figure 50**). However, significant differences in BV/TV between control mice transferred to colitis caging and DSS-treated mice transferred to non-colitis caging disappeared, perhaps indicating a subtle intermediate phenotype (**Figure 50**). To assess if manipulating the microbiota through housing changes impacted skeletal cytokines, we assessed cytokine within the femur of mice with and without colitis that had undergone cage transfers. Transferring mice with colitis into cages that had previously housed mice without colitis did not detectably alter cytokine abundances within homogenized femurs (**Figure 50**).

To complement this approach, we also utilized mice from different vendors to test different baseline microbial community composition. Mice bred in our colony demonstrated increased sensitivity to DSS colitis, as measured by increased weight loss and mortality (**Figure 51**). We did not detect differences in survival, weight loss, or histologic injury in mice purchased from Jackson Laboratories or Taconic. We found that mice purchased from Jackson Laboratories mice were susceptible to bone loss during compared to mice purchased from Taconic, despite similar weight loss and intestinal inflammation (**Figure 51**).

We next set out to determine if colonization of germ-free mice with stool from mice with or without colitis impacted trabecular bone volume. To accomplish this, we collaborated with Taconic to colonize germ-free mice with stool from mice with DSS colitis or controls. Fecal samples from prior studies with DSS-colitis had previously been collected and were screened for specific criteria as follow. Samples were collected at day seven from mice where femurs had been evaluated for trabecular bone loss and colons were scored for histologic injury at day 14. Samples from control mice demonstrated BV/TV within one standard deviation of the mean and no evidence of histologic injury. Samples from mice treated with DSS came from mice with a histologic injury score ≥ 10 and evidence of reduced BV/TV compared to control samples. Mice were gavaged twice with 100 μL of resuspended fecal pellets and colonized for 28 days. We did not detect differences weight at day 0 or day 28 (**Figure 52**). Male mice colonized with fecal contents from mice with DSS colitis demonstrated a significant reduction in trabecular BV/TV compared to mice colonized with control fecal contents (**Figure 52**).

These studies demonstrate that manipulation of the microbiota through coprophagy is insufficient to alter trabecular bone in conventionally housed mice. However, we did observe that WT mice from different vendors were differentially susceptible to bone loss during colitis despite equivalent evidence of colonic injury. More direct manipulation of the microbiota by colonizing germ-free mice with stool from mice with or without DSS colitis demonstrate that male mice colonized with fecal samples from mice with colitis led to a significant reduction in trabecular BV/TV. Future work should evaluate the specific changes to the microbiota that contribute to altered BV/TV in colonized germ-free mice.

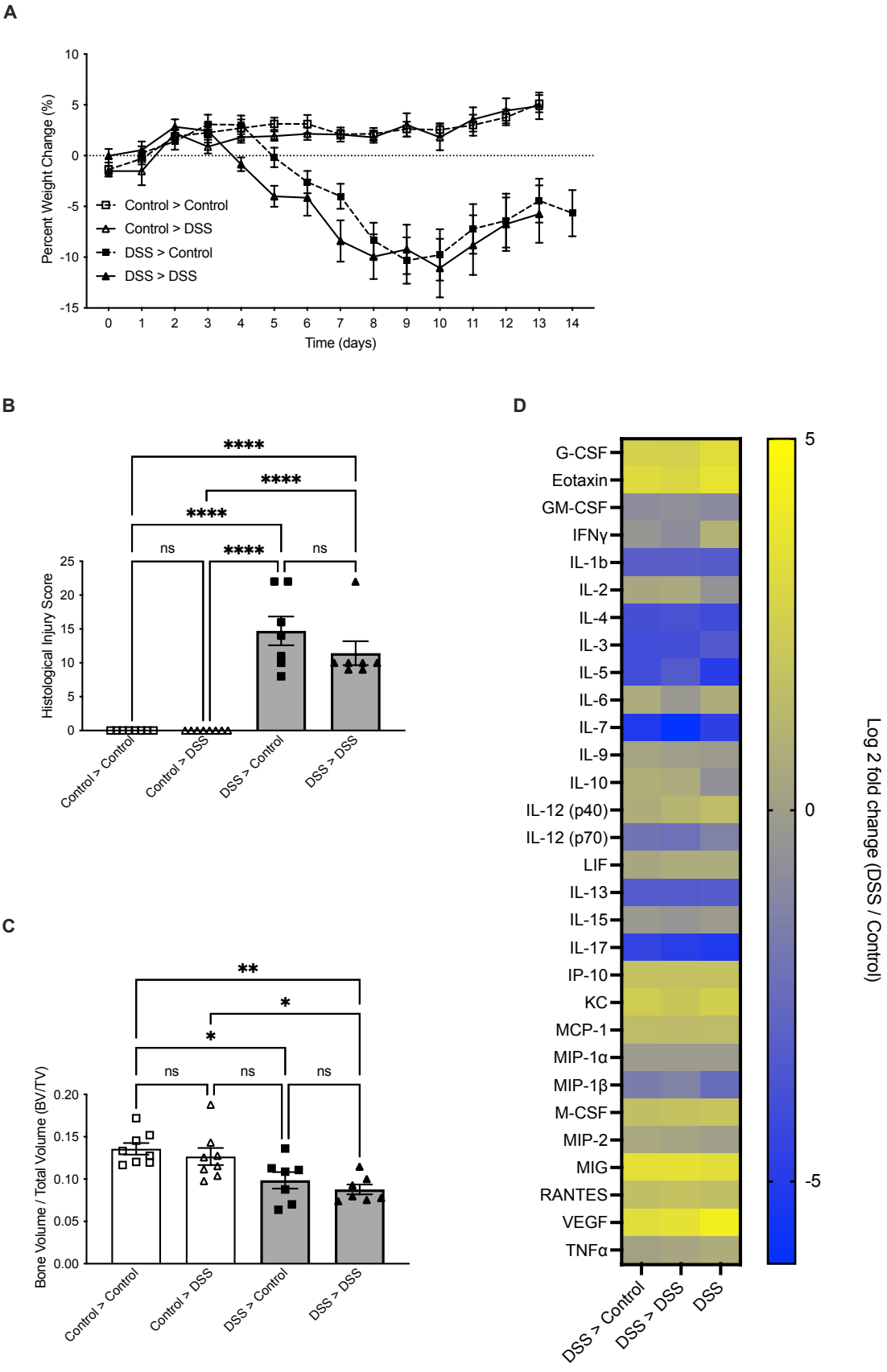
A
Percent Weight Change (%)
Time (days)
Control > Control
Control > DSS
DSS > Control
DSS > DSS
B
Histological Injury Score
****
****
****
ns
****
ns
Control > Control
Control > DSS
DSS > Control
DSS > DSS
C
Bone Volume / Total Volume (BV/TV)
**
*
*
ns
ns
ns
Control > Control
Control > DSS
DSS > Control
DSS > DSS
D
G-CSF
Eotaxin
GM-CSF
IFNγ
IL-1b
IL-2
IL-4
IL-3
IL-5
IL-6
IL-7
IL-9
IL-10
IL-12 (p40)
IL-12 (p70)
LIF
IL-13
IL-15
IL-17
IP-10
KC
MCP-1
MIP-1α
MIP-1β
M-CSF
MIP-2
MIG
RANTES
VEGF
TNFα
DSS > Control
DSS > DSS
DSS
Log 2 fold change (DSS / Control)

Figure 50. Microbiota manipulation through coprophagy does not impact bone loss during DSS-colitis.

Mice were administered 3% DSS or water (control) for 7 days. After 7 days, mice were switched to cages that had originally housed mouse in the indicated condition and maintained for additional 7 days on normal drinking water. Mice were weighed daily to monitor disease progression (A). After 14 days, colons were collected and processed for histologic injury scoring (B). Femurs were harvested and assess for trabecular bone volume via micro CT (C) or homogenized and assessed for cytokine abundances via Luminex (D) and normalized to control mice in matched housing conditions. Error bars represent mean ± S.E.M. Data analyzed via One-way ANOVA with Tukey's multiple comparison's test. * $p<0.05$, ** $p<0.01$, **** $p<0.0001$.

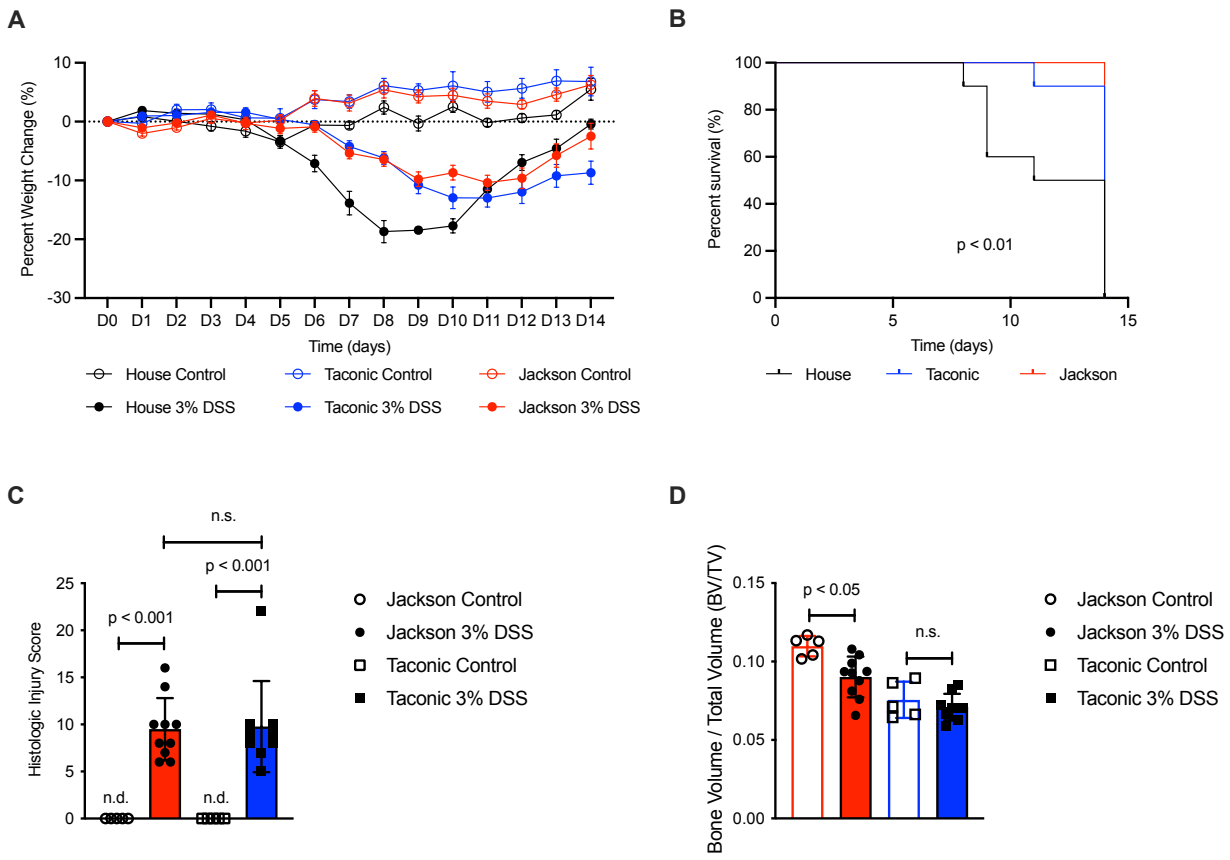

Figure 51. Taconic mice are protected from bone loss during DSS colitis.

Mice purchased directly from Jackson Laboratories, Taconic, or bred in SPF housing conditions were administered 3% DSS or water (control) for 7 days, after which mice were switched to normal drinking water for an additional 7 days. Mice were weighed daily to monitor disease progression (A). Survival was monitored through the study (B). After 14 days, colons were collected and processed for histologic injury scoring (C). Femurs were harvested and assessed for trabecular bone volume via micro CT (D). Error bars represent mean ± S.E.M. Data analyzed via Log-rank (Mantel-Cox) survival (B), or One-way ANOVA with Tukey's multiple comparison's test (C-D).

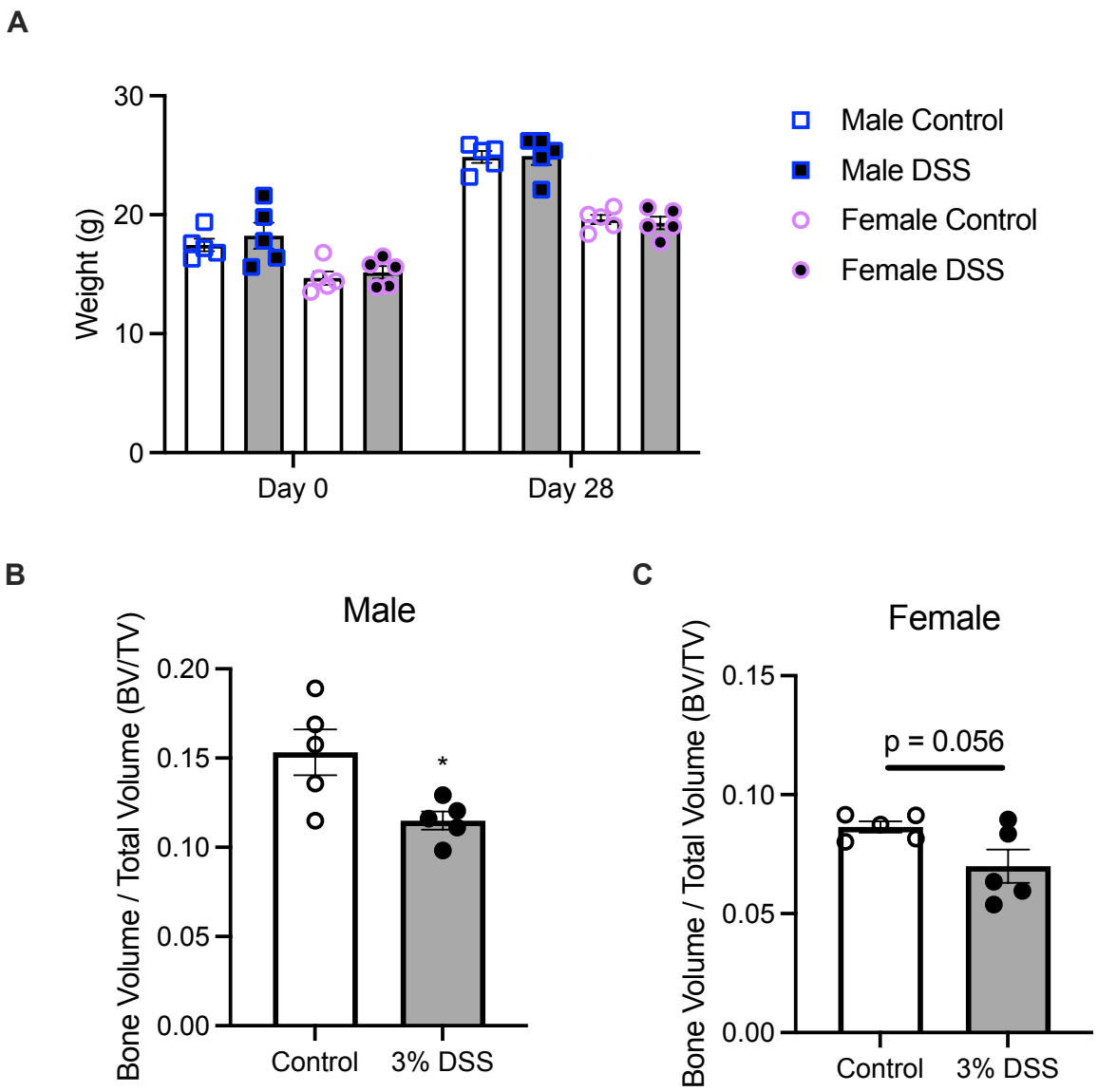

Figure 52. Colonization of germ-free mice with DSS-derived microbiota alters trabecular bone in male mice.

Germ-free mice were colonized with sex-matched stool derived from mice with or without DSS colitis for 28 days. Mice were weighed at d0 and d28 of the study (A). At d28, femurs were collected and analyzed via micro CT for trabecular bone volume / total volume (BV/TV) (B-C). Error bars represent mean ± S.E.M. Data analyzed via Student's t-test. * $p<0.05$.

REFERENCES

1. Xu F, Dahlhamer JM, Zammitti EP, Wheaton AG, Croft JB. Health-Risk Behaviors and Chronic Conditions Among Adults with Inflammatory Bowel Disease — United States, 2015 and 2016. *Morbidity Mortal Wkly Rep* 2018;67(6):190–195.

2. Souza HSP de, Fiocchi C. Immunopathogenesis of IBD: current state of the art. *Nat Rev Gastroenterol* 2016;13(1):13–27.

3. Bernstein CN, Blanchard JF, Rawsthorne P, Yu N. The prevalence of extraintestinal diseases in inflammatory bowel disease: a population-based study. *The American journal of gastroenterology* 2001;96(4):1116–1122.

4. Ott C, Schölmerich J. Extraintestinal manifestations and complications in IBD. *Nature reviews. Gastroenterology & hepatology* 2013;10(10):585–595.

5. Levine JS, Burakoff R. Extraintestinal manifestations of inflammatory bowel disease. *Gastroenterology Hepatology* 2011;7(4):235–41.

6. Aghazadeh R et al. Inflammatory bowel disease in Iran: A review of 457 cases. *J Gastroen Hepatol* 2005;20(11):1691–1695.

7. Lamb EJ et al. Metabolic bone disease is present at diagnosis in patients with inflammatory bowel disease. *Aliment Pharm Therap* 2002;16(11):1895–1902.

8. Sylvester FA et al. Natural history of bone metabolism and bone mineral density in children with inflammatory bowel disease. *Inflammatory bowel diseases* 2007;13(1):42–50.

9. Bjarnason I et al. Reduced bone density in patients with inflammatory bowel disease. *Gut* 1997;40(2):228–233.

10. Pigot F et al. Low bone mineral density in patients with inflammatory bowel disease. *Digest Dis Sci* 1992;37(9):1396–1403.

11. Pollak RD et al. Femoral neck osteopenia in patients with inflammatory bowel disease. *The American journal of gastroenterology* 1998;93(9):1483–1490.

12. Oostlander AE et al. Histomorphometric analysis reveals reduced bone mass and bone formation in patients with quiescent Crohn's disease. *Gastroenterology* 2011;140(1):116–123.

13. Genant HK, Mall JC, Wagonfeld JB, Horst JV, Lanzi LH. Comparisons Between X-Ray Photodensitometric and Gamma-Ray Absorptiometric Findings of Bone Mineral Measurements, and the Evidence of Their Convertibility. *Invest Radiol* 1976;11(6):550–555.

14. Bernstein CN, Blanchard JF, Leslie W, Wajda A, Yu BN. The Incidence of Fracture among Patients with Inflammatory Bowel Disease: A Population-Based Cohort Study. *Ann Intern Med* 2000;133(10):795.

15. Bernstein CN, Leslie WD, Leboff MS. AGA technical review on osteoporosis in gastrointestinal diseases. *Gastroenterology* 2003;124(3):795–841.

16. Abreu MT et al. Treatment with infliximab is associated with increased markers of bone formation in patients with Crohn's disease. *Journal of clinical gastroenterology* 2006;40(1):55–63.

17. Miheller P et al. Changes of OPG and RANKL concentrations in Crohn's disease after infliximab therapy. *Inflammatory bowel diseases* 2007;13(11):1379–1384.

18. Bernstein CN et al. Decreased bone density in inflammatory bowel disease is related to corticosteroid use and not disease diagnosis. *J Bone Miner Res* 1995;10(2):250–256.

19. Ghishan FK, Kiela PR. Advances in the understanding of mineral and bone metabolism in inflammatory bowel diseases. *American journal of physiology. Gastrointestinal and liver physiology* 2011;300(2):G191-201.

20. Benchimol EI et al. Effect of calcium and vitamin D supplementation on bone mineral density in children with inflammatory bowel disease. *Journal of Pediatric Gastroenterology and Nutrition* 2007;45(5):538–545.

21. Bernstein CN et al. A randomized, placebo-controlled trial of calcium supplementation for decreased bone density in corticosteroid-using patients with inflammatory bowel disease: A pilot study. *Alimentary pharmacology & therapeutics* 1996;10(5):777–786.

22. Pazianas M, Rhim AD, Weinberg AM, Su C, Lichtenstein GR. The effect of anti-TNF-alpha therapy on spinal bone mineral density in patients with Crohn's disease. *Annals of the New York Academy of Sciences* 2006;1068:543–556.

23. Mizoguchi A. Animal models of inflammatory bowel disease. *Progress in molecular biology and translational science* 2012;105:263–320.

24. OKAYASU I et al. A Novel Method in the Induction of Reliable Experimental Acute and Chronic Ulcerative-Colitis in Mice. *Gastroenterology* 1990;98(3):694–702.

25. Morris GP et al. Hapten-induced model of chronic inflammation and ulceration in the rat colon. *Gastroenterology* 1989;96(3):795–803.

26. Kühn R, Löhler J, Rennick D, Rajewsky K, Müller W. Interleukin-10-deficient mice develop chronic enterocolitis. *Cell* 1993;75(2):263–274.

27. Morrissey PJ, Charrier K, Braddy S, Liggitt D, Watson JD. CD4+ T cells that express high levels of CD45RB induce wasting disease when transferred into congenic severe combined immunodeficient mice. Disease development is prevented by cotransfer of purified CD4+ T cells. *J Exp Medicine* 1993;178(1):237–244.

28. Powrie F et al. Inhibition of Thl responses prevents inflammatory bowel disease in scid mice reconstituted with CD45RBhi CD4+ T cells. *Immunity* 1994;1(7):553–562.

29. Powrie F, Leach MW, Mauze S, Caddie LB, Coffman RL. Phenotypically distinct subsets of CD4 + T cells induce or protect from chronic intestinal inflammation in C. B-17 scid mice. *Int Immunol* 1993;5(11):1461–1471.

30. Powrie F, Correa-Oliveira R, Mauze S, Coffman RL. Regulatory interactions between CD45RBhigh and CD45RBlow CD4+ T cells are important for the balance between protective and pathogenic cell-mediated immunity. *J Exp Medicine* 1994;179(2):589–600.

31. Cahill RJ et al. Inflammatory bowel disease: an immunity-mediated condition triggered by bacterial infection with Helicobacter hepaticus. *Infect Immun* 1997;65(8):3126–3131.

32. Sartor RB. Mechanisms of Disease: pathogenesis of Crohn's disease and ulcerative colitis. *Nat Clin Pract Gastr* 2006;3(7):390–407.

33. Nell S, Suerbaum S, Josenhans C. The impact of the microbiota on the pathogenesis of IBD: lessons from mouse infection models. *Nat Rev Microbiol* 2010;8(8):564–577.

34. Higgins LM, Frankel G, Douce G, Dougan G, MacDonald TT. Citrobacter rodentium Infection in Mice Elicits a Mucosal Th1 Cytokine Response and Lesions Similar to Those in Murine Inflammatory Bowel Disease. *Infect Immun* 1999;67(6):3031–3039.

35. Foltz CJ et al. Spontaneous Inflammatory Bowel Disease in Multiple Mutant Mouse Lines: Association with Colonization by Helicobacter hepaticus. *Helicobacter* 1998;3(2):69–78.

36. McGovern VJ, Slavutin LJ. Pathology of *Salmonella* colitis. *Am J Surg Pathology* 1979;3(6):483–490.

37. DAY DW, MANDAL BK, MORSON BC. The rectal biopsy appearances in Salmonella colitis. *Histopathology* 1978;2(2):117–131.

38. Dresner-Pollak R, Gelb N, Rachmilewitz D, Karmeli F, Weinreb M. Interleukin 10-deficient mice develop osteopenia, decreased bone formation, and mechanical fragility of long bones. *Gastroenterology* 2004;127(3):792–801.

39. Byrne FR et al. CD4+CD45RBHi T cell transfer induced colitis in mice is accompanied by osteopenia which is treatable with recombinant human osteoprotegerin. *Gut* 2005;54(1):78–86.

40. Irwin R, Raehtz S, Parameswaran N, McCabe LR. Intestinal inflammation without weight loss decreases bone density and growth. *American journal of physiology. Regulatory, integrative and comparative physiology* 2016;311(6):R1149–R1157.

41. Uno JK et al. The Role of Tumor Necrosis Factor α in Down-Regulation of Osteoblast Phex Gene Expression in Experimental Murine Colitis. *Gastroenterology* 2006;131(2):497–509.

42. Thurston RD et al. Tumor necrosis factor and interferon-gamma down-regulate Klotho in mice with colitis. *Gastroenterology* 2010;138(4):1384-94-1394.e1–2.

43. Ibáñez L et al. Inflammatory Osteoclasts Prime TNFα-Producing CD4+ T Cells and Express CX_3CR1. *Journal of Bone and Mineral Research* 2016;31(10):1899–1908.

44. Ciucci T et al. Bone marrow Th17 TNFα cells induce osteoclast differentiation, and link bone destruction to IBD. *Gut* 2015;64(7):1072–1081.

45. Fries W, Giacomin D, Plebani M, Martin A. Effect of Experimental Colitis on Bone Metabolism in the Rat. *Digestion* 1994;55(4):229–233.

46. Lin CL, Moniz C, Chambers TJ, Chow J. Colitis causes bone loss in rats through suppression of bone formation. *Gastroenterology* 1996;111(5):1263–1271.

47. Ashcroft AJ et al. Colonic dendritic cells, intestinal inflammation, and T cell-mediated bone destruction are modulated by recombinant osteoprotegerin. *Immunity* 2003;19(6):849–861.

48. Cohen SL, Moore AM, Ward WE. Interleukin-10 knockout mouse: A model for studying bone metabolism during intestinal inflammation. *Inflammatory bowel diseases* 2004;10(5):557–563.

49. Melgar S, Karlsson A, Michaëlsson E. Acute colitis induced by dextran sulfate sodium progresses to chronicity in C57BL/6 but not in BALB/c mice: correlation between symptoms and inflammation. *American journal of physiology. Gastrointestinal and liver physiology* 2005;288(6):G1328-38.

50. Hamdani G et al. Dextran sodium sulfate-induced colitis causes rapid bone loss in mice. *Bone* 2008;43(5):945–950.

51. Harris L, Senagore P, Young VB, McCabe LR. Inflammatory bowel disease causes reversible suppression of osteoblast and chondrocyte function in mice. *American journal of physiology. Gastrointestinal and liver physiology* 2009;296(5):G1020-9.

52. Trottier MD, Irwin R, Li Y, McCabe LR, Fraker PJ. Enhanced production of early lineages of monocytic and granulocytic cells in mice with colitis. *Proceedings of the National Academy of Sciences of the United States of America* 2012;109(41):16594–16599.

53. Irwin R, Lee T, Young VB, Parameswaran N, McCabe LR. Colitis-induced bone loss is gender dependent and associated with increased inflammation. *Inflammatory bowel diseases* 2013;19(8):1586–1597.

54. Ke K et al. Attenuation of NF-κB in Intestinal Epithelial Cells Is Sufficient to Mitigate the Bone Loss Comorbidity of Experimental Mouse Colitis. *Journal of Bone and Mineral Research* 2019;34(10):1880–1893.

55. Kodama H, Nose M, Niida S, Yamasaki A. Essential role of macrophage colony-stimulating factor in the osteoclast differentiation supported by stromal cells. *J Exp Medicine* 1991;173(5):1291–1294.

56. Lacey DL et al. Osteoprotegerin Ligand Is a Cytokine that Regulates Osteoclast Differentiation and Activation. *Cell* 1998;93(2):165–176.

57. Yasuda H et al. Osteoclast differentiation factor is a ligand for osteoprotegerin/osteoclastogenesis-inhibitory factor and is identical to TRANCE/RANKL. *Proceedings of the National Academy of Sciences* 1998;95(7):3597–3602.

58. Yoshida H et al. The murine mutation osteopetrosis is in the coding region of the macrophage colony stimulating factor gene. *Nature* 1990;345(6274):442–444.

59. Wiktor-Jedrzejczak W et al. Total absence of colony-stimulating factor 1 in the macrophage-deficient osteopetrotic (op/op) mouse. *Proc National Acad Sci* 1990;87(12):4828–4832.

60. Kong Y-Y et al. OPGL is a key regulator of osteoclastogenesis, lymphocyte development and lymph-node organogenesis. *Nature* 1999;397(6717):315–323.

61. Li J et al. RANK is the intrinsic hematopoietic cell surface receptor that controls osteoclastogenesis and regulation of bone mass and calcium metabolism. *Proc National Acad Sci* 2000;97(4):1566–1571.

62. Dougall WC et al. RANK is essential for osteoclast and lymph node development. *Gene Dev* 1999;13(18):2412–2424.

63. Yasuda H et al. Identity of Osteoclastogenesis Inhibitory Factor (OCIF) and Osteoprotegerin (OPG): A Mechanism by which OPG/OCIF Inhibits Osteoclastogenesis in Vitro. *Endocrinology* 1998;139(3):1329–1337.

64. Tsuda E et al. Isolation of a Novel Cytokine from Human Fibroblasts That Specifically Inhibits Osteoclastogenesis. *Biochem Bioph Res Co* 1997;234(1):137–142.

65. Xiong J et al. Matrix-embedded cells control osteoclast formation. *Nat Med* 2011;17(10):1235–1241.

66. Chen X et al. Osteoblast–osteoclast interactions. *Connect Tissue Res* 2017;59(2):99–107.

67. Weivoda MM et al. Identification of osteoclast-osteoblast coupling factors in humans reveals links between bone and energy metabolism. *Nature Communications* 2020;11(1):87–13.

68. Hu K, Olsen BR. Osteoblast-derived VEGF regulates osteoblast differentiation and bone formation during bone repair. *The Journal of clinical investigation* 2016;126(2):509–526.

69. Martin TJ, Sims NA. Osteoclast-derived activity in the coupling of bone formation to resorption. *Trends in molecular medicine* 2005;11(2):76–81.

70. Nakamura T et al. Estrogen prevents bone loss via estrogen receptor alpha and induction of Fas ligand in osteoclasts. *Cell* 2007;130(5):811–823.

71. Mundy GR, Elefteriou F. Boning up on Ephrin Signaling. *Cell* 2006;126(3):441–443.

72. Negishi-Koga T et al. Suppression of bone formation by osteoclastic expression of semaphorin 4D. *Nat Med* 2011;17(11):1473–1480.

73. Tang Y et al. TGF-β1–induced migration of bone mesenchymal stem cells couples bone resorption with formation. *Nat Med* 2009;15(7):757–765.

74. Ikebuchi Y et al. Coupling of bone resorption and formation by RANKL reverse signalling. *Nature* 2018;561(7722):195–200.

75. Walker DG. Control of bone resorption by hematopoietic tissue. The induction and reversal of congenital osteopetrosis in mice through use of bone marrow and splenic transplants. *J Exp Medicine* 1975;142(3):651–663.

76. Walker DG. Bone Resorption Restored in Osteopetrotic Mice by Transplants of Normal Bone Marrow and Spleen Cells. *Science* 1975;190(4216):784–785.

77. Walker DG. Osteopetrosis Cured by Temporary Parabiosis. *Science* 1973;180(4088):875–875.

78. Walker DG. Spleen Cells Transmit Osteopetrosis in Mice. *Science* 1975;190(4216):785–787.

79. Marks SC, Walker DG. The hematogenous origin of osteoclasts: Experimental evidence from osteopetrotic (microphthalmic) mice treated with spleen cells from beige mouse donors. *Am J Anat* 1981;161(1):1–10.

80. Okada S et al. In vivo and in vitro stem cell function of c-kit- and Sca-1-positive murine hematopoietic cells. *Blood* 1992;80(12):3044–3050.

81. Jacquin C, Gran DE, Lee SK, Lorenzo JA, Aguila HL. Identification of multiple osteoclast precursor populations in murine bone marrow. *Journal of Bone and Mineral Research* 2006;21(1):67–77.

82. Charles JF et al. Inflammatory arthritis increases mouse osteoclast precursors with myeloid suppressor function. *The Journal of clinical investigation* 2012;122(12):4592–4605.

83. Muto A et al. Lineage-committed osteoclast precursors circulate in blood and settle down into bone. *Journal of Bone and Mineral Research* 2011;26(12):2978–2990.

84. Miyamoto T et al. Bifurcation of osteoclasts and dendritic cells from common progenitors. *Blood* 2001;98(8):2544–2554.

85. Rivollier A et al. Immature dendritic cell transdifferentiation into osteoclasts: a novel pathway sustained by the rheumatoid arthritis microenvironment. *Blood* 2004;104(13):4029–4037.

86. Sawant A et al. Myeloid-Derived Suppressor Cells Function as Novel Osteoclast Progenitors Enhancing Bone Loss in Breast Cancer. *Cancer Res* 2013;73(2):672–682.

87. Nakamichi Y et al. Spleen serves as a reservoir of osteoclast precursors through vitamin D-induced IL-34 expression in osteopetrotic op/op mice. *Proc National Acad Sci* 2012;109(25):10006–10011.

88. Jacome-Galarza CE, Lee SK, Lorenzo JA, Aguila HL. Identification, characterization, and isolation of a common progenitor for osteoclasts, macrophages, and dendritic cells from murine bone marrow and periphery. *Journal of Bone and Mineral Research* 2013;28(5):1203–1213.

89. Novak S et al. Osteoclasts Derive Predominantly from Bone Marrow-Resident CX3CR1+ Precursor Cells in Homeostasis, whereas Circulating CX3CR1+ Cells Contribute to Osteoclast Development during Fracture Repair. *Journal of immunology (Baltimore, Md. : 1950)* 2020;204(4):868–878.

90. Yahara Y et al. Erythromyeloid progenitors give rise to a population of osteoclasts that contribute to bone homeostasis and repair. *Nature cell biology* 2020;22(1):49–59.

91. Jacome-Galarza CE et al. Developmental origin, functional maintenance and genetic rescue of osteoclasts. *Nature* 2019;568(7753):541–545.

92. McDonald MM et al. Osteoclasts recycle via osteomorphs during RANKL-stimulated bone resorption. *Cell* 2021;184(5):1330-1347.e13.

93. Mundy GR, Varani J, Orr W, Gondek MD, Ward PA. Resorbing bone is chemotactic for monocytes. *Nature* 1978;275(5676):132–135.

94. Ishii M, Kikuta J, Shimazu Y, Meier-Schellersheim M, Germain RN. Chemorepulsion by blood S1P regulates osteoclast precursor mobilization and bone remodeling in vivo. *The Journal of experimental medicine* 2010;207(13):2793–2798.

95. Ishii M et al. Sphingosine-1-phosphate mobilizes osteoclast precursors and regulates bone homeostasis. *Nature* 2009;458(7237):524–528.

96. Kotani M et al. Systemic circulation and bone recruitment of osteoclast precursors tracked by using fluorescent imaging techniques. *Journal of immunology (Baltimore, Md. : 1950)* 2013;190(2):605–612.

97. Khan UA, Hashimi SM, Bakr MM, Forwood MR, Morrison NA. CCL2 and CCR2 are Essential for the Formation of Osteoclasts and Foreign Body Giant Cells. *Journal of cellular biochemistry* 2016;117(2):382–389.

98. Sucur A et al. Chemokine signals are crucial for enhanced homing and differentiation of circulating osteoclast progenitor cells. *Arthritis research & therapy* 2017;19(1):142–16.

99. Matijašević MI et al. Increased chemotaxis and activity of circulatory myeloid progenitor cells may contribute to enhanced osteoclastogenesis and bone loss in the C57BL/6 mouse model of collagen-induced arthritis. *Clinical and experimental immunology* 2016;186(3):321–335.

100. Mulholland BS, Forwood MR, Morrison NA. Monocyte Chemoattractant Protein-1 (MCP-1/CCL2) Drives Activation of Bone Remodelling and Skeletal Metastasis. *Current osteoporosis reports* 2019;17(6):538–547.

101. Li X et al. A destructive cascade mediated by CCL2 facilitates prostate cancer growth in bone. *Cancer Research* 2009;69(4):1685–1692.

102. Boyce BF, Xing L. Functions of RANKL/RANK/OPG in bone modeling and remodeling. *Archives of biochemistry and biophysics* 2008;473(2):139–146.

103. Okamoto K et al. Osteoimmunology: The Conceptual Framework Unifying the Immune and Skeletal Systems. *Physiological Reviews* 2017;97(4):1295–1349.

104. Takayanagi H. Mechanistic insight into osteoclast differentiation in osteoimmunology. *J Mol Med* 2005;83(3):170–179.

105. Takayanagi H. The role of NFAT in osteoclast formation. *Annals of the New York Academy of Sciences* 2007;1116:227–237.

106. Lacey DL et al. Osteoprotegerin Ligand Modulates Murine Osteoclast Survival in Vitro and in Vivo. *Am J Pathology* 2000;157(2):435–448.

107. Ross FP. M-CSF, c-Fms, and signaling in osteoclasts and their precursors. *Annals of the New York Academy of Sciences* 2006;1068:110–116.

108. Koga T et al. Costimulatory signals mediated by the ITAM motif cooperate with RANKL for bone homeostasis. *Nature* 2004;428(6984):758–763.

109. Mócsai A et al. The immunomodulatory adapter proteins DAP12 and Fc receptor γ-chain (FcRγ) regulate development of functional osteoclasts through the Syk tyrosine kinase. *P Natl Acad Sci Usa* 2004;101(16):6158–6163.

110. Humphrey MB, Nakamura MC. A Comprehensive Review of Immunoreceptor Regulation of Osteoclasts. *Clin Rev Allerg Immu* 2016;51(1):48–58.

111. Bar-Shavit Z. The osteoclast: a multinucleated, hematopoietic-origin, bone-resorbing osteoimmune cell. *Journal of cellular biochemistry* 2007;102(5):1130–1139.

112. Zhao H. Membrane trafficking in osteoblasts and osteoclasts: new avenues for understanding and treating skeletal diseases. *Traffic (Copenhagen, Denmark)* 2012;13(10):1307–1314.

113. Teitelbaum SL. Bone resorption by osteoclasts. *Science* 2000;289(5484):1504–1508.

114. Takayanagi H. Osteoimmunology: shared mechanisms and crosstalk between the immune and bone systems. *Nat Rev Immunol* 2007;7(4):292–304.

115. Charles JF, Aliprantis AO. Osteoclasts: more than 'bone eaters'. *Trends Mol Med* 2014;20(8):449–459.

116. Krisher T, Bar-Shavit Z. Regulation of osteoclastogenesis by integrated signals from toll-like receptors. *Journal of cellular biochemistry* 2014;115(12):2146–2154.

117. Sato N et al. MyD88 But Not TRIF Is Essential for Osteoclastogenesis Induced by Lipopolysaccharide, Diacyl Lipopeptide, and IL-1α. *J Exp Medicine* 2004;200(5):601–611.

118. Bar-Shavit Z. Taking a toll on the bones: regulation of bone metabolism by innate immune regulators. *Autoimmunity* 2008;41(3):195–203.

119. Takami M, Kim N, Rho J, Choi Y. Stimulation by toll-like receptors inhibits osteoclast differentiation. *The Journal of Immunology* 2002;169(3):1516–1523.

120. Ji J-D et al. Inhibition of RANK Expression and Osteoclastogenesis by TLRs and IFN-γ in Human Osteoclast Precursors. *J Immunol* 2009;183(11):7223–7233.

121. Ivashkiv LB. A signal-switch hypothesis for cross-regulation of cytokine and TLR signalling pathways. *Nat Rev Immunol* 2008;8(10):816–822.

122. Ivashkiv LB. Cross-regulation of signaling by ITAM-associated receptors. *Nat Immunol* 2009;10(4):340–347.

123. Yu M et al. PTH induces bone loss via microbial-dependent expansion of intestinal TNF+ T cells and Th17 cells. *Nature Communications* 2020;11(1):468.

124. Gao Y et al. IFN-gamma stimulates osteoclast formation and bone loss in vivo via antigen-driven T cell activation. *Journal of Clinical Investigation* 2007;117(1):122–132.

125. Yu M et al. Ovariectomy induces bone loss via microbial-dependent trafficking of intestinal TNF+ T cells and Th17 cells. *J Clin Invest* 2021;131(4):e143137.

126. Tsukasaki M et al. Host defense against oral microbiota by bone-damaging T cells. *Nature Communications* 2018;9(1):701.

127. Ono T et al. IL-17-producing γδ T cells enhance bone regeneration. *Nature Communications* 2016;7(1):10928.

128. Komatsu N et al. Pathogenic conversion of Foxp3+ T cells into TH17 cells in autoimmune arthritis. *Nature Medicine* 2014;20(1):62–68.

129. Sato K et al. Th17 functions as an osteoclastogenic helper T cell subset that links T cell activation and bone destruction. *The Journal of experimental medicine* 2006;203(12):2673–2682.

130. Tang M, Tian L, Luo G, Yu X. Interferon-Gamma-Mediated Osteoimmunology. *Frontiers in immunology* 2018;9:1508.

131. Nagata N, Kitaura H, Yoshida A, Nakayama K. Inhibition of RANKL-induced osteoclast formation in mouse bone marrow cells by IL-12: involvement of IFN-gamma possibly induced from non-T cell population. *Bone* 2003;33(4):721–732.

132. Pöllinger B et al. Th17 cells, not IL-17+ γδ T cells, drive arthritic bone destruction in mice and humans. *Journal of immunology (Baltimore, Md. : 1950)* 2011;186(4):2602–2612.

133. Yu M et al. Regulatory T cells are expanded by Teriparatide treatment in humans and mediate intermittent PTH-induced bone anabolism in mice. *EMBO reports* 2018;19(1):156–171.

134. Tyagi AM et al. The Microbial Metabolite Butyrate Stimulates Bone Formation via T Regulatory Cell-Mediated Regulation of WNT10B Expression. *Immunity* 2018;49(6):1116-1131.e7.

135. Wei S, Kitaura H, Zhou P, Ross FP, Teitelbaum SL. IL-1 mediates TNF-induced osteoclastogenesis. *Journal of Clinical Investigation* 2005;115(2):282–290.

136. Lam J et al. TNF-alpha induces osteoclastogenesis by direct stimulation of macrophages exposed to permissive levels of RANK ligand. *Journal of Clinical Investigation* 2000;106(12):1481–1488.

137. Dewhirst FE, Stashenko PP, Mole JE, Tsurumachi T. Purification and partial sequence of human osteoclast-activating factor: identity with interleukin 1 beta. *J Immunol Baltim Md 1950* 1985;135(4):2562–8.

138. Horton JE, Raisz LG, Simmons HA, Oppenheim JJ, Mergenhagen SE. Bone Resorbing Activity in Supernatant Fluid from Cultured Human Peripheral Blood Leukocytes. *Science* 1972;177(4051):793–795.

139. Joyce-Shaikh B et al. Myeloid DAP12-associating lectin (MDL)-1 regulates synovial inflammation and bone erosion associated with autoimmune arthritis. *J Exp Medicine* 2010;207(3):579–589.

140. Ochi S et al. Pathological role of osteoclast costimulation in arthritis-induced bone loss. *Proc National Acad Sci* 2007;104(27):11394–11399.

141. Zhang YH, Heulsmann A, Tondravi MM, Mukherjee A, Abu-Amer Y. Tumor necrosis factor-alpha (TNF) stimulates RANKL-induced osteoclastogenesis via coupling of TNF type 1 receptor and RANK signaling pathways. *The Journal of biological chemistry* 2001;276(1):563–568.

142. Gong JK. Endosteal marrow: a rich source of hematopoietic stem cells. *Science* 1978;199(4336):1443–1445.

143. Orkin SH, Zon LI. Hematopoiesis: An Evolving Paradigm for Stem Cell Biology. *Cell* 2008;132(4):631–644.

144. Kollet O et al. Osteoclasts degrade endosteal components and promote mobilization of hematopoietic progenitor cells. *Nat Med* 2006;12(6):657–664.

145. Mansour A et al. Osteoclasts promote the formation of hematopoietic stem cell niches in the bone marrow. *The Journal of experimental medicine* 2012;209(3):537–549.

146. Kollet O et al. Osteoclasts Are Involved in Stem Cell Mobilization: Cleavage of SDF-1 by Cathepsin K. *Blood* 2004;104(11):1291–1291.

147. Takamatsu Y et al. Osteoclast-mediated bone resorption is stimulated during short-term administration of granulocyte colony-stimulating factor but is not responsible for hematopoietic progenitor cell mobilization. *Blood* 1998;92(9):3465–3473.

148. Cheung R et al. Activation of MDL-1 (CLEC5A) on immature myeloid cells triggers lethal shock in mice. *J Clin Invest* 2011;121(11):4446–4461.

149. Caiado F, Pietras EM, Manz MG. Inflammation as a regulator of hematopoietic stem cell function in disease, aging, and clonal selection. *J Exp Med* 2021;218(7):e20201541.

150. Griseri T, McKenzie BS, Schiering C, Powrie F. Dysregulated Hematopoietic Stem and Progenitor Cell Activity Promotes Interleukin-23-Driven Chronic Intestinal Inflammation. *Immunity* 2012;37(6):1116–1129.

151. Chang CF, Pollard M. Effects of Microbial Flora on Levels of Colony Stimulating Factor in Serums of Irradiated CFW Mice 1. *P Soc Exp Biol Med* 1973;144(1):177–180.

152. Staber FG, Tarcsay L, Dukor P. Modulation of Myelopoiesis In Vivo by Chemically Pure Preparations of Cell Wall Components from Gram-Negative Bacteria: Effects at Different Stages. *Infect Immun* 1978;20(1):40–49.

153. Joshi JH, Entringer MA, Robinson WA. Bacterial Stimulation of Serum Colony-Stimulating Activity and Neutrophil Production in Germ-Free Mice 1. *P Soc Exp Biol Med* 1979;162(1):44–47.

154. Goris H, Boer F de, Waaij D van der. Myelopoiesis in experimentally contaminated specific-pathogen-free and germfree mice during oral administration of polymyxin. *Infect Immun* 1985;50(2):437–441.

155. Cho I et al. Antibiotics in early life alter the murine colonic microbiome and adiposity. *Nature* 2012;488(7413):621–626.

156. Yan J et al. Gut microbiota induce IGF-1 and promote bone formation and growth. *Proceedings of the National Academy of Sciences of the United States of America* 2016;113(47):E7554–E7563.

157. Sjögren K et al. The gut microbiota regulates bone mass in mice. *Journal of Bone and Mineral Research* 2012;27(6):1357–1367.

158. Quach D, Collins F, Parameswaran N, McCabe L, Britton RA. Microbiota Reconstitution Does Not Cause Bone Loss in Germ-Free Mice. *mSphere* 2018;3(1). doi:10.1128/mspheredirect.00545-17

159. Tyagi AM et al. The gut microbiota is a transmissible determinant of skeletal maturation. *Elife* 2021;10:e64237.

160. Collins FL et al. Beneficial effects of Lactobacillus reuteri 6475 on bone density in male mice is dependent on lymphocytes. *Scientific Reports* 2019;9(1):14708.

161. Britton RA et al. Probiotic L. reuteri treatment prevents bone loss in a menopausal ovariectomized mouse model. *Journal of cellular physiology* 2014;229(11):1822–1830.

162. Schepper JD et al. Probiotic Lactobacillus reuteri Prevents Postantibiotic Bone Loss by Reducing Intestinal Dysbiosis and Preventing Barrier Disruption. *Journal of Bone and Mineral Research* 2019;34(4):681–698.

163. McCabe LR, Irwin R, Schaefer L, Britton RA. Probiotic use decreases intestinal inflammation and increases bone density in healthy male but not female mice. *Journal of cellular physiology* 2013;228(8):1793–1798.

164. Li J-Y et al. Sex steroid deficiency-associated bone loss is microbiota dependent and prevented by probiotics. *The Journal of clinical investigation* 2016;126(6):2049–2063.

165. Lucas S et al. Short-chain fatty acids regulate systemic bone mass and protect from pathological bone loss. *Nature Communications* 2018;9(1):55.

166. Bäumler AJ, Tsolis RM, Ficht TA, Adams LG. Evolution of Host Adaptation in Salmonella enterica. *Infect Immun* 1998;66(10):4579–4587.

167. Tsolis RM, Xavier MN, Santos RL, Bäumler AJ. How To Become a Top Model: Impact of Animal Experimentation on Human Salmonella Disease Research. *Infect Immun* 2011;79(5):1806–1814.

168. Scallan E et al. Foodborne Illness Acquired in the United States—Major Pathogens - Volume 17, Number 1—January 2011 - Emerging Infectious Diseases journal - CDC. *Emerg Infect Dis* 2011;17(1):7–15.

169. Anand AJ, Glatt AE. Salmonella osteomyelitis and arthritis in sickle cell disease. *Semin Arthritis Rheu* 1994;24(3):211–221.

170. Huang Z et al. Salmonella Osteomyelitis in Adults: A Systematic Review. *Orthop Surg* 2021;13(4):1135–1140.

171. Farooqui BJ, Khurshid M, Ashfaq MK, Khan MA. Comparative yield of Salmonella typhi from blood and bone marrow cultures in patients with fever of unknown origin. *J Clin Pathol* 1991;44(3):258.

172. Santos RL et al. Animal models of Salmonella infections: enteritis versus typhoid fever. *Microbes Infect* 2001;3(14–15):1335–1344.

173. Vidal S et al. The Ity/Lsh/Bcg locus: natural resistance to infection with intracellular parasites is abrogated by disruption of the Nramp1 gene. *J Exp Medicine* 1995;182(3):655–666.

174. Barthel M et al. Pretreatment of Mice with Streptomycin Provides a Salmonella enterica Serovar Typhimurium Colitis Model That Allows Analysis of Both Pathogen and Host. *Infect Immun* 2003;71(5):2839–2858.

175. Andrews-Polymenis HL, Bäumler AJ, McCormick BA, Fang FC. Taming the Elephant: Salmonella Biology, Pathogenesis, and Prevention. *Infect Immun* 2010;78(6):2356–2369.

176. Rauch I et al. NAIP-NLRC4 Inflammasomes Coordinate Intestinal Epithelial Cell Expulsion with Eicosanoid and IL-18 Release via Activation of Caspase-1 and -8. *Immunity* 2017;46(4):649–659.

177. Crowley SM et al. Intestinal restriction of Salmonella Typhimurium requires caspase-1 and caspase-11 epithelial intrinsic inflammasomes. *Plos Pathog* 2020;16(4):e1008498.

178. Knodler LA et al. Dissemination of invasive Salmonella via bacterial-induced extrusion of mucosal epithelia. *Proc National Acad Sci* 2010;107(41):17733–17738.

179. Santos M de S, Orth K. Subversion of the cytoskeleton by intracellular bacteria: lessons from Listeria, Salmonella and Vibrio. *Cellular microbiology* 2015;17(2):164–173.

180. Santos AMP dos, Ferrari RG, Conte-Junior CA. Type three secretion system in Salmonella Typhimurium: the key to infection. *Genes Genom* 2020;42(5):495–506.

181. Arpaia N et al. TLR Signaling Is Required for Salmonella typhimurium Virulence. *Cell* 2011;144(5):675–688.

182. Sellin ME et al. Epithelium-Intrinsic NAIP/NLRC4 Inflammasome Drives Infected Enterocyte Expulsion to Restrict Salmonella Replication in the Intestinal Mucosa. *Cell Host Microbe* 2014;16(2):237–248.

183. Karki R et al. IRF8 Regulates Transcription of Naips for NLRC4 Inflammasome Activation. *Cell* 2018;173(4):920-933.e13.

184. Qu Y et al. NLRP3 recruitment by NLRC4 during Salmonella infectionNLRP3 recruitment by NLRC4. *J Exp Medicine* 2016;213(6):877–885.

185. Gram AM et al. Salmonella Flagellin Activates NAIP/NLRC4 and Canonical NLRP3 Inflammasomes in Human Macrophages. *J Immunol Author Choice* 2021;206(3):631–640.

186. Matusiak M et al. Flagellin-induced NLRC4 phosphorylation primes the inflammasome for activation by NAIP5. *Proc National Acad Sci* 2015;112(5):1541–1546.

187. Shi J et al. Inflammatory caspases are innate immune receptors for intracellular LPS. *Nature* 2014;514(7521):187–192.

188. Kimura S et al. Osteoprotegerin-dependent M cell self-regulation balances gut infection and immunity. *Nat Commun* 2020;11(1):234.

189. Fang C et al. Cutting Edge: EZH2 Promotes Osteoclastogenesis by Epigenetic Silencing of the Negative Regulator IRF8. *J Immunol* 2016;196(11):4452–4456.

190. Zhao B et al. Interferon regulatory factor-8 regulates bone metabolism by suppressing osteoclastogenesis. *Nat Med* 2009;15(9):1066–1071.

191. Nishikawa K et al. DNA methyltransferase 3a regulates osteoclast differentiation by coupling to an S-adenosylmethionine–producing metabolic pathway. *Nat Med* 2015;21(3):281–287.

192. Targownik LE, Bernstein CN, Leslie WD. Inflammatory bowel disease and the risk of osteoporosis and fracture. *Maturitas* 2013;76(4):315–319.

193. Ghosh S, Cowen S, Hannan WJ, Ferguson A. Low Bone-Mineral Density in Crohns-Disease, but Not in Ulcerative-Colitis, at Diagnosis. *YGAST* 1994;107(4):1031–1039.

194. Moschen AR et al. The RANKL/OPG system is activated in inflammatory bowel disease and relates to the state of bone loss. *Gut* 2005;54(4):479–487.

195. Shin H-S et al. Crosstalk among IL-23 and DNAX activating protein of 12 kDa-dependent pathways promotes osteoclastogenesis. *Journal of immunology (Baltimore, Md. : 1950)* 2015;194(1):316–324.

196. Chen S-T et al. CLEC5A is critical for dengue-virus-induced lethal disease. *Nature* 2008;453(7195):672–676.

197. Aoki N et al. Expression and functional role of MDL-1 (CLEC5A) in mouse myeloid lineage cells. *J Leukocyte Biol* 2009;85(3):508–517.

198. Singh UP et al. Chemokine and cytokine levels in inflammatory bowel disease patients. *Cytokine* 2016;77:44–49.

199. Neurath MF. Cytokines in inflammatory bowel disease. *Nature Reviews Immunology* 2014;14(5):329–342.

200. Friedrich M, Pohin M, Powrie F. Cytokine Networks in the Pathophysiology of Inflammatory Bowel Disease. *Immunity* 2019;50(4):992–1006.

201. Melgar S et al. Mice with experimental colitis show an altered metabolism with decreased metabolic rate. *American journal of physiology. Gastrointestinal and liver physiology* 2007;292(1):G165-72.

202. DeBoer MD, Steinman J, Li Y. Partial normalization of pubertal timing in female mice with DSS colitis treated with anti-TNF-α antibody. *Journal of gastroenterology* 2012;47(6):647–654.

203. Oz HS, Ebersole JL. A novel murine model for chronic inflammatory alveolar bone loss. *Journal of periodontal research* 2010;45(1):94–99.

204. Gobert AP et al. Hypusination Orchestrates the Antimicrobial Response of Macrophages. *Cell Reports* 2020;33(11):108510–108510.

205. Hardbower DM et al. Ornithine decarboxylase regulates M1 macrophage activation and mucosal inflammation via histone modifications. *Proc National Acad Sci* 2017;114(5):E751–E760.

206. Rivera-Chávez F et al. Depletion of Butyrate-Producing Clostridia from the Gut Microbiota Drives an Aerobic Luminal Expansion of Salmonella. *Cell Host Microbe* 2016;19(4):443–454.

207. Dieleman LA et al. Chronic experimental colitis induced by dextran sulphate sodium (DSS) is characterized by Th1 and Th2 cytokines. *Clinical and experimental immunology* 1998;114(3):385–391.

208. Kennedy RJ et al. Interleukin 10-deficient colitis: new similarities to human inflammatory bowel disease. *Brit J Surg* 2000;87(10):1346–1351.

209. Bouxsein ML et al. Guidelines for assessment of bone microstructure in rodents using micro-computed tomography. *Journal of Bone and Mineral Research* 2010;25(7):1468–1486.

210. Dempster DW et al. Standardized nomenclature, symbols, and units for bone histomorphometry: A 2012 update of the report of the ASBMR Histomorphometry Nomenclature Committee. *J Bone Miner Res* 2013;28(1):2–17.

211. Raffatellu M et al. Lipocalin-2 resistance confers an advantage to Salmonella enterica serotype Typhimurium for growth and survival in the inflamed intestine. *Cell Host & Microbe* 2009;5(5):476–486.

212. Chong SZ et al. CXCR4 identifies transitional bone marrow premonocytes that replenish the mature monocyte pool for peripheral responses. *The Journal of experimental medicine* 2016;213(11):2293–2314.

213. González-Domínguez érika et al. CD163L1 and CLEC5A discriminate subsets of human resident and inflammatory macrophages in vivo. *J Leukocyte Biol* 2015;98(4):453–466.

214. Aschenbrenner D et al. Deconvolution of monocyte responses in inflammatory bowel disease reveals an IL-1 cytokine network that regulates IL-23 in genetic and acquired IL-10 resistance. *Gut* 2020;gutjnl-2020-321731.

215. Inui M et al. Signal adaptor DAP10 associates with MDL-1 and triggers osteoclastogenesis in cooperation with DAP12. *Proc National Acad Sci* 2009;106(12):4816–4821.

216. Kim HK, Sierra MDLL, Williams CK, Gulino AV, Tosato G. G-CSF down-regulation of CXCR4 expression identified as a mechanism for mobilization of myeloid cells. *Blood* 2006;108(3):812–820.

217. Petit I et al. G-CSF induces stem cell mobilization by decreasing bone marrow SDF-1 and up-regulating CXCR4. *Nat Immunol* 2002;3(7):687–694.

218. Herman S et al. Induction of osteoclast-associated receptor, a key osteoclast costimulation molecule, in rheumatoid arthritis. *Arthritis Rheumatism* 2008;58(10):3041–3050.

219. Radhakrishnan VM, Gilpatrick MM, Parsa NA, Kiela PR, Ghishan FK. Expression of Cav1.3 calcium channel in the human and mouse colon: posttranscriptional inhibition by IFNγ. *American journal of physiology. Gastrointestinal and liver physiology* 2017;312(1):G77–G84.

220. Radhakrishnan VM et al. Post-translational loss of renal TRPV5 calcium channel expression, Ca(2+) wasting, and bone loss in experimental colitis.. *Gastroenterology* 2013;145(3):613–624.

221. Knoop KA et al. RANKL Is Necessary and Sufficient to Initiate Development of Antigen-Sampling M Cells in the Intestinal Epithelium. *J Immunol* 2009;183(9):5738–5747.

222. Tsukasaki M et al. OPG Production Matters Where It Happened. *Cell Reports* 2020;32(10):108124.

223. Tahoun A et al. Salmonella Transforms Follicle-Associated Epithelial Cells into M Cells to Promote Intestinal Invasion. *Cell Host Microbe* 2012;12(5):645–656.

224. Hoffman D et al. A non-classical monocyte-derived macrophage subset provides a splenic replication niche for intracellular Salmonella. *Immunity* 2021;54(12):2712-2723.e6.

225. Vazquez-Torres A et al. Extraintestinal dissemination of Salmonella by CD18-expressing phagocytes. *Nature* 1999;401(6755):804–808.

226. Kikuta J et al. Dynamic visualization of RANKL and Th17-mediated osteoclast function. *The Journal of clinical investigation* 2013;123(2):866–873.

227. Wu J et al. High-throughput assay to phenotype Salmonella enterica Typhimurium association, invasion, and replication in macrophages. *Journal of Visualized Experiments* 2014;(90):e51759.

228. Nishikawa K et al. Blimp1-mediated repression of negative regulators is required for osteoclast differentiation. *Proceedings of the National Academy of Sciences of the United States of America* 2010;107(7):3117–3122.

229. Lightfield KL et al. Differential Requirements for NAIP5 in Activation of the NLRC4 Inflammasome. *Infect Immun* 2011;79(4):1606–1614.

230. Rauch I et al. NAIP proteins are required for cytosolic detection of specific bacterial ligands in vivo. *J Exp Medicine* 2016;213(5):657–665.

231. Uematsu S et al. Detection of pathogenic intestinal bacteria by Toll-like receptor 5 on intestinal CD11c+ lamina propria cells. *Nat Immunol* 2006;7(8):868–874.

232. Chen KW et al. The Neutrophil NLRC4 Inflammasome Selectively Promotes IL-1β Maturation without Pyroptosis during Acute Salmonella Challenge. *Cell Reports* 2014;8(2):570–582.

233. Hapfelmeier S et al. The Salmonella Pathogenicity Island (SPI)-2 and SPI-1 Type III Secretion Systems Allow Salmonella Serovar typhimurium to Trigger Colitis via MyD88-Dependent and MyD88-Independent Mechanisms. *J Immunol* 2005;174(3):1675–1685.

234. Fournier BM, Parkos CA. The role of neutrophils during intestinal inflammation. *Mucosal Immunol* 2012;5(4):354–366.

235. Kasten TP et al. Potentiation of osteoclast bone-resorption activity by inhibition of nitric oxide synthase. *Proc National Acad Sci* 1994;91(9):3569–3573.

236. Armour KE, Hof RJV 'T, Grabowski PS, Reid DM, Ralston SH. Evidence for a Pathogenic Role of Nitric Oxide in Inflammation-Induced Osteoporosis. *J Bone Miner Res* 1999;14(12):2137–2142.

237. Bakker ABH, Baker E, Sutherland GR, Phillips JH, Lanier LL. Myeloid DAP12-associating lectin (MDL)-1 is a cell surface receptor involved in the activation of myeloid cells. *Proc National Acad Sci* 1999;96(17):9792–9796.

238. Abdallah D et al. An Optimized Method to Generate Human Active Osteoclasts From Peripheral Blood Monocytes. *Front Immunol* 2018;9:632.

239. Martin JC et al. Single-Cell Analysis of Crohn's Disease Lesions Identifies a Pathogenic Cellular Module Associated with Resistance to Anti-TNF Therapy. *Cell* 2019;178(6):1493-1508.e20.

240. Aune TM et al. Expression of long non-coding RNAs in autoimmunity and linkage to enhancer function and autoimmune disease risk genetic variants. *J Autoimmun* 2017;81:99–109.

241. Barbara JS, et al, inventors; Merck Sharp & Dohme Corp, assignee. MDL-1 Ligand. U.S. Patent No. 9,284,377. March 15, 2016.

242. Yang R et al. Galectin-9 interacts with PD-1 and TIM-3 to regulate T cell death and is a target for cancer immunotherapy. *Nat Commun* 2021;12(1):832.

243. Zhu C et al. The Tim-3 ligand galectin-9 negatively regulates T helper type 1 immunity. *Nat Immunol* 2005;6(12):1245–1252.

244. Dardalhon V et al. Tim-3/Galectin-9 Pathway: Regulation of Th1 Immunity through Promotion of CD11b+Ly-6G+ Myeloid Cells. *J Immunol* 2010;185(3):1383–1392.

245. Shinohara M et al. Tyrosine Kinases Btk and Tec Regulate Osteoclast Differentiation by Linking RANK and ITAM Signals. *Cell* 2008;132(5):794–806.

246. Lee SH, Kim T, Jeong D, Kim N, Choi Y. The Tec Family Tyrosine Kinase Btk Regulates RANKL-induced Osteoclast Maturation*. *J Biol Chem* 2008;283(17):11526–11534.

247. Murata K et al. Hypoxia-Sensitive COMMD1 Integrates Signaling and Cellular Metabolism in Human Macrophages and Suppresses Osteoclastogenesis. *Immunity* 2017;47(1):66-79.e5.

248. Ivashkiv LB. Metabolic-epigenetic coupling in osteoclast differentiation. *Nat Med* 2015;21(3):212–213.

249. Kubatzky KF, Uhle F, Eigenbrod T. From macrophage to osteoclast - How metabolism determines function and activity. *Cytokine* 2018;112:102–115.

250. Indo Y et al. Metabolic regulation of osteoclast differentiation and function. *J Bone Miner Res* 2013;28(11):2392–2399.

251. Ishii K et al. Coordination of PGC-1β and iron uptake in mitochondrial biogenesis and osteoclast activation. *Nat Med* 2009;15(3):259–266.

252. Jiang L et al. Salmonella Typhimurium reprograms macrophage metabolism via T3SS effector SopE2 to promote intracellular replication and virulence. *Nat Commun* 2021;12(1):879.

253. Powers TR et al. Intracellular niche-specific profiling reveals transcriptional adaptations required for the cytosolic lifestyle of Salmonella enterica. *Plos Pathog* 2021;17(8):e1009280.

254. Ford CA et al. Diflunisal-loaded poly(propylene sulfide) nanoparticles decrease S. aureus-mediated bone destruction during osteomyelitis. *J Orthop Res* 2021;39(2):426–437.

255. Putnam NE et al. MyD88 and IL-1R signaling drive antibacterial immunity and osteoclast-driven bone loss during Staphylococcus aureus osteomyelitis. *PLOS Pathogens* 2019;15(4):e1007744.

256. Cassat JE, Skaar EP. Recent advances in experimental models of osteomyelitis. *Expert review of anti-infective therapy* 2013;11(12):1263–1265.

257. Hendrix AS et al. Repurposing the Nonsteroidal Anti-inflammatory Drug Diflunisal as an Osteoprotective, Antivirulence Therapy for Staphylococcus aureus Osteomyelitis. *Antimicrobial agents and chemotherapy* 2016;60(9):5322–5330.

258. Cassat JE et al. A secreted bacterial protease tailors the Staphylococcus aureus virulence repertoire to modulate bone remodeling during osteomyelitis. *Cell Host & Microbe* 2013;13(6):759–772.

259. Adamopoulos IE et al. IL-23 is critical for induction of arthritis, osteoclast formation, and maintenance of bone mass. *Journal of immunology (Baltimore, Md. : 1950)* 2011;187(2):951–959.

260. Horwood NJ, Elliott J, Martin TJ, Gillespie MT. IL-12 alone and in synergy with IL-18 inhibits osteoclast formation in vitro. *The Journal of Immunology* 2001;166(8):4915–4921.

261. Yoshimatsu M et al. IL-12 Inhibits Lipopolysaccharide Stimulated Osteoclastogenesis in Mice. *Journal of immunology research* 2015;2015(2):214878–8.

262. Chen L, Wei X-Q, Evans B, Jiang W, Aeschlimann D. IL-23 promotes osteoclast formation by up-regulation of receptor activator of NF-kappaB (RANK) expression in myeloid precursor cells. *European Journal of Immunology* 2008;38(10):2845–2854.

263. Ju J-H et al. IL-23 induces receptor activator of NF-kappaB ligand expression on CD4+ T cells and promotes osteoclastogenesis in an autoimmune arthritis model. *Journal of immunology (Baltimore, Md. : 1950)* 2008;181(2):1507–1518.